

Low mantle plume component in 370 Ma old Kola ultrabasic-alkaline-carbonatite complexes: Evidences from rare gas isotopes and related trace elements

I. N. Tolstikhin, I. L. Kamensky, V. A. Nivin, V. R. Vetrin,
E. G. Balaganskaya, S. V. Ikorsky, M. A. Gannibal, and Yu. M. Kirnarsky

Geological Institute, Kola Scientific Centre, Russian Academy of Sciences, Apatity 184200, Russia

B. Marty

Centre National de la Recherche Scientifique Centre de Recherches Petrographiques et
Geochimiques(C.R.P.G.) B.P. 20, 54501 Vandoeuvre-Nancy Cedex, France

D. Weiss, A. Verhulst, and D. Demaiffe

Petrologie et Geodynamique Chimique Department des Sciences de la Terre et de l'Environnement
Faculte des Sciences Universite Libre de Bruxelles Avenue F. D. Roosevelt 50 B-1050 Bruxelles,
Belgique

Abstract. During Devonian pulse of alkaline magmatism (370 Ma ago) 18 ultrabasic-alkaline-carbonatite complexes were formed on the Kola Peninsula. Rare gas isotope abundances were studied in ~300 samples from 8 complexes and also from Devonian dikes. A comparison of expected from in-situ closed-system production (calc) and measured (meas) abundances has shown that ${}^4\text{He}_{\text{meas}} \leq {}^4\text{He}_{\text{calc}}$ whereas in some rocks and minerals ${}^3\text{He}_{\text{meas}}$ exceeded ${}^3\text{He}_{\text{calc}}$ up to 1,000 times indicating occurrence of a mantle fluid in a majority of samples. Gas extraction liberated fluid-related helium with as low ${}^4\text{He}/{}^3\text{He}$ ratios as 3×10^4 . These values show a contribution of ${}^3\text{He}$ -rich plume-like component.

A reason for highly variable ${}^4\text{He}/{}^3\text{He}$ ratios is not well understood yet. Isotope composition of Ne supports the occurrence of plume component: ${}^{20}\text{Ne}/{}^{22}\text{Ne}$ ratio varies from 10.4 to 12.0 and ${}^{20}\text{Ne}/{}^{22}\text{Ne}$ versus ${}^{21}\text{Ne}/{}^{22}\text{Ne}$ correlation is quite similar to that observed for Loihi hot spot, Hawaii.

A comparison of these data with rare gas systematic in the mantle enable us to suggest a contribution of material from the less degassed deep mantle reservoir, source of primordial rare gases, to Devonian ultrabasic-alkaline and carbonatite rocks on the Kola Peninsula.

1. Introduction

Several reasons encourage studies of trace element and isotope systematics of Ultrabasic-Alkaline-Carbonatites Complexes (UACC). Petrologic [*Le Bas*, 1987; *Wyllie et al.*, 1990], geochemical [*Nelson et al.*, 1988] and isotopic [*Grunenfelder et al.*, 1986; *Andersen*, 1987;

Bell and Blenkinsop, 1989; *Kwan et al.*, 1989] features of UACC all indicate mantle source for parent melts. Generally manifestations of alkaline and carbonatite magmatism are small; however low-viscous carbonatite- and alkaline melts could sample large volumes of mantle. Concentrations of some elements, such as Sr and REE, in alkaline and carbonatitic rocks and related melts are rather high when compared to crustal average abundances; therefore these melts are able to deliver characteristics of mantle composition and processes through the continental crust with a limited crustal contamination [*Nelson et al.*, 1988; *Woolley and Kempe*, 1989; *Bell and Blenkinsop*, 1989].

©1998 Russian Journal of Earth Sciences.

Paper No. TJE99015.

Online version of this paper was published on February 12, 1999.
URL: <http://eos.wdcb.rssi.ru/tjes/TJE99015/TJE99015.htm>

Studies of the UACC have led to the following results important for this contribution: 1) Petrology and trace element chemistry of UACC both indicate a metasomatically-processed volatile-element-enriched mantle source for the alkaline and carbonatite melts [Andersen, 1987; Hawkesworth *et al.*, 1990; Kramm and Kogarko, 1994]. 2) Isotopic signatures of UACC show certain similarities with oceanic island alkaline rocks suggesting similar sources and processes [Grunenfelder *et al.*, 1986; Nelson *et al.*, 1988; Bell and Blenkinsop, 1989; Kwon *et al.*, 1989].

Because of a high abundance of volatiles is required to form alkaline and especially carbonatite melts, and noble gases are the meaningful tracers of volatiles, noble gas studies of UACC appears to be quite promising. However only a few relevant papers are available [Staudacher and Allegre, 1982; Sasada *et al.*, 1997], excepting systematic studies of the Kola UACC [Tolstikhin *et al.*, 1985; Mitrofanov *et al.*, 1995a; Ikorsky *et al.*, 1997, 1998; Marty *et al.*, 1999].

Within the Kola Peninsula, the eastern segment of the Baltic shield, several pulses of the alkaline magmatism occurred from 2760 Ma till 370 Ma ago [Pushkarev, 1990; Kramm *et al.*, 1993; Kogarko *et al.*, 1995]. During the last (Devonian) magmatic event about 20 ultrabasic-alkaline-carbonatite intrusive Complexes, from giant Khibiny to quite small dikes, were formed [Kuharenko *et al.*, 1965; Kogarko *et al.*, 1995; Beard *et al.*, 1996, 1998]. The isotopic signatures of Sr, Nd and abundances of REE indeed show rather low crustal contamination of the Devonian Kola UACC [Kramm and Kogarko, 1994; Zaitsev and Bell., 1995]. Considerable development of the UACC by later metamorphic processes has not been observed.

In this paper new noble gas and parent trace element analyses obtained for 8 Devonian Kola UACC are presented and previous available data are compiled. Solar-like isotopic signatures of trapped rare gases definitely identify a contribution from plume component similar to that observed in the most active spot of the archipelago Hawaii, the Loihi seamount. A subcontinental lithosphere source for this component is discussed, with a negative conclusion. A contribution from the lower mantle reservoir is suggested and evaluated for different models of the lower mantle fractionation-degassing history.

2. Geological Background

2.1. Alkaline Magmatism on the Kola Peninsula

Extension of alkaline-subalkaline rocks of different ages, from 2.76 till 0.36 Ga, appears to be a specific feature of the Kola Geological Province situated on the north-east segment of the Baltic Shield. The total con-

tribution of these rocks is $\sim 4\%$ (four times the mean world contribution). The Kola Province consists of several Late Archaean blocks separated by Late Archaean greenstone belts and Early Proterozoic riftogenic structures (Figure 1). Hercynian activation was the last powerful magmatic event within the Kola Province. Proterozoic Granulite belt separates the Kola Province from the southward Karelian one [Kratz *et al.*, 1978; Bertherson and Marker, 1985; Mitrofanov *et al.*, 1995b].

Tonalite trondhjemite-granodiorite gneisses (TTG) are the most ancient rocks of the Kola Province forming the basement for Early Proterozoic structures. The gneisses were originated 2.95–2.75 Ga ago. According to Sm-Nd studies of TTG and komatiites, the upper mantle of this age was substantially depleted [Timmerman and Daly, 1995; Vrevsky and Krymsky, 1997] due to melting and removal of large masses of basalt melts which serve as a parent material for the TTG gneisses [Balashov *et al.*, 1992; Levchenkov *et al.*, 1995].

Several massifs of subalkaline lepidomelane-ferrohastingsite granitoids were formed in the north-eastern part of the Kola Peninsula during cratonisation period of the Late Archaean tectono-magmatic stage at 2.76 ± 0.08 Ga (Figure 1). Approximately simultaneously alkaline granites formed the largest in the world province, about 3,000 square km, in the Central part of the Peninsula.

The composition of mantle sources were essentially changed in Early Proterozoic. Basic-ultrabasic layered intrusions having 2.5 – 2.4 Ga U-Pb and Sm-Nd ages show similar geochemical and isotopic characteristics, e.g., negative $\varepsilon_{Nd} = -1.2$ to -2.3 implying an enriched reservoir [Balashov *et al.*, 1993; Amelin *et al.*, 1995, Amelin and Semenov, 1996]. A number of such intrusions within the Kola, the Karelia and the northern Finland suggests uprising of a large mantle plume at that time [Amelin *et al.*, 1995]. Evolution of this plume determined sequence of tectonic events and peculiarities of mantle and crustal magmatism during Early Proterozoic. Approximately simultaneously with the layered intrusions, the first alkaline syenite Sakharyok massif was formed within the Kola Province.

The Svekofennian activation, 1800 Ma ago, gave rise to multy-phase gabbro-nepheline syenite and alkaline granite intrusions, such as Gremyakh-Vyrmes, Soustova and other. Simultaneously porphyritic granitoid melts were intruded along the faults of north-eastern direction, giving rise to Litsa, Lebyazhka and other massifs with the total area of 900 km².

The latest intense alkaline magmatism was related to Devonian plume [Beard *et al.*, 1996; Ikorsky *et al.*, 1997]. At that time two giant nepheline syenite massifs, Khibiny and Lovozero, several ultrabasic-alkaline-carbonatite Complexes [Kovdor, Sebyavv and other], and swarms of dykes were formed. Metasomatic enrichment of the depleted mantle material with certain

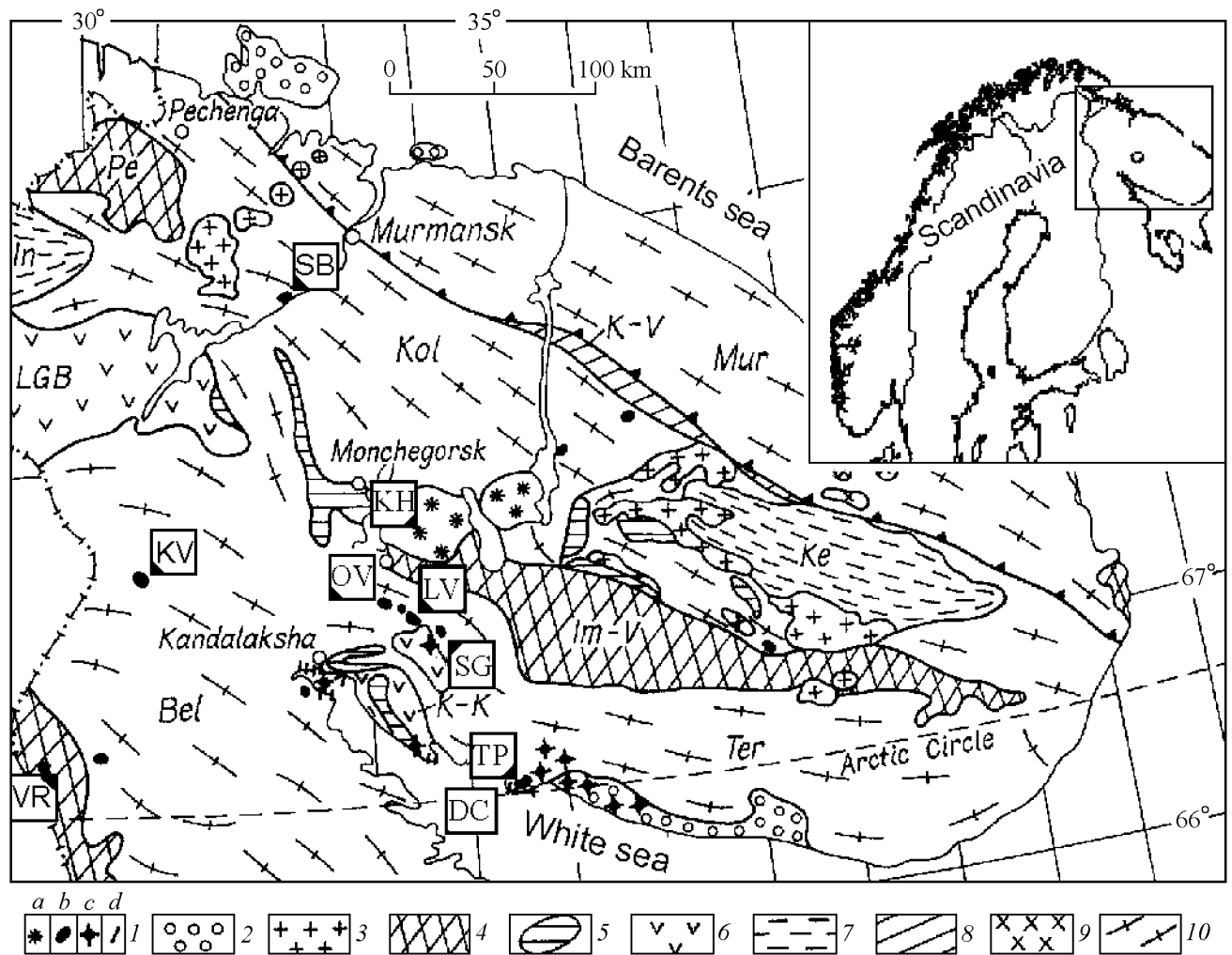


Figure 1. Schematic geological map of the Kola Peninsula. 1 - The Palaeozoic Complexes of: nepheline syenites (a), ultrabasic-alkaline-carbonatite rocks (b), explosion pipes (c) and dykes (d). 2 - Upper Proterozoic sedimentary rocks. Early Proterozoic: 3 - granites, 4 - volcanic-sedimentary rocks, 5 - basic-ultrabasic rocks, 6 - granulites. Late Archaean: 7 - gneisses, 8 - gneisses, amphibolites, and komatiites (fragments of greenstone belts), 9 - granites, 10 - granite-gneiss basement of Proterozoic structure. Domains: Mur - Murmansk, Kol - Kola, Bel - Belomorian, Ter - Tersky, Ke - Keivy, In - Inary. Belts: K-V - Kolmipozero-Voronja, LGB - Lapland, K-K - Kolvitsa-Kandalaksha, Pe - Pechenga, Im-V - Imandra-Varsuga. Complexes from which samples were collected (numbers in squares): 1 - Khibiny (abbreviation KH), 2 - Kovdor (KV), 3 - Seblyavr (SB), 4 - Ozernaya Varaka (OV), 5 - Lesnaya Varaka (LV), 6 - Salmagora (SG), 7 - Vuoriyarvy (VR), 8 - Turyi peninsula (TP), 9 - Dyke Complex (DC).

elements, e.g., Rb, Sr, REE, is suggested to occur before the alkaline melts emplacement [Kramm and Kogarko, 1994]. The melts were probably originated from two or three different mantle sources and were not contaminated considerably by crustal material during ascending through the continental crust [Kramm, 1993; Zaitsev and Bell, 1995].

2.2. Devonian Ultrabasic-Alkaline-Carbonatite and Dyke Complexes

2.2.1. The giant Khibiny alkaline pluton

with exposed area 1327 km², is situated in the central part of Kola Peninsula (Figure 1) between Archaean gneisses and granitoids of the Kola block to north and volcano-

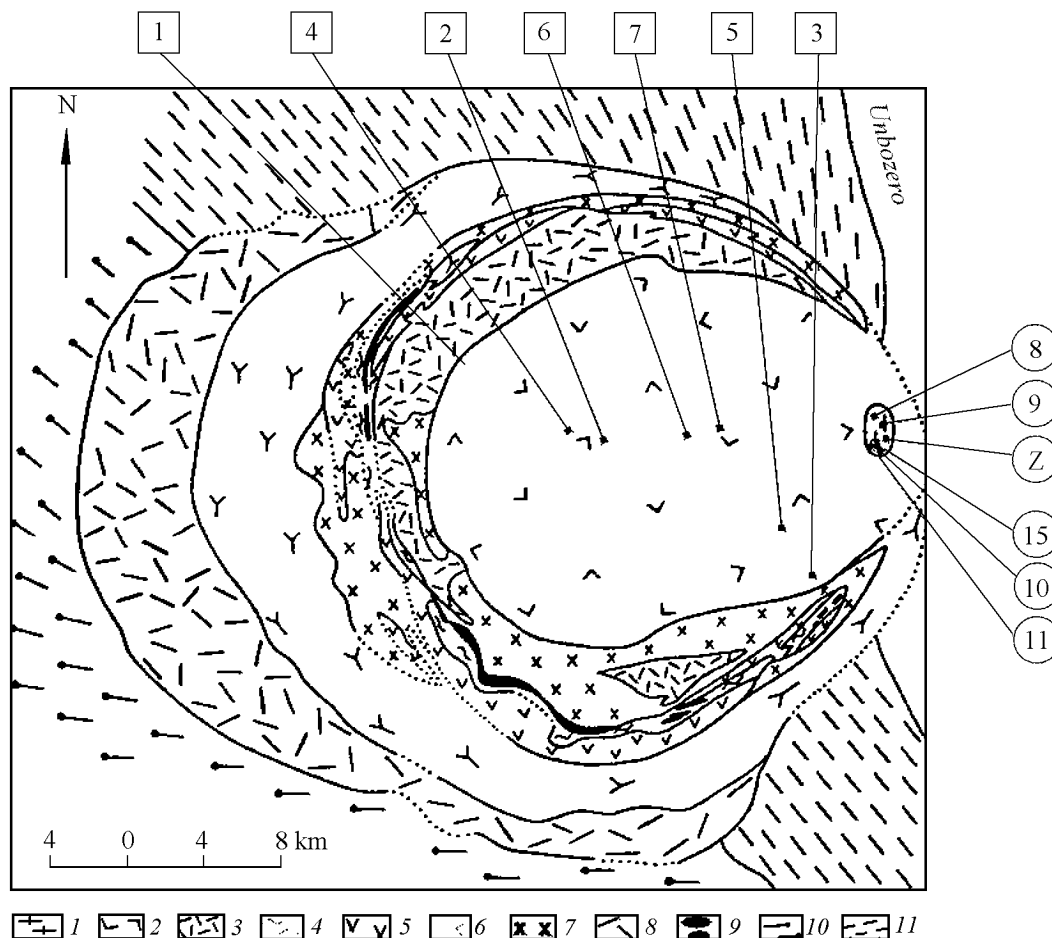


Figure 2. Schematic Geological map of Khibiny pluton (after *Arzamastseva et al.*, 1991).

1 - carbonatites, 2 - rocks of foyaite complex, 3 - unregular-grained nepheline syenites (lyavochorrites), 4 - massive urtites, 5 - gneissic ijolites, 6 - trachytoid khibinites, 7 - poikilitic nepheline syenites (rischorrites), 8 - massive khibinites, 9 - apatite-nepheline ores, 10 - Early Proterozoic volcanic-sedimentary rocks of Imandra - Varsuga structure, 11 - Archean gneisses of the Kola domain.

Sample sites: square - outcrop, circle - borehole, number - number of sample (Tables 1-5), letter shows - several samples at one and the same location; after slash depth of a sample is shown 8/128; 9/1547; 10/282; 11/287; Z: 12/177, 13/216, 14/393.

genic-sedimentary rocks of the Early-Proterozoic riftogenic Imandra-Varzuga structure to south (Figure 2).

The Khibiny pluton is nepheline-syenites polyphase central-type intrusion characterised by a cone-like shape and a concentric-zoned (arc-like at horizontal plane) structure. Rocks of different intrusive phases exposed the following time-spatial sequence (from periphery to centre): (I) volcanic alkaline syenites; (II) massive khibinites; (III) trachytoid khibinites; (IV) rischorrites; (V) ijolite-urtites; this phase is of complicated structure and composition and includes a number of bodies of apatite-

nepheline rocks; (VI) unregular-grained nepheline-syenites (lyavochorrites); and (VII) foyaite [*Ivanova et al.*, 1970; *Galakhov*, 1975].

Olivinite, pyroxenite and jacupirangite xenoliths found within the Khibiny imply that the earliest protopluton could be formed by alkaline-ultrabasic rocks which were then intruded and partially assimilated by nepheline-syenite melts [*Galakhov*, 1975, 1978; *Shpachenko and Stepanov*, 1991; *Balaganskaya and Savchenko*, 1998].

A stock of carbonatite and ferrocarnatite-silicate

rocks (phase VIII) intruded foyaites (VII) displaying the following time sequence: phoscorites, i.e., biotite-aegirine-apatite rocks, (a), early carbonatites, calcite, with biotite and aegirine, (b), late calcite (c), and carbonate-zeolite veins (d) [Zaitsev, 1996].

Kramm and Kogarko [1994] obtained Rb-Sr rock-mineral isochrone age at 367.5 ± 5.5 Ma for nepheline-syenites and quite a similar age was found for mineral separates from Khibiny carbonatites, 366.6 ± 47 Ma [Zaitsev et al., 1997].

Table 1 comprises indexes and description of samples selected from the Khibiny massif and other Complexes.

2.2.2. The Kovdor (5.5 x 8 km size) is situated on the south-west segment of Kola Peninsula (Figure 1), gneisses of the Belomorian domain being the host rocks [Kukharensko et al., 1965; Ternovoy, 1977; Dudkin and Kirnarsky, 1994; Balaganskaya, 1994]. The Complex has a stock-like shape and concentric-zoned structure (Figure 3). Its central core is composed by olivinites which are surrounded by olivine-clinopyroxene, phlogopite-clinopyroxene, and clinopyroxene rocks including giant pegmatitic body with meter-size crystals of olivine, clinopyroxene and phlogopite. The peripheral circle consists of melilite-bearing rocks, earlier ijolite-melteigites and later ijolite-urtites.

Between olivine-clinopyroxene and ijolite rocks in the south-west part of the Complex there is 1.2 x 0.8 km size body of apatite-forsterite rocks, calcite-apatite-phlogopite-magnetite phoscorites, earlier calcite carbonatites and later dolomite ones. Further to the west – south-west calcite carbonatites form a vein-stockwerk zone among fenitized host rocks of the frame. (Figure 3).

The 380 ± 3 Ma age was obtained by applying U-Pb systematics to baddeite from the calcite carbonatites [Bayanova et al., 1997].

2.2.3. The Sebyavr Complex is situated in the north-west part of Kola Peninsula (Figure 1). The Complex is a stock-like oval body intruding Archean gneisses of the Kola domain and having the exposed area 5 x 4 km. The Complex is characterised by a concentric zoned structure (Figure 4). The core is composed by clinopyroxenites, including blocks of olivinites, and surrounded by the thin unlocked oval of nepheline clinopyroxenites and ijolite. In some parts of the Complex clinopyroxenites were transformed by pneumatolithic and autometasomatic processes into scarn-like apatite-phlogopite-garnet-amphibole rocks and apatite clinopyroxenites [Kukharensko et al., 1965; Subbotin and Mihaels, 1986].

Phoscorites and carbonatites intruded the core at four stages producing a concentric net of dykes and veins.

The 409 ± 5 Ma Rb-Sr rocks and minerals isochrone age was obtained for clinopyroxenite, phoscorite and carbonatite of the 1 stage, whereas U-Pb age of bad-

deite from phoscorite of the 2 stage gave 378 ± 4 Ma [Gogol et al., 1998] and Rb-Sr isochrone age of carbonatite (ibid) 376 ± 6 Ma [Balaganskaya and Gogol, unpublished data]. In the following discussion the age of the Complex obtained by Kramm and Kogarko [1993], 370 ± 10 Ma, is accepted.

2.2.4. The Ozernaya Varaka is situated in the central part of Kola Peninsula (Figure 1). This is a small almost isometric zoned body, 0.8 x 1 km (Figure 5), intruded biotite-plagioclase Late Archean gneisses of the Tersky block. The central core, ~25% of the exposed area, is composed by coarse-grained clinopyroxene rocks with nepheline, Ti-magnetite, perovskite, sometimes with apatite, amphibole, and schorlomite. The core is surrounded by intermediate ~0.2 km thick zone of ijolite-urtites. The western periphery segment is composed by ijolite-melteigites. Small blocks of clinopyroxenites (same as in the core) with characteristic reaction rims and breccias spots are observed within the ijolite-melteigites [Borodin, 1961; Kukharensko et al., 1965; Dudkin et al., 1980; Arzamastzeva and Arzamastzev, 1990].

Veins of aegirine-calcite and phlogopite-calcite carbonatites and dykes of ijolite-porphyrates, feldspatoid syenites, monchiquites and tinguaite cut rocks of the massif and its fenitized 0.2–0.3 km thick rim. Kramm et al. [1993] presented 376 ± 3 Ma Rb-Sr isochrone age for clinopyroxenites and 370 ± 5 Ma for carbonatites of this Complex.

2.2.5. The Lesnaya Varaka Complex is situated 8 km to the south-east from the Ozernaya Varaka (Figure 1) also within the north-west section of Tersky domain. The massif is a stock-like body. The most abundant rocks are olivinites covering up to 85% of the oval-like 2.5 x 4 km exposed area (Figure 6). Among olivinites ore-bearing (with Ti-magnetite and perovskite) and pure varieties are distinguished. Veins of fine-grained ijolites, coarse-grained ijolite-pegmatites, dolomite-tremolite-carbonatites, and later tinguaite dykes are observed within olivinites. In the western and southern segments olivinites are rimmed by narrow (< 0.2 km) zone of clinopyroxenites. In contact zones the host rocks are transformed into typical aegirine-feldspar fenites.

2.2.6. The Salmagorsky Complex is situated 20 km to the south-east from Ozernaya Varaka (Figure 1). A stock-like body of the Complex intruded Late Archean gneisses of the north-west segment of Tersky domain (Figure 7). Near the contact gneisses are fenitized. The Complex, having exposed area 5.5 x 6.5 km, is characterised by clearly zoned structure. Its periphery segment is composed by olivinites and clinopyroxenites, at some places with elevated concentrations of Ti-

Table 1. Brief description of samples

Sample	Rock/mineral	Description
Khibiny		
KH-1	Foyaite	Clinopyroxene foyaite, coarse-grained, with Ti-magnetite and titanite
KH-2	Foyaite	Biotite foyaite, coarse-grained
KH-3	Foyaite	Clinopyroxene foyaite, coarse-grained, albite-bearing
KH-4	Foyaite	Clinopyroxene foyaite, albite-bearing, with titanite and biotite
KH-5	Foyaite	Clinopyroxene foyaite, albitized, with titanite
KH-6	Foyaite	Foyaite
KH-7	Foyaite	Amphibole-biotite-clinopyroxene foyaite, titanite-bearing
KH-8	Carbonatite	Biotite-calcite carbonatite, fine-grained, with sulfides, apatite, pyrochlore
KH-9	Carbonatite	Manganocalcite carbonatite
KH-10	Carbonatite	Biotite-feldspar-manganocalcite carbonatite
KH-11	Carbonatite	Manganocalcite carbonatite, feldspar-bearing, with biotite and burbankite
KH-12	Carbonatite	Manganocalcite carbonatite
KH-13	Carbonatite	Manganocalcite carbonatite
KH-14	Carbonatite	Manganocalcite carbonatite
KH-15	Carbonatite	Ankerite carbonatite
Kovdor		
KV-1	Olivinite	Olivinite, massive, coarse-grained
KV-2	Olivinite	Olivinite medium-grained, Ti-magnetite-bearing, with phlogopite and clinohumite
KV-3	Olivinite	Phlogopite olivinite Ti-magnetite-bearing, with serpentine and clinohumite
KV-4	Olivinite	Ore olivinite Ti-magnetite-bearing, altered (serpentine, clinohumite, carbonate)
KV-5	Olivinite	Olivinite phlogopite- and clinohumite-bearing, with Ti-magnetite
KV-6	Olivinite	Olivinite medium-fine-grained, with phlogopite, Ti-magnetite and calcite
KV-7	Melteygite	Melteygite fine-medium-grained, with perovskite
KV-8	Olivinite	Phlogopite olivinite with perovskite and Ti-magnetite
KV-9	Olivinite	Olivinite serpentinous, fine-grained, Ti-magnetite- and clinohumite-bearing
KV-10	Olivinite	Olivinite serpentinous, clinopyroxene- and Ti-magnetite-bearing, with clinohumite and phlogopite
KV-11	Clinopyroxenite	Ore clinopyroxenite medium-grained, Ti-magnetite- and olivine-bearing
KV-12	Clinopyroxenite	Ore nepheline-phlogopite clinopyroxenite zeolitized
KV-13	**Diopside	From clinopyroxenite
KV-14	**Ti-Magnetite	From clinopyroxenite
KV-15	Melilitolite	Melilitolite with garnet
KV-16	Melilitite	Melilitite with biotite, coarse-grained
KV-17	Turjaite	Turjaite with olivine, coarse-grained
KV-18	Ijolite	Ijolite porphyreous
KV-19	Ijolite	Ijolite fine-grained carbonate-bearing
KV-20	Ijolite	Ijolite, fine-medium-grained with titanite
KV-21	**Magnetite	Magnetite from phoscorite
KV-22	Phoscorite	Apatite-forsterite rock with magnetite, contain phlogopite and baddeleyite, fine-medium-grained
KV-23	Phoscorite	Forsterite-magnetite phoscorite with calcite and green phlogopite
KV-24	Phoscorite	Apatite-forsterite-magnetite rock with phlogopite, calcite and baddeleyite, medium-grained
KV-25	Phoscorite	Calcite-magnetite rock with forsterite, phlogopite, apatite and baddeleyite, medium-grained
KV-26	Phoscorite	Apatite-forsterite-calcite-magnetite rock with clinohumite, red phlogopite and pyrochlore
KV-27	Carbonatite	Clinopyroxene-calcite carbonatite
KV-28	Carbonatite	Phlogopite-clinopyroxene-calcite carbonatite
KV-29	*Clinopyroxene	From biotite-clinopyroxene-calcite carbonatite

Table 1. Continuation

Sample	Rock/mineral	Description
KV-30	*Biotite	From biotite-clinopyroxene-calcite carbonatite
KV-31	*Calcite	From biotite-clinopyroxene-calcite carbonatite
KV-32	Carbonatite	Clinopyroxene-calcite carbonatite
KV-33	Carbonatite	Calcite carbonatite, apatite and phlogopite-bearing, with dolomite
KV-34	Carbonatite	Apatite-calcite rock with magnetite, green phlogopite and baddeleyite, medium-grained
KV-35	Carbonatite	Calcite rock with apatite, magnetite, green phlogopite and baddeleyite, medium-grained
KV-36	Carbonatite	Calcite rock with forsterite, magnetite, green phlogopite and baddeleyite, medium-grained
KV-37	Carbonatite	Coarse-grained calcite carbonatite, contains rare fine grains of red phlogopite
KV-38	**Magnetite	From dolomite-phlogopite-calcite carbonatite
KV-39	**Calcite	From dolomite-phlogopite-calcite carbonatite
KV-40	Carbonatite	Calcite-dolomite rock with red phlogopite
KV-41	Carbonatite	Dolomite-calcite carbonatite with red phlogopite
KV-42	Carbonatite	Dolomite carbonatite
KV-43	Carbonatite	Dolomite carbonatite, coarse-grained
KV-44	Carbonatite	Dolomite carbonatite with apatite and red phlogopite, fine-medium-grained
KV-45	Carbonatite	Dolomite carbonatite with magnetite and rare grains of apatite and pyrochlore, medium-grained
KV-46	Carbonatite	Dolomite carbonatite with calcite, apatite and red phlogopite
Seblyavr		
SB-1	Olivinite	Olivinite with Ti-magnetite, perovskite, phlogopite, serpentine, fine-grained
SB-2	*Magn, fraction	From olivinite with Ti-magnetite, perovskite, phlogopite, serpentine, fine-grained
SB-3	Olivinite	Olivinite clinopyroxene-, phlogopite-, Ti-magnetite-bearing, with serpentine
SB-4	Olivinite	Ore olivinite, medium-fine-grained, clinopyroxene- and Ti-magnetite-bearing
SB-5	Olivinite	Olivinite fine-grained, clinopyroxene- and Ti-magnetite-bearing, with phlogopite and serpentine
SB-6	Clinopyroxenite	Clinopyroxenite with perovskite, Ti-magnetite, phlogopite and amphibole
SB-7	Clinopyroxenite	Ore clinopyroxenite, perovskite- and Ti-magnetite-bearing, with phlogopite and amphibole
SB-8	*Magn, fraction	From ore clinopyroxenite, perovskite- and Ti-magnetite-bearing, with phlogopite and amphibole
SB-9	*clinopyroxene	From ore clinopyroxenite, perovskite- and Ti-magnetite-bearing, with phlogopite and amphibole
SB-10	*Perovskite	From ore clinopyroxenite, perovskite- and Ti-magnetite-bearing, with phlogopite and amphibole
SB-11	Clinopyroxenite	Phlogopite clinopyroxenite with perovskite and Ti-magnetite
SB-12	Clinopyroxenite	Ore clinopyroxenite, Ti-magnetite- and phlogopite-bearing, with perovskite and amphibole
SB-13	Clinopyroxenite	Perovskite-Ti-magnetite-clinopyroxene rock with phlogopite and calcite, medium-grained
SB-14	Ijolite	Ijolite medium-grained, contains titanite and baddeleyite, slightly shpreushteinized, medium-grained
SB-15	Phoscorite	Apatite-phlogopite-diopside-magnetite rock with calcite and amphibole
SB-16	Phoscorite	Apatite-forsterite-magnetite rock contains phlogopite, baddeleyite, chlorite after forsterite

Table 1. Continuation

Sample	Rock/mineral	Description
SB-17	Phoscorite	Apatite-phlogopite-diopside-magnetite rock with baddeleyite and amphibole
SB-18	Carbonatite	Calcite rock, contain apatite, phlogopite, baddeleyite and zircon
SB-19	Phoscorite	Apatite-calcite-magnetite rock with red phlogopite and baddeleyite
SB-20	Carbonatite	Calcite carbonatite
SB-21	Carbonatite	Calcite carbonatite with green phlogopite and red phlogopite, magnetite and apatite
SB-22	Carbonatite	Calcite rock with green phlogopite, amphibole after clinopyroxene, apatite, magnetite, zircon, baddeleyite
SB-23	Carbonatite	Calcite carbonatite, with green and red phlogopite, dolomite, apatite, amphibole and pyrochlore
SB-24	Carbonatite	Phlogopite-calcite carbonatite (green and red phlogopite) with Ti-magnetite, apatite
SB-25	Carbonatite	Calcite carbonatite with red phlogopite, dolomite and baddeleyite, fine-grained
SB-26	Carbonatite	Calcite carbonatite with red phlogopite, apatite, magnetite, ilmenite, pyrochlore and baddeleyite
SB-27	Carbonatite	Calcite carbonatite, medium-grained, with dolomite, red phlogopite, apatite, baddeleyite
SB-28	Carbonatite	Calcite carbonatite fine-grained, with dolomite, red phlogopite, forsterite, pyrochlore, Ti-magnetite
SB-29	Carbonatite	Calcite-dolomite carbonatite with ancyllite, pyrochlore and magnetite, medium-grained
SB-30	Carbonatite	Dolomite-calcite carbonatite, medium-fine-grained, with apatite, pyrochlore
SB-31	Carbonatite	Dolomite-calcite carbonatite with red phlogopite, amphibole, baddeleyite, Ti-magnetite, apatite
SB-32	Carbonatite	Dolomite carbonatite
SB-33	*Pyrrhotite	From dolomite carbonatite
SB-34	*Dolomite	From dolomite carbonatite
SB-35	*Ankerite	From dolomite carbonatite
SB-36	Carbonatite	Dolomite carbonatite
SB-37	Carbonatite	Dolomite carbonatite with red phlogopite, pyrrhotite, chalcopyrite, sphalerite, galena and zircon
SB-38	*Pyrrhotite	From dolomite carbonatite with red phlogopite, pyrrhotite, chalcopyrite, phalerite, galena and zircon
SB-39	*Dolomite	From dolomite carbonatite with red phlogopite, pyrrhotite, chalcopyrite, sphalerite, galena and zircon
SB-40	Carbonatite	Dolomite carbonatite, fine-grained, with calcite, sulfides
Ozernaya Varaka		
OV-1	Clinopyroxenite	Nepheline clinopyroxenite medium-grained
OV-2	Clinopyroxenite	Nepheline clinopyroxenite fine-grained, with amphibole and Ti-magnetite
OV-3	Clinopyroxenite	Nepheline clinopyroxenite with perovskite, Ti-magnetite and phlogopite
OV-4	*Clinopyroxene	From nepheline clinopyroxenite with perovskite, Ti-magnetite and phlogopite
OV-5	*Ti-magnetite	From nepheline clinopyroxenite with perovskite, Ti-magnetite and phlogopite
OV-6	Clinopyroxenite	Nepheline clinopyroxenite with Ti-magnetite, phlogopite, apatite, titanite, melanite and amphibole
OV-7	Clinopyroxenite	Rock consist of prismatic crystals of clinipyroxene, contain nepheline and calcite, medium-grained
OV-8	Ijolite	Ijolite with apatite, melanite and titanomagnetite
OV-9	Ijolite	Perovskite ijolite with apatite and phlogopite, fine-grained, banded
OV-10	Ijolite	Ijolite with titanite and biotite fine-grained

Table 1. Continuation

Sample	Rock/mineral	Description
OV-11	Ijolite	Ijolite with titanite and apatite, fine-grained
OV-12	Ijolite-urtite	Ijolite-urtite with apatite, titanomagnetite and perovskite
OV-13	Syenite	Cancrinite-nepheline syenite fine-grained, with titanite
OV-14	Syenite	Cancrinite syenite with biotite, fine-grained
OV-15	Carbonatite	Clinopyroxene-calcite carbonatite
OV-16	*Clinopyroxene	From clinopyroxene-calcite carbonatite
OV-17	*Calcite	From clinopyroxene-calcite carbonatite
OV-18	Carbonatite	Phlogopite-calcite carbonatite
OV-19	Carbonatite	Phlogopite-calcite carbonatite
OV-20	Carbonatite	Biotite-calcite carbonatite, coarse-grained
Lesnaya Varaka		
LV-1	Olivinite	Olivinite coarse-grained
LV-2	Olivinite	Ore olivinite with Ti-magnetite and perovskite, medium-grained
LV-3	Olivinite	Ore olivinite with Ti-magnetite and perovskite
LV-4	*Olivine	From ore olivinite with Ti-magnetite and perovskite
LV-5	*Ti-magnetite	From ore olivinite with Ti-magnetite and perovskite
LV-6	**Ti-magnetite	From Ti-magnetite shlieren in rough-banded ore olivinite
LV-7	**Ti-magnetite	From rough-banded ore olivinite
LV-8	**Clinopyroxene	From ore clinopyroxenite with Ti-magnetite, perovskite and phlogopite
LV-9	**Ti-magnetite	From ore clinopyroxenite with Ti-magnetite, perovskite and phlogopite
Salmagorsky		
SG-1	Olivinite	Ore olivinite, coarse-grained, Ti-magnetite-bearing, with perovskite
SG-2	Olivinite	Olivinite clinopyroxene-bearing, with Ti-magnetite, perovskite and phlogopite
SG-3	Olivinite	Olivinite with Ti-magnetite and perovskite, medium-grained
SG-4	Olivinite	Ore olivinite, coarse-grained, Ti-magnetite-bearing, with perovskite
SG-5	*Olivine	From ore olivinite, coarse-grained, Ti-magnetite-bearing, with perovskite
SG-6	*Ti-magnetite	From ore olivinite, coarse-grained, Ti-magnetite-bearing, with perovskite
SG-7	Olivinite	Ore olivinite, with Ti-magnetite and perovskite, coarse-grained
SG-8	Olivinite	Ore olivinite with Ti-magnetite and perovskite, coarse-grained
SG-9	Olivinite	Olivinite with Ti-magnetite, perovskite and phlogopite, fine-grained
SG-10	Olivinite	Ore olivinite medium-fine-grained, Ti-magnetite-bearing, with clinopyroxene and perovskite
SG-11	Olivinite	Olivinite fine-grained, clinopyroxene-bearing, with perovskite and Ti-magnetite
SG-12	Olivinite	Olivinite medium-fine-grained, with phlogopite, clinopyroxene and Ti-magnetite
SG-13	Olivinite	Ore olivinite, clinopyroxene and perovskite-bearing with Ti-magnetite
SG-14	Olivinite	Ore olivinite finely banded, clinopyroxene- and perovskite-bearing, with Ti-magnetite
SG-15	Clinopyroxenite	Olivine clinopyroxenite, Ti-magnetite- and perovskite-bearing
SG-16	Clinopyroxenite	Olivine clinopyroxenite, Ti-magnetite-bearing
SG-17	Clinopyroxenite	Ore clinopyroxenite, Ti-magnetite and nepheline-bearing, with perovskite
SG-18	Clinopyroxenite	Olivine clinopyroxenite, trachytoid, Ti-magnetite-bearing, with perovskite
SG-19	Ijolite-urtite	Ijolite-urtite with Ti-magnetite, coarse-grained
SG-20	Turjaite	Phlogopite-diopside turyaite
SG-21	Turjaite	Clinopyroxene turyaite phlogopite-bearing
SG-22	Turjaite	Turyaite medium-fine-grained, Ti-magnetite-bearing, with phlogopite
SG-23	Melteygite	Phlogopite-diopside melteygite
SG-24	Ijolite-melteygite	Ijolite-melteygite medium-grained, with apatite and titanite
SG-25	Ijolite-melteygite	Ijolite-melteygite Ti-magnetite-bearing, with titanite
SG-26	Ijolite-melteygite	Ijolite-melteygite, trachytoid, perovskite- and Ti-magnetite-bearing

Table 1. Continuation

Sample	Rock/mineral	Description
SG-27	Ijolite	Ijolite with Ti-magnetite, perovskite and titanite, fine-grained
SG-28	Ijolite	Ijolite coarse-grained
SG-29	Carbonatite	Calcite carbonatite, coarse-grained, with sulfides, biotite and cancrinite
SG-30	Carbonatite	Calcite carbonatite
Vuoriyarvy		
VR-1	Olivinite	Olivinite fine-grained, clinopyroxene- and Ti-magnetite-bearing
VR-2	Olivinite	Olivinite fine-grained with Ti-magnetite and perovskite
VR-3	Olivinite	Olivinite with Ti-magnetite, perovskite, phlogopite, medium-grained
VR-4	Olivinite	Ore olivinite
VR-5	Olivinite	Olivinite with clinopyroxene, Ti-magnetite, phlogopite and amphibole, medium-grained
VR-6	Clinopyroxenite	Phlogopite clinopyroxenite
VR-7	**Ti-magnetite	From ore clinopyroxenite with Ti-magnetite, perovskite and phlogopite
VR-8	Clinopyroxenite	Clinopyroxenite with Ti-magnetite and perovskite, coarse-grained
VR-9	Clinopyroxenite	Ore clinopyroxenite with olivine, Ti-magnetite and perovskite, coarse-grained
VR-10	*Clinopyroxene	From ore clinopyroxenite with olivine, Ti-magnetite and perovskite, coarse-grained
VR-11	*Ti-Magnetite	From ore clinopyroxenite with olivine, Ti-magnetite and perovskite, coarse-grained
VR-12	Clinopyroxenite	Nepheline clinopyroxenite with apatite, medium-grained
VR-13	Ijolite	Ijolite coarse-grained
VR-14	Ijolite-urtite	Ijolite-urtite medium-grained
VR-15	Ijolite	Ijolite medium-fine-grained, Ti-magnetite- and apatite-bearing
VR-16	Ijolite-urtite	Ijolite-urtite, fine-grained, shpreushteinized
VR-17	Carbonatite	Calcite carbonatite with biotite and aegirine
VR-18	Carbonatite	Calcite carbonatite with dolomite, phlogopite and magnetite
VR-19	Carbonatite	Magnetite-phlogopite(green)-calcite carbonatite with clinopyroxene and apatite
VR-20	Carbonatite	Calcite carbonatite with green phlogopite and diopside
VR-21	Carbonatite	Calcite carbonatite with red phlogopite and apatite
VR-22	Carbonatite	Calcite carbonatite with red phlogopite
VR-23	Carbonatite	Dolomite-calcite carbonatite with apatite and sulphides
VR-24	Carbonatite	Calcite-dolomite carbonatite ancylite-bearing
VR-25	Carbonatite	Dolomite carbonatite with calcite and sulfides
VR-26	Carbonatite	Dolomite carbonatite, medium-grained, with calcite, phlogopite, ancylite and zircon
VR-27	Carbonatite	Dolomite carbonatite, fine-grained, with amphibole, calcite and pyrochlore
VR-28	Carbonatite	Dolomite-calcite carbonatite, fine-grained
Turiy Peninsula		
TP-1	Clinopyroxenite	Clinopyroxenite with Ti-magnetite
TP-2	Clinopyroxenite	Nepheline clinopyroxenite with Ti-magnetite, phlogopite and perovskite
TP-3	Clinopyroxenite	Nepheline-olivine clinopyroxenite, phlogopite and Ti-magnetite-bearing, medium-coarse-grained
TP-4	Turjaite	Turyaite zeolitized, with Ti-magnetite and perovskite
TP-5	Turjaite	Turyaite zeolitized, coarse-grained, with Ti-magnetite, carbonate and perovskite
TP-6	Turjaite	Turjaite, coarse-grained
TP-7	Turjaite	Ti-magnetite-clinopyroxene turyaite, olivine-bearing, medium-grained
TP-8	Carbonatite	Phlogopite-calcite carbonatite with clinopyroxene, sulfides, magnetite, apatite and zircon
TP-9	Carbonatite	Calcite carbonatite, medium-fine-grained, with amphibole, pyrochlore, apatite and zircon

Table 1. Continuation

Sample	Rock/mineral	Description
TP-10	Carbonatite	Calcite carbonatite, fine-medium-grained, with red phlogopite, apatite, baddeleyite
TP-11	Carbonatite	Dolomite carbonatite, medium-grained, with green phlogopite, apatite and sulfides
TP-12	Carbonatite	Calcite carbonatite with fluorite, fine-grained
Dyke Complex		
DC-1	Lamprophyre	Olivine-pyroxene-phlogopite ultramafic lamprophyre
DC-2	*Amphibole	From olivine-pyroxene-phlogopite ultramafic lamprophyre
DC-3	*Amphibole	From olivine-pyroxene-phlogopite ultramafic lamprophyre
DC-4	Lamprophyre	Olivine-pyroxene-phlogopite ultramafic lamprophyre
DC-5	Lamprophyre	Olivine-pyroxene-phlogopite ultramafic lamprophyre
DC-6	*Amphibole	From olivine-pyroxene-phlogopite ultramafic lamprophyre
DC-7	*Amphibole	From olivine-pyroxene-phlogopite ultramafic lamprophyre
DC-8	Lamprophyre	Rim of ultramafic lamprophyre
DC-9	Lamprophyre	Rim of ultramafic lamprophyre
DC-10	Lamprophyre	Olivine-pyroxene-phlogopite ultramafic lamprophyre
DC-11	Lamprophyre	Olivine-pyroxene-phlogopite ultramafic lamprophyre
DC-12	Carbonatite	Ankerite carbonatite with aegirine, phlogopite and apatite
DC-13	*Amphibole	From ankerite carbonatite with aegirine, phlogopite and apatite
DC-14	Kimberlite	Olivine-monticellite-phlogopite kimberlite
DC-15	Kimberlite	Olivine-phlogopite kimberlite
DC-16	Kimberlite	Olivine-phlogopite kimberlite
DC-17	Kimberlite	Olivine-phlogopite kimberlite
DC-18	Nephelinite	Phlogopite-garnet nephelinite
DC-19	*Amphibole	From nephelinite
DC-20	Carbonatite	Calcite carbonatite with phlogopite and amphibole
DC-21	*Amphibole	From calcite carbonatite with phlogopite and amphibole
DC-22	Granulite	Xenolith of garnet granulite in ultramafic lamprophyre
DC-23	Granulite	Xenolith of garnet granulite in ultramafic lamprophyre
DC-24	Granulite	Xenolith of garnet granulite in ultramafic lamprophyre
DC-25	*Garnet	From xenolith of garnet granulite
DC-26	*Pyroxene	From xenolith of garnet granulite
DC-27	Granulite	Garnet granulite mesocratic
DC-28	Granulite	Garnet granulite leucocratic
DC-29	Granulite	Garnet granulite melanocratic
DC-30	Granulite	Garnet granulite leucocratic
DC-31	Granulite	Garnet granulite
DC-32	Carbonatite	Calcite carbonatite with phlogopite and amphibole
DC-33	Carbonatite	Calcite carbonatite
DC-34	Carbonatite	Xenolith of calcite carbonatite with phlogopite and apatite in ankerite carbonatite
DC-35	Carbonatite	Xenolith of calcite carbonatite with phlogopite and apatite in ankerite carbonatite
DC-36	Carbonatite	Xenolith of calcite carbonatite with phlogopite and apatite in ankerite carbonatite
DC-37	Carbonatite	Xenolith of calcite carbonatite with phlogopite and apatite in ankerite carbonatite
DC-38	Carbonatite	Ankerite carbonatite with aegirine, phlogopite and apatite
DC-39	Carbonatite	Ankerite carbonatite with aegirine, phlogopite and apatite
DC-40	Carbonatite	Ankerite carbonatite with pyroxene and phlogopite
DC-41	*Amphibole	From ankerite carbonatite with pyroxene and phlogopite

Table 1. Continuation

Sample	Rock/mineral	Description
DC-42	**Amphibole	From ankerite carbonatite with phlogopite and opaques
DC-43	Carbonatite	Ankerite carbonatite
DC-44	Amphibolite	Xenolith of amphibolite in ankerite carbonatite
DC-45	Amphibolite	Amphibolite with carbonate and phlogopite, xenolith in ankerite carbonatite
DC-46	Amphibolite	Xenolith of amphibolite in ultramafic lamprophyre
DC-47	Amphibolite	Host amphibolite 5 m from an explosion pipe
DC-48	Amphibolite	Host amphibolite 10 m from an explosion pipe
DC-49	Amphibolite	Host amphibolite 15 m from an explosion pipe
DC-50	Pyroxenite	Xenolith of garnet pyroxenite in ultramafic lamprophyre
DC-51	Pyroxenite	Hornblende-bearing pyroxenite of xenolith in garnet melanephelinite
DC-52	Pyroxenite	Xenolith of pyroxenite in ankerite carbonatite
DC-53	Pyroxenite	Xenolith of pyroxenite in ultramafic lamprophyre
DC-54	Metasomatite	Xenolith of amphibole-phlogopite-garnet-calcite-pyroxene rock in ultramafic lamprophyre
DC-55	Metasomatite	Xenolith of amphibole-rutile-phlogopite-garnet rock in ultramafic lamprophyre

magnetite and perovskite. Internal core of the massif is composed by rocks varying in texture and composition; coarse-grained melteyites, ijolites and urtites are most abundant. In south-west part, between the core and outer zone, there are melilite-bearing rocks: melilitites, amphibole-phlogopite-melilite rocks, turjaites and other [Orlova, 1959; Kukharensko *et al.*, 1965; Panina, 1975]. A few thin veins and small spots of early calcite and later dolomite-ankerite-calcite carbonatites with accessory pyrochlore occur within the massif, mainly in its core.

2.2.7. Vuorijarvi Complex is situated in the south-west part of the Peninsula (Figure 8) intruding host Archaean gneisses of the Belomorian Block. The size of exposed area is 3.5 x 5.5 km. Clinopyroxenites cover ~60% of the central core rimmed by 500 m thick nepheline clinopyroxenites and the periphery circle of ijolites which thickness varies from 10 to 500 m. In the eastern part a sub-vertical phoscorite stock intruded clinopyroxenites of the core. Numerical veins of calcite and dolomite carbonatites cut the phoscorites. Small single bodies of phoscorites and carbonatite veins with thickness up to 50 m and length up to 1 km are observed in various parts of the massif and within host rocks.

Rb-Sr rock-minerals isochrone age of carbonatite is 375 ± 7 Ma [Gogol and Delenitsyn, 1999].

2.2.8. The Turiy Peninsula Complex is situated on the southern coast of Kola peninsula (Figure 1). The host rocks are Early-Proterozoic granitoids of the Tersky domain overlapped by Upper-Proterozoic quartzite sandstones and aleurolites (Figure 9).

The Complex includes several isometric bodies which exposed areas vary from 20 to 6 km², the total exposed area being ~40 km². These bodies are supposed to be apophyses of a single large intrusive located at least at 400 m depth. The rime, 0.2 to 1.5 km thick, of fenitised rocks surrounds the bodies (Evdokimov, 1982; Bulakh and Ivanikov, 1984). All the bodies show similar concentric-zoned structure. Periphery segments are composed by ijolite-melteigite rocks containing relics of nepheline clinopyroxenites. The central cores consist of melilite-bearing rocks, mainly unkomphagrites and turjaites and (less abundant) okaites and melilitolites. In the centre of the largest body phoscorites and carbonatites form up to 150 m thick veins. Rocks of the massif and host rocks are cut by dykes of olivine nephelinites, melilitites, monchiquites and other rocks.

Kramm *et al.* [1993] obtained 373 ± 6 Ma Rb-Sr isochrone age for ijolites and Dunworth *et al.* [1997] presented Rb-Sr isochrone age for phoscorites, 363 ± 3.5 Ma.

2.2.9. Dyke Complex of the Kandalaksha Gulf. More than 1000 dykes and explosion pipes are situated mainly within a 250 km long belt along the northern coast of Kandalaksha Gulf (Figure 1). According to Kukharensko [1967] the dykes do not relate to any known magmatic Complexes; probably they were subsurface roots of an explosion lava flow removed by erosion [Bulakh and Ivanikov, 1984]. Their emplacement was controlled by the Kandalaksha Graben belonging to the regional Onega-Kandalaksha paleorift.

Dykes within the western segment were investigated with some details. The dykes are characterised by 0.8 to 1.2 m thickness, up to 300 m length, and presumably

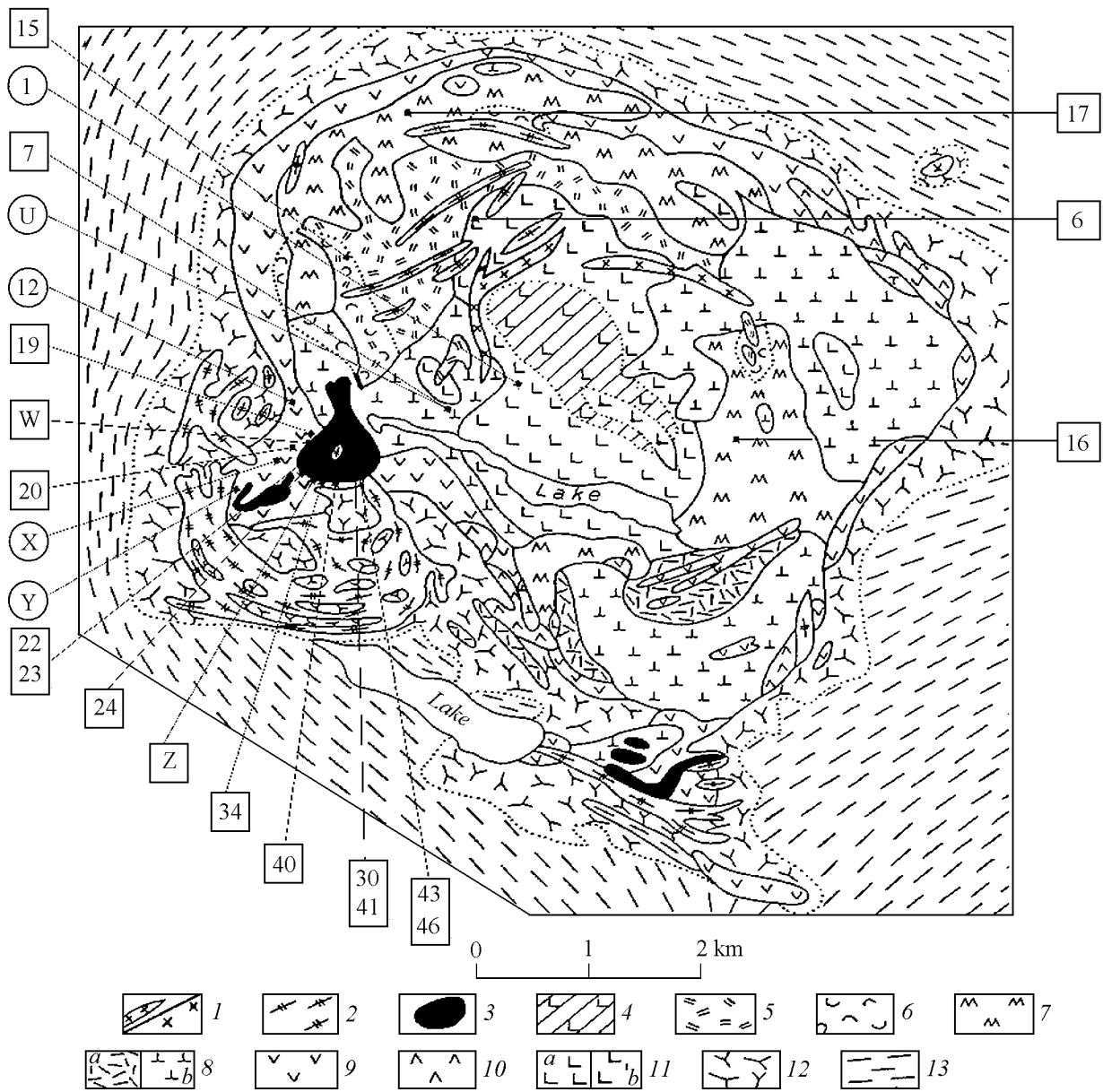


Figure 3. Schematic geological map of Kovdor Complex (modified from *Ternovoy et al.*, 1969, *Ternovoy*, 1977;).

1 - feldspar ijolites, nepheline and alkaline syenites: a-dyke complex, b-rocks of Maliy massif, 2 - calcite and dolomite carbonatites, 3 - phoscorites, 4 - forsterite-magnetite rocks, 5 - phlogopite-olivine rocks, 6 - garnet-amphibole-monticellite rocks with diopside, vesuvianite, calcite, 7 - monticellite-melilite rocks, melilitolites, 8 - mica-pyroxene rocks: a-essential biotite ("glimmerites"), b-essential clinopyroxene ("clinopyroxenites"), 9 - coarse-grained ijolite-urtites and urtites, 10 - medium-grained ijolite-melteigites, 11 - olivinites: a - without ores, b - ore-bearing, 12 - fenites and fenitized gneisses, 13 - gneisses and granite-gneisses.

1/595; 12/1598; U: 2/268, 3/276, 4/199, 5/358, 8/997, 9/126, 10/258, 11/171, 33/305, 42/796; W: 25,35,36,37; X: 27/1370; 28/1385; 29/1385; 30/1385; 31/1385; 32/1391; Y: 18/83, 38/83, 39/83; Z: 26,44,45. See Figure 2 for explanation of sample sites.

north to north-east orientation (Figure 10). According to the field relationships, early and late dykes can be distinguished.

The early dykes are composed by carbonatites, mon-

tichellite kimberlites, ultrabasic lamprophyres, and monchiquites; these rocks contain lower crustal and host rock xenoliths. Conventional K-Ar dating of ultrabasic lamprophyres and monticellite kimberlites gives 360 -

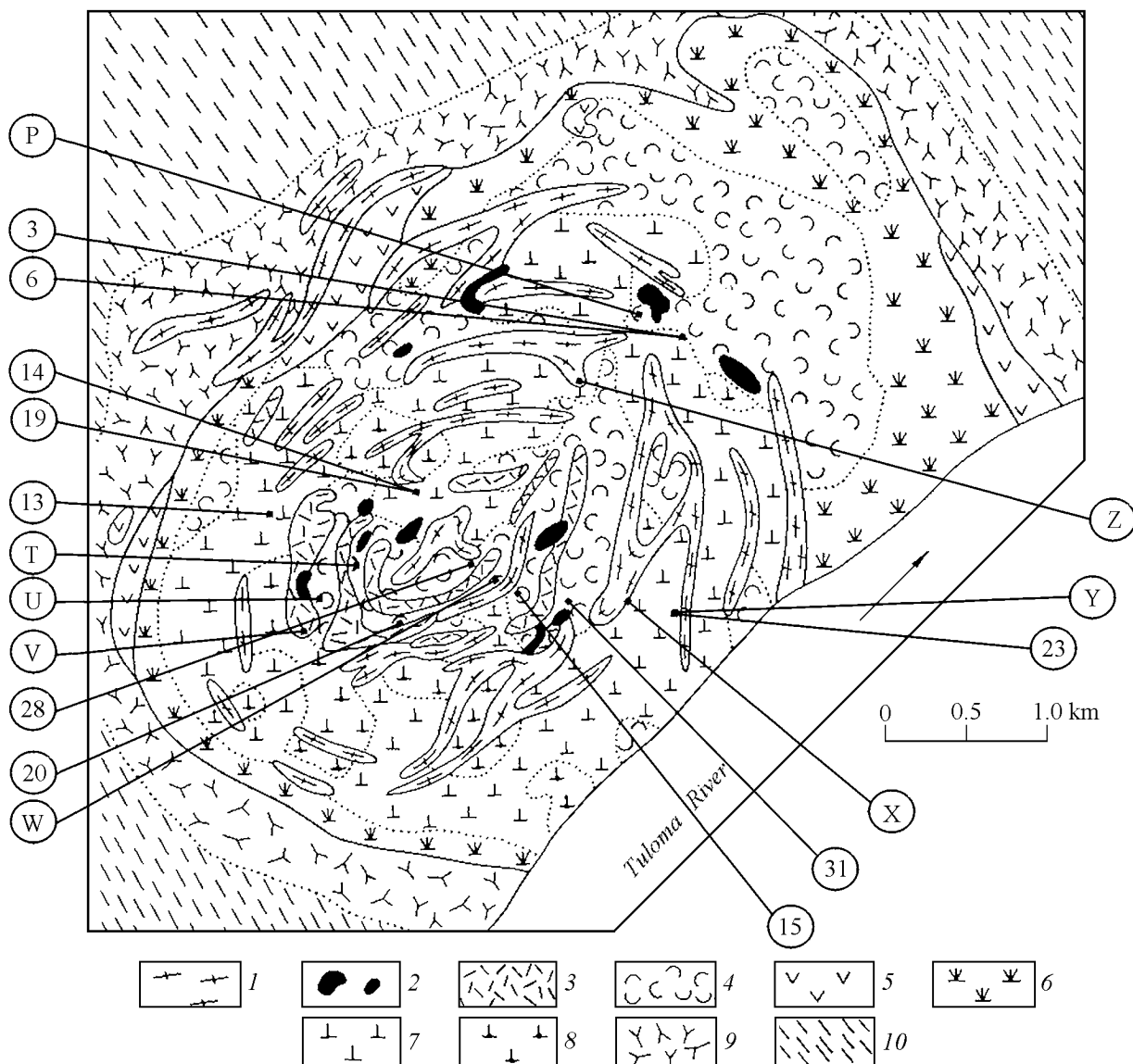


Figure 4. Schematic geological map of Sebyavr Complex (after *Subbotin and Michaelis, 1986*). 1 - carbonatites, 2 - phoscorites, 3 - apatite-phlogopite-diopside rocks, 4 - apatite-garnet-amphibole rocks and apatite clinopyroxenites, 5 - ijolites, 6 - nepheline clinopyroxenites, 7 - clinopyroxenites, 8 - ore-bearing clinopyroxenites and olivinites, 9 - fenites and fenitized gneisses, 10 - gneisses and migmatites.

3/ 160; 6/70; 14/24; 19/336; 13/52; 28/353; 20/180; 15/350; 31/352; 23/132; P: 7/55, 8/55, 9/55, 10/55, 11/65; T: 32/250, 33/250, 34/250, 35/250, 36/19; U: 26/406, 30/325, 40/242; V: 37/243, 38/243, 39/243; W: 16/841, 17/841, 18/580, 21/930, 22/539, 24/462, 25/460, 27/467, 29/495; X: 4/82, 5/80; Y: 12/130, 23/132; Z: 1/49, 2/49. (See Figure 2).

368 Ma, and $^{40}\text{Ar} - ^{39}\text{Ar}$ age of carbonatites is 386–396 Ma [*Beard et al., 1996, 1998*].

The late dykes are represented by alkaline picrites, melanephelinites, nephelinites and alkaline syenite-porphyrates. Within the eastern segment a number of ex-

plosive pipes are situated together with the dykes. The pipes are composed by foidites, melilitites, and olivine-phlogopite diamond-bearing kimberlites. K-Ar phlogopite ages of the kimberlites are within 337 – 384 Ma [*Kalinkin et al., 1993*].

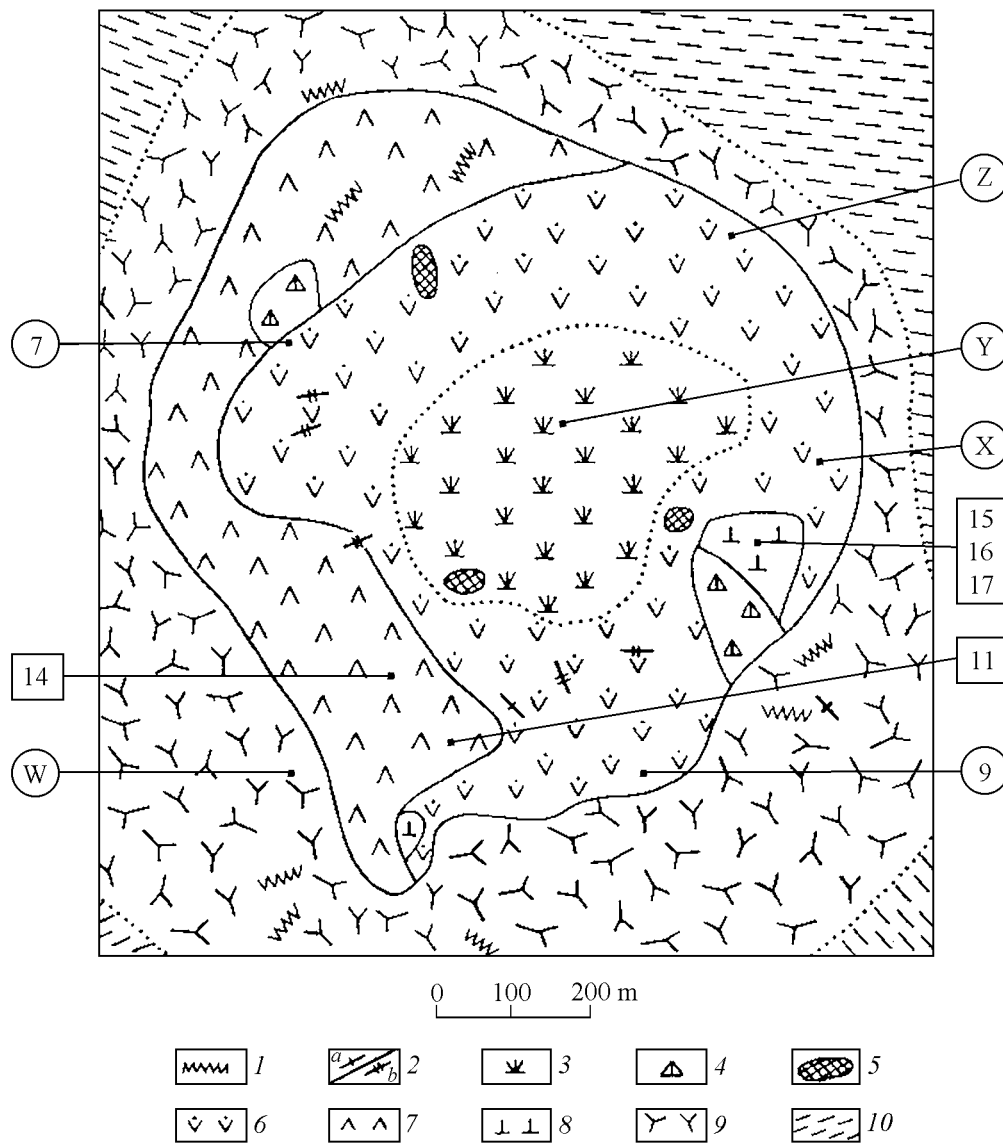


Figure 5. Schematic geological map of Ozernaya Varaka Complex (after *Kukharenko et al.*, 1965; *Dudkin et al.*, 1980).

1 - dykes of ijolite-porphyrites, monchiquites, tinguaite, 2 - carbonatites and related rocks: a-aegirine-calcite, b-phlogopite-calcite, 3 - nepheline-clinopyroxene rocks with titanomagnetite, perovskite, apatite, 4 - breccias of biotite-diopside rocks with ijolite cement, 5 - rocks with apatite-titanomagnetite-perovskite mineralization, 6 - ijolite-urtites, ijolites, cancrinite syenites, 7 - fine-grained ijolite-melteigites, 8 - fine-grained clinopyroxene rocks, 9 - fenite and fenitized gneisses, 10 - gneisses and granite gneisses.

7/95; 9/215; W: 10/230, 18/121, 19/282; X: 6/116, 8/212, 12/12; Y: 3/303, 4/303, 5/303, 20/140; Z: 1/117, 2/118, 13/88; (See Figure 2).

3. Experimental Techniques

3.1. Rare Gas Measurements at Laboratory of Geochronology, Apatity, Russia

Two extraction lines for (1) heating and (2) milling of samples were operating. (1) After weighting 0.25 – 0.64

mm chips of rocks were wrapped in Al foil and mounted in a sample holder able to store up to 7 samples. The holder was evacuated and intermittently baked up to 200 °C for one week. The samples were sequentially dropped into a furnace and heated to a required temperature, up to 1700°C, in a Mo crucible. For the complete extraction this temperature was applied for 30 minutes.

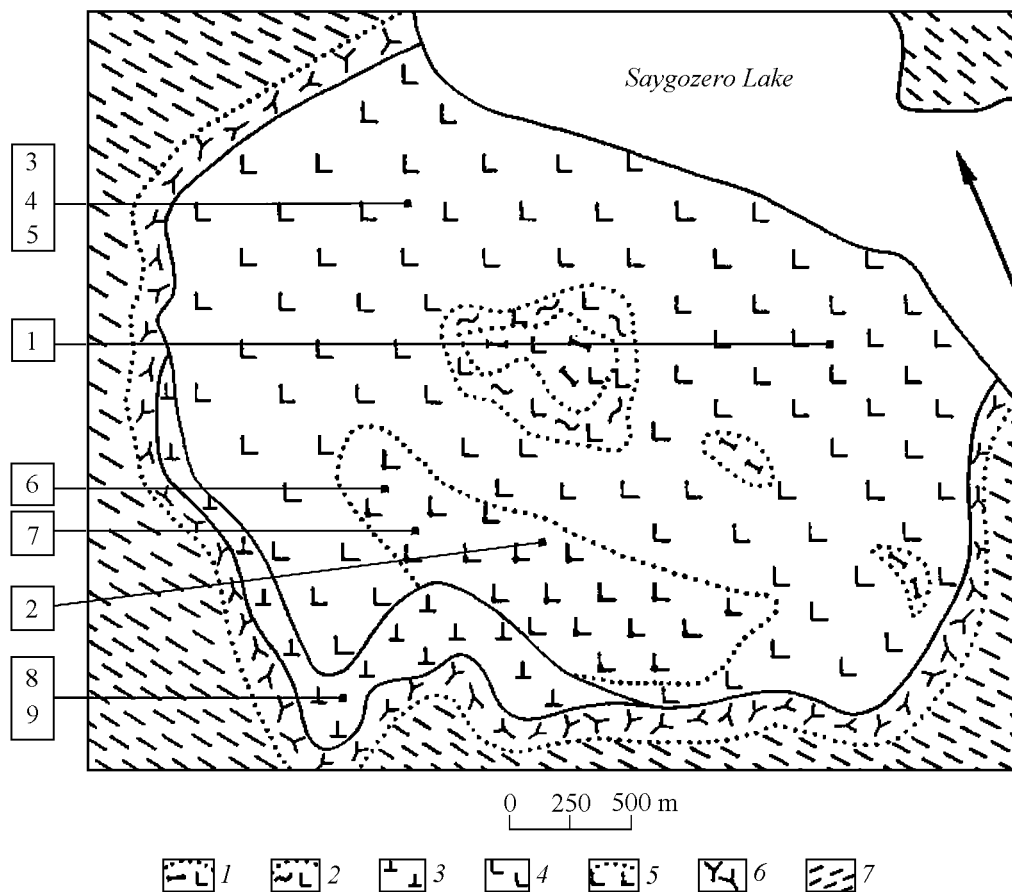


Figure 6. Schematic geological map of Lesnaya Varaka Complex (after *Kukhareno et al., 1965; Solopov, 1977*).

1 - tremolitized olivinites, tremolite-dolomite rocks, dolomite carbonatites, 2 - serpentized olivinites, 3 - clinopyroxenites, 4 - olivinites, 5 - ore-bearing olivinites, 6 - fenites and fenitized gneisses, 7- gneisses and granite-gneisses (Figure 2).

(2) For milling 0.25 – 0.64 mm size chips of a sample and several small metal milling balls were loaded in a glass ampoule which then was evacuated and sealed off. The ampoule was settled on a vibration table and milling was carried out by simultaneous vibrating and rotating [*Ikorsky and Kusth, 1992*]. After milling, the ampoule was mounted in an ampoule breaker which was pumped out. Then the ampoule was broken. In both cases (1 and 2) the extracted gases were admitted to an all-metal line and purified using Ti-Zr getters. He (and Ne) were separated from Ar and heavier gases using a charcoal trap cooled by liquid nitrogen.

The isotope compositions and elemental abundances of He and Ar were determined using a static mass spectrometer (MI 1201). A special trap reduced background (first of all background of hydrogen) in the chamber. By heating of Ti-Mo wire Ti was vaporised onto a metal surface of the trap which was cooled down by liquid nitro-

gen during He isotope analysis. The resolving power of mass-spectrometer was ~ 1000 , allowing complete separation of ${}^3\text{He}^+$ from ${}^3\text{H}^+$ and HD^+ . The sensitivity for He was 5×10^{-5} A/Torr, allowing measurements of ${}^4\text{He}/{}^3\text{He}$ ratios as high as 10^8 typical of crustal samples. The sensitivity for Ar was 3×10^{-4} A/Torr. Artificial mixture of ${}^3\text{He}$, He from a high-pressure tank (${}^4\text{He}/{}^3\text{He} = 5 \times 10^7$) and air Ne, Ar, Kr and Xe was used as a standard for the calibration of the mass-spectrometer. ${}^4\text{He}/{}^3\text{He} = 6.29 \times 10^5$ and ${}^4\text{He}/{}^{20}\text{Ne} = 47$ ratios were normalised against air and verified at CRPG (Nancy).

The concentrations were determined by the peak height method with an uncertainty of $\sim 5\%$ (hereafter 1σ is shown). Uncertainties in the ${}^4\text{He}/{}^3\text{He}$ ratios of $\sim 10^6$ and $\sim 10^8$ were 2% and 20%, respectively, and uncertainties in the ${}^{40}\text{Ar}/{}^{36}\text{Ar}$ ratios of 300 and 50,000 were 0.3% and 25%, respectively. The analytical blanks measured twice a week under exactly the same condi-

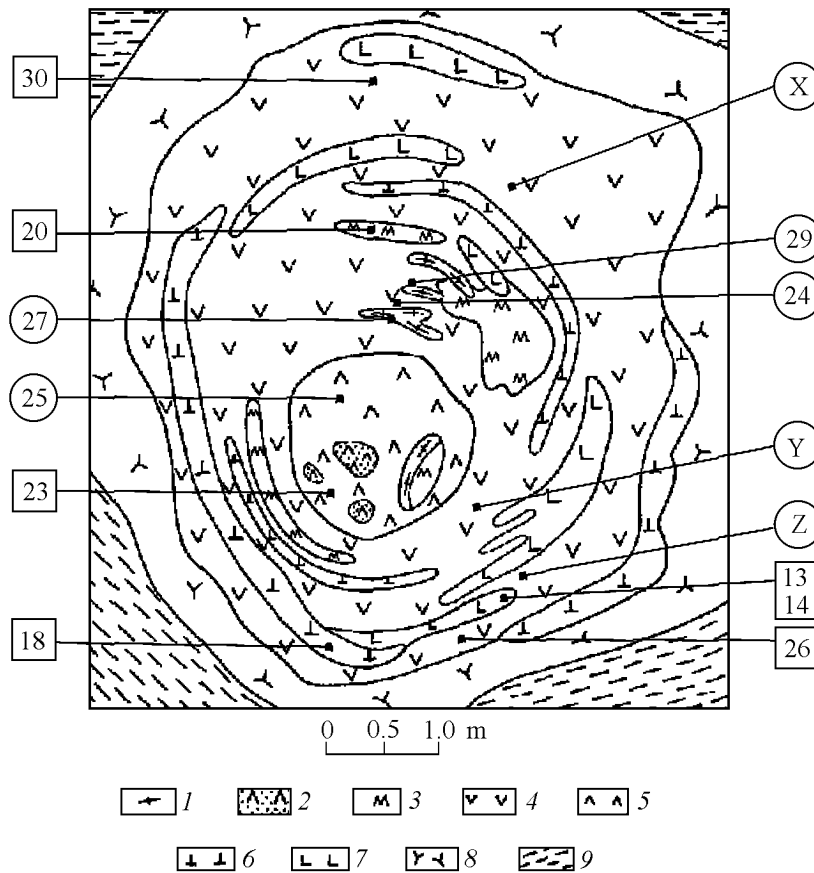


Figure 7. Schematic geological map of Salmagora Complex (after Orlova, 1959; Kukharensko *et al.*, 1965; Ternovoy *et al.*, 1977).

1 - carbonatites, 2 - apatitized rocks, 3 - melilite-bearing rocks, 4 - ijolites, 5 - melteigites, 6 - clinopyroxenites, 7 - olivinites, 8 - fenites and fenitized gneisses, 9 - gneisses and granite-gneisses. 27/349; 25/20; 24/157; 29/257; Z: 12/268, 16/13; Y: 21/261, 22/290; X: 1/118, 2/13, 3/183, 4/189, 5/189, 6/189, 7/191, 8/195, 9/199, 10/253, 11/304, 15/72, 17/183, 19/199, 28/184; (See Figure 2).

tions as the samples, were 1×10^{-9} , 2×10^{-10} , and 1×10^{-10} cm³ STP for ⁴He, ²⁰Ne and ³⁶Ar, respectively [Kamensky *et al.*, 1984; Tolstikhin *et al.*, 1991].

3.2. Rare Gas Measurements at CRPG, Nancy, France

Rare gases were extracted by vacuum crushing [Richard *et al.*, 1996; Marty and Humbert, 1997]. About one gram of sample was loaded in a stainless steel crusher with a magnetic piston and baked under high vacuum for one night at 100°C. 500 strokes were applied on line using an external solenoid activating the piston, and the released gases were cleaned over two Ti-sponge getters cycled between 750°C and room temperature. After purification neon and argon were adsorbed on a stainless steel grid cooled at 17 K.

Helium was first analysed (⁴He on a Faraday collector, ³He using an electron multiplier and an ion counter).

The mass spectrometer was adjusted for the analysis of all rare gases (electron energy of 60 eV, trap current of 200 mA), resulting in a low He sensitivity of 1.6×10^{-5} A/Torr, which was fortunately compensated by the generally high amounts of both He isotopes in the samples. The He isotope ratios were normalised against a secondary standard (Irénée mineral spring gas, Réunion Island, 12.41 ± 0.09 Ra as measured in CRPG).

After He analyses, Ne was admitted in the mass spectrometer. To suppress interfering ions, e.g., doubly charged ⁴⁰Ar, ²⁰NeH at mass 21, and doubly charged CO₂ at mass 22, the mass spectrometer comprises two SAES@ getters at room temperature and a stainless steel finger containing active charcoal directly connected to the mass spectrometer ion source. The finger was cooled down to liquid nitrogen temperature before Ne admission. Neon was then desorbed from the cryogenic trap at 40°K, admitted into the mass spectrometer, and

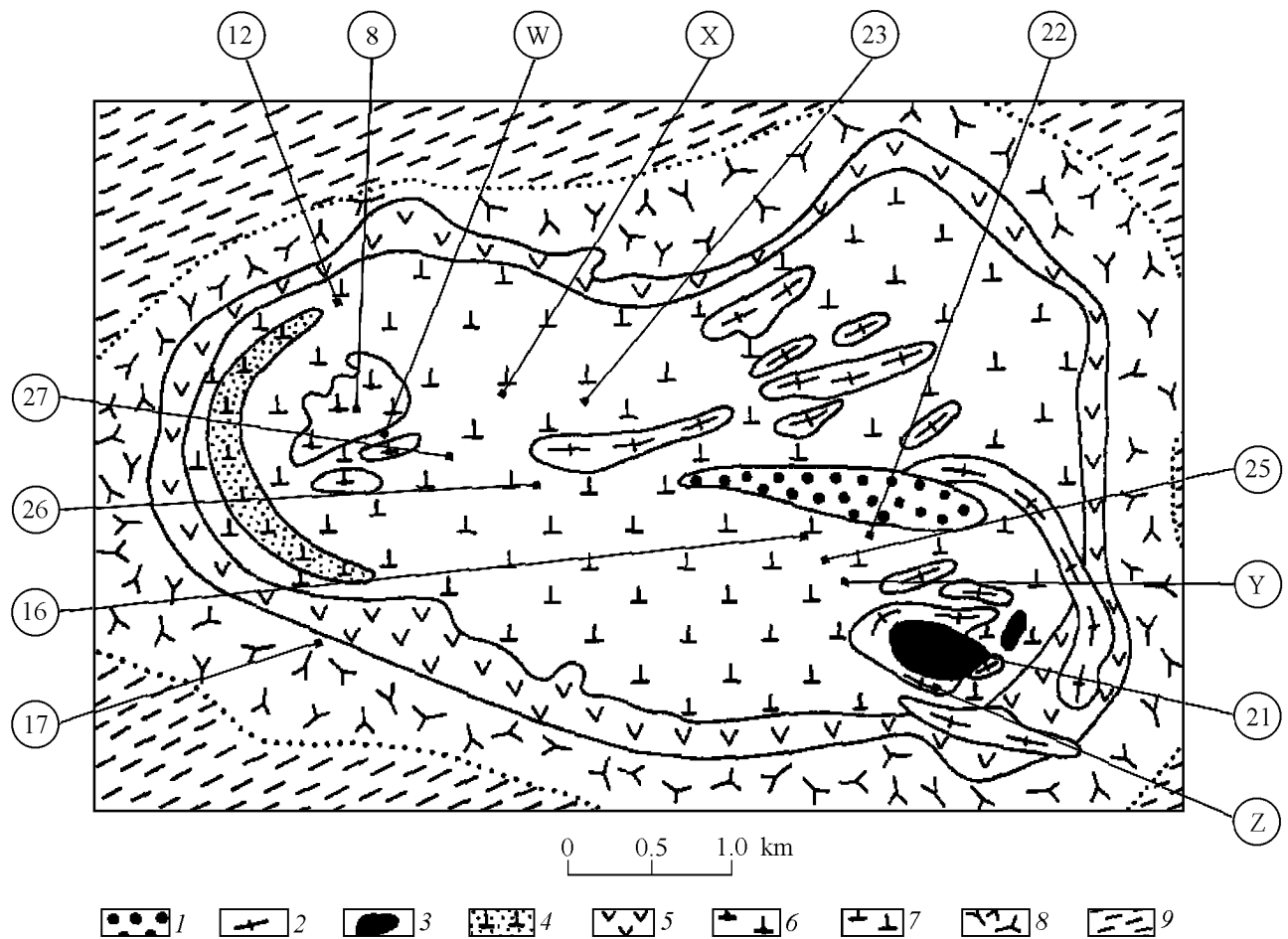


Figure 8. Schematic geological map of Vuorijarvi Complex (after *Solopov, 1978; Subbotin, 1990*). 1 - field of veined rare-metals phosphorites and carbonatites, 2 - calcite carbonatites, 3 - phosphorites, 4 - apatitized pyroxenites, 5 - ijolites, ijolite-urtites, 6 - ore (perovskite-titanomagnetite) pyroxenites, 7 - pyroxenites with olivinite relics, 8 - fenites, 9 - gneisses and granite gneisses. 27/158; 26/202; 16/102; 17/174; 21/56; 22/127; 25/248; 23/84 12/140 8/96; Z: 20/680, 28/311; Y: 3/202, 4/296, 5/152; X: 14/325, 15/325; W: 9/126, 10/126, 11/126;. (See Figure 2).

left in the chamber for five more minutes before measurement started. The amount of neon and its isotopic composition were determined by analysing Ne isotope masses during 12 cycles. The peak heights and the isotopic ratios were extrapolated to the time when counting started. After the measurements, the blank and mass discrimination corrections were applied [*Marty et al., 1998*].

After Ne analysis, argon was desorbed from the cryogenic trap tuned at 85°K and admitted into the mass spectrometer, with the charcoal finger valved off. ^{40}Ar was analysed using the Faraday collector, and ^{36}Ar , ^{38}Ar were analysed with electron amplification and ion counting (10 cycles). During these analyses, the ^{36}Ar

blanks were typically 4×10^{-12} cc STP, and therefore small in comparison to the ^{36}Ar contents of the samples, representing only 0.2–4.0 % of the total signals at mass 36.

3.3. U, Th, K and Li Measurements

The concentrations of U and Th were measured by X-radiography in Neva Expedition, St. Petersburg, Russia. The lowest measurable concentration is about 0.5 ppm. K and Li were determined by spectrophotometry after acid attack and solution in distilled water in the Geological Institute, Apatity. The reproducibility of the analyses of these four elements is within $\pm 10\%$.

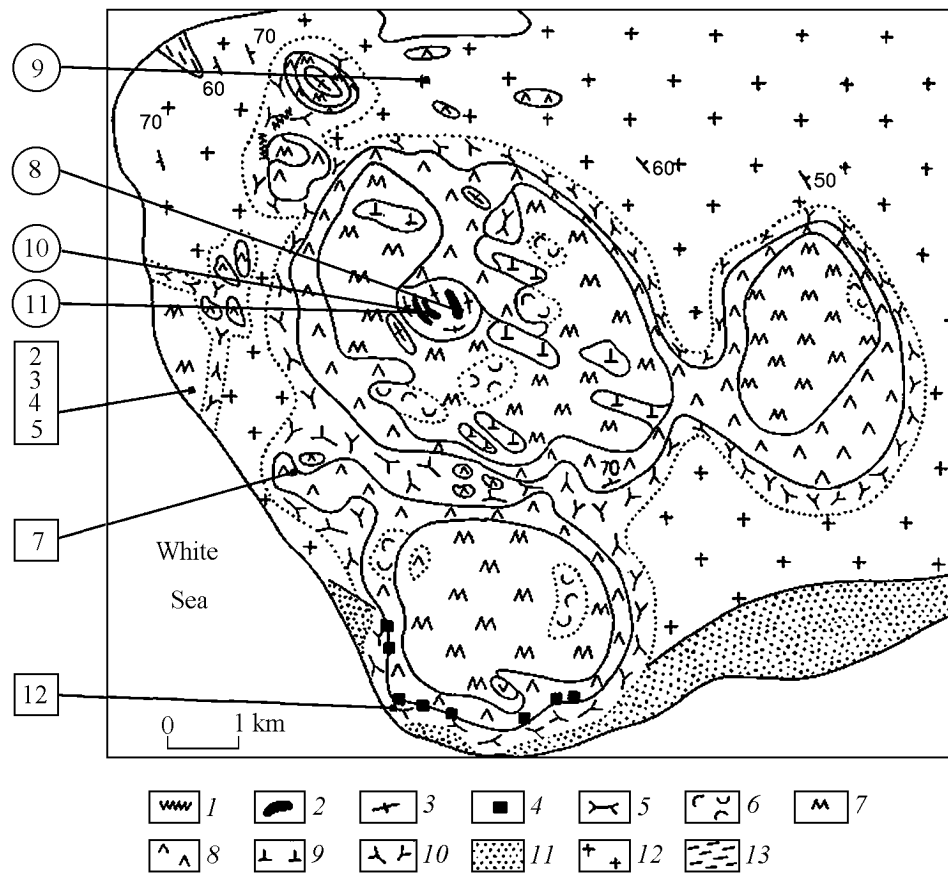


Figure 9. Schematic geological map of Turiy Complex (after *Samoylov, Afanas'jev, 1978; Evdokimov, 1982; Bulakh, Ivanikov, 1984*).

1 - dyke rocks (olivine melanephelinites, nephelinites, monchiquites, etc.), 2 - phoscorites, 3 - carbonatites, 4 - olivine melteigite-porphry, 5 - aegirine and aegirine-apatite rocks, 6 - skarned rocks with vesuvianite, garnet, diopside, hastingsite, 7 - melilite rocks (turjaite), 8 - ijolite-melteigites, 9 - clinopyroxenites with olivinites relics, 10 - fenites, 11 - sandstones, quartzito-sandstones, conglomerates, 12 - granitoids of Uмба Complex, 13 - gneisses and schists. 9/224; 8/210; 10/182; 11/191 (See Figure 2).

4. Results

4.1. Helium

4.1.1. Abundances of He isotopes in whole-rock samples. Whole-rock (mineral) concentrations of helium isotopes and $^4\text{He}/^3\text{He}$ ratios vary within a great range $\sim 10^4$ (Table 2, Figure 11). Generally ultrabasic rocks show somewhat higher concentrations of ^3He and lower $^4\text{He}/^3\text{He}$ ratios; carbonatites contain widely variable abundances of He isotopes; intermediate concentrations and ratios are typical of alkaline rocks. The lowest abundances of ^3He , down to 5×10^{-13} cm^3 STP g^{-1} , and ^4He , down to 2×10^{-7} cm^3 STP g^{-1} , are typ-

ical of carbonatites from the Khibiny and some rocks from dyke Complexes. Some rocks from these Complexes also show quite high $^4\text{He}/^3\text{He}$ ratios, similar to those in radiogenic crustal helium, $\sim 10^8$ [*Mamyrin and Tolstikhin, 1984*].

In contrast, ultrabasic rocks, carbonatites and related minerals from the Seblyavr and the Kovdor show high concentrations of ^3He , from 5×10^{-9} to 5×10^{-10} cm^3 STP g^{-1} , along with the low $^4\text{He}/^3\text{He}$ ratios. Rocks and minerals from the Seblyavr appear to retain He isotopes better than any other and contain helium with $^4\text{He}/^3\text{He} \sim 1000$ times below the radiogenic ratio. Two olivinites, from the Seblyavr and the Lesnaya Varaka (Table 2) contain He with as low $^4\text{He}/^3\text{He}$ as 6.4×10^4 and 6.8×10^4 , respectively, which are substantially lower than the

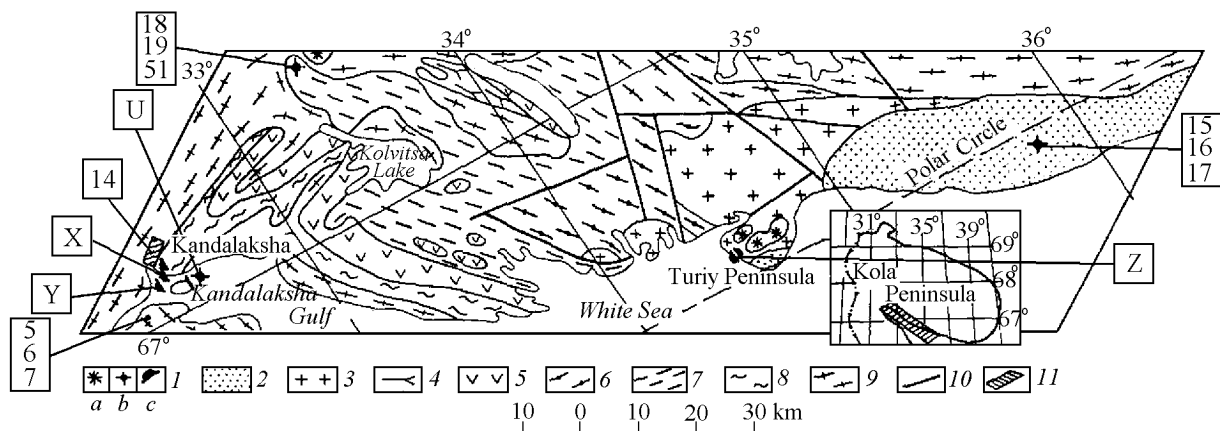


Figure 10. Schematic geological map of Southern part of the Kola Peninsula (after *Vetrin, Kalinkin, 1997*).

1 - Ultrabasic-alkaline rocks of the Paleozoic age: a-Complexes, b-explosion pipes, c-dykes, 2 - the Upper Proterozoic sandstones and conglomerates. 3-5 the Lower Proterozoic rocks: 3- porphyry granites, 4 - alkaline granites, 5 - basic and ultrabasic rocks. 6-9 the Late Archean rocks: 6 - garnet-biotite gneisses, 7 - biotite and amphibole -biotite gneisses, 8 - amphibolites, 9 - granite-gneisses, 10 - faults, 11- boundaries of investigated region. (See Figure 2).

mean value in mid-oceanic ridge basalts, $(8.9 \pm 0.9) \times 10^4$, implying a contribution of plume-related materials to Kola UACC. However, nuclear reactions could also produce high abundances of ^3He and low $^4\text{He}/^3\text{He}$ ratios

in certain environments, e.g., in Li-bearing rocks and minerals, and to identify sources of helium the measured concentrations should be compared with those expected for radiogenic in-situ produced helium.

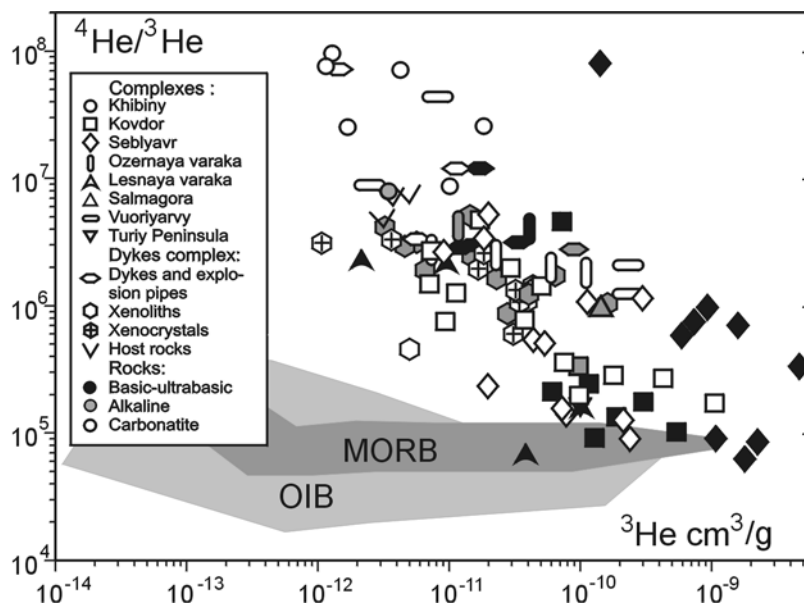


Figure 11. Helium isotope abundance in samples from Kola ultrabasic-alkaline- carbonatite Complexes: whole-rock abundances (gas extraction by melting). Samples from Sebyavr, Kovdor and Lesnaya Varaka show low $^4\text{He}/^3\text{He}$ ratios similar to or even slightly below the mean MORB ratio. ^3He abundances in ultrabasic rocks and carbonatites from these massifs are higher than those typical for MORB and OIB glasses. Sources of data for helium isotope abundances in MORB (170 samples) and OIB (280): *Hiyagon et al., [1992]*; *Honda et al., [1991, 1993]*; *Kaneoka et al., [1986]*; *Marty, [1989]*; *Moreira et al., [1995]*; *Ozima and Zashu, [1983, 1991]*; *Poreda and Farley, [1992]*; *Poreda and Radicati, [1984]*; *Sarda et al., [1985, 1988]*; *Staudacher and Allegre, [1989]*; *Staudacher et al., [1986, 1989]*; *Valbracht et al., [1996]*.

4.1.2. Helium isotope inventories: Measured and expected from in-situ production. The concentrations of radiogenic $^4\text{He}^*$ are calculated from measured U and Th concentrations (Table 2), and the age of the massifs, 370 ± 10 Ma [Kramm *et al.*, 1993; Kramm and Kogarko, 1994, see Section 2).

Estimates of the in-situ produced $^3\text{He}^*$ appears to be a more complicated and less reliable than $^4\text{He}^*$. The relevant nuclear reaction is $^6\text{Li}(n_t, \alpha)^3\text{H} \rightarrow \beta^- \rightarrow ^3\text{He}^*$ with $\lambda(^3\text{H}) = 12.2$ yr where n_t defines thermal neutron and α is α -particle. The production of $^3\text{He}^*$ per one $^4\text{He}^*$ atom depends on abundance of major and some trace elements in a rock, peculiarities of U and Th distribution and Th/U ratio. Among trace elements Li is the most important but also Gd, Be, B could influence the flux of thermal neutrons.

Morrison and Pine [1955] were the first who invented method for estimation $^3\text{He}^*/^4\text{He}^*$ production ratio. Gorshkov *et al.* [1966] illustrated a good agreement, within 20%, between measured and calculated thermal neutron fluxes in natural rocks. Gerling *et al.* [1976] and Mamyrin and Tolstikhin [1984] presented measured and calculated $^3\text{He}/^4\text{He}$ ratios for different rocks and inferred that the measured ratios are mainly controlled by Li and U+Th distribution among minerals and He losses from these minerals. Therefore a direct comparison of measured and calculated ratios can not be used to estimate the accuracy of calculations. Tolstikhin *et al.* [1996] illustrated a similarity (also within 20 %) between the calculated production ratio of $^3\text{He}^*/^4\text{He}^* = 7.2 \times 10^{-8}$ for Permian shists (the Molasses basin, Northern Switzerland) and the measured ratio, 9.4×10^{-8} , in adjacent aquifer having stagnant waters with quite high helium concentrations, 4.5×10^{-3} cm³ STP per g H₂O. From this brief review we consider that the accuracy of calculated $^3\text{He}^*$ concentrations are most probably within 50%.

Figure 12 comprises measured (m) over calculated (c) abundances of helium isotopes in ~ 40 rocks of different compositions and localities. All samples show $^4\text{He}_m/^4\text{He}_c \leq 1$ implying that an additional source for ^4He is not required. This is in a great contrast to extremely high $^3\text{He}_m/^3\text{He}_c$ ratios in these very samples, up to 105. A great excess of ^3He in UACC samples can not be attributed to spallogenic production of this nuclide simply because more than 50% of the samples were collected from prospecting boreholes and quarries (Figures 2 – 10).

The comparison of measured and calculated abundances gives unambiguous evidence on contribution of mantle ^3He -bearing fluid to a majority of ultrabasic, alkaline rocks and carbonatites. The crushing and stepwise heating experiments allow fluid-related helium to be separated, at least partially, from in-situ produced He^* .

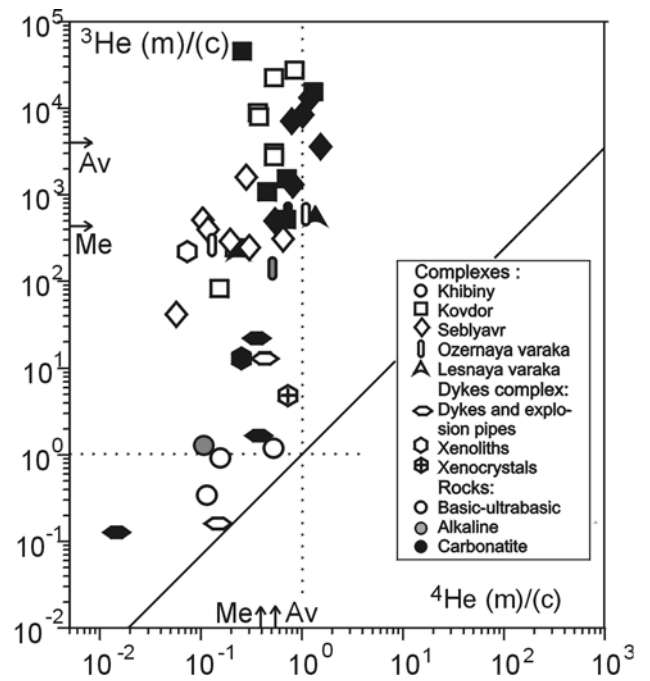


Figure 12. Comparison of measured (m) abundances of ^4He and ^3He and those calculated (c) assuming closed system evolution.

While $^4\text{He}(m)/^4\text{He}(c)$ ratios are similar to or less than 1 in all samples, a great excess of $^3\text{He}(m)$ is observed implying a contribution of mantle fluid retained by almost all samples. Carbonatites and alkaline rocks from Khibiny show small excess of ^3He in contrast to ultrabasic rocks and carbonatites from Kovdor and Sebyavr. Av - the average values, Me- the medians.

4.1.3. He isotope abundances in fluid inclusions. Generally a substantial portion of ^3He is related to vesicles and readily extracted by milling (the Average and Median are 0.42 and 0.37, respectively, Figure 13), whereas ^4He appears to be better fixed within crystalline lattices (Av = 0.13, Me = 0.075).

Helium isotope abundances in fluid-related He vary in a wide range (Figure 14) similar to that observed for the whole-rock data (see Figure 11). However in a number of samples from different massifs $^4\text{He}/^3\text{He}$ ratios are substantially below the MORB value indicating a contribution of high- ^3He plume-related fluid. Olivine SV-1 from the Sebyavr massif and magnetic fraction SV-2 separated from this rock both show the lowest $^4\text{He}/^3\text{He} = (3.02 \pm 0.01) \times 10^4$ whereas ^3He concentration in the magnetic fraction is by a factor of 4.5 exceeds that in the parent rock (Table 3). These relationships, also seen in Figure 14, indicate independence of the lowest ratios $^4\text{He}/^3\text{He}$ from helium concentrations exceeded some threshold, $^3\text{He} \geq 10^{-10}$ cm³ STP g⁻¹.

According to Figure 14, the $^4\text{He}/^3\text{He}$ range is getting narrower with increasing ^3He . However samples

Table 2. Bulk He and Ar isotope abundances and concentrations of parent elements

Sample	Rock/ mineral	Number	^3He 10^{-12}cc/g	$^4\text{He}/^3\text{He}$ 10^6	(^{36}Ar) 10^{-9}cc/g	$(^{40}\text{Ar})/^{36}\text{Ar}$ g	U ppm	Th ppm	K %wt	Li ppm
KH-7	Foyaite	KH-2945	3.38	8.00	7.34	11418	3	11		
KH-8	Carbonatite	NKH-581-1	10.2	8.85	6.78	1253			0.356	17.2
KH-9	Carbonatite	81-KHC	18.4	26.3	22.05	662				
KH-12	Carbonatite	633/176,6	1.63	35.7	4.29	676	1	33	0.050	
KH-13	Carbonatite	633/216,2	1.12	76.9	3.29	607	1	70	0.040	
KH-14	Carbonatite	633/393,3	1.26	100.0	5.30	1850	1	19	0.260	
KH-15	Carbonatite	4	4.30	71.4	13.95	430				
KV-3	Olivinite	KR-62-1/276	305.8	0.18	3.56	2303	0.4	6	0.431	2.7
KV-4	Olivinite	KR41-1/199	61.1	0.213	5.89	662	0.4	1	0.070	1.6
KV-5	Olivinite	KR80-1/357,8	192.5	0.137	6.58	1749	0.6	1	0.257	2.8
KV-6	Olivinite	KI-22-V	129.0	0.092	3.79	3962				
KV-7	Olivinite	D-63	69.9	4.88	5.08	7327				
KV-13	**Diopside	KD-2	111.5	0.246	9.97	632	2.3	0.5	0.085	0.0
KV-14	**Magnetite	KD-1	522.2	0.103	3.19	3507	0.8	0.5	0.058	7.8
KV-19	Ijolite	KR-193	94.5	0.330	2.85	20707	0.7	3	3.275	1.0
KV-21	**Magnetite	KD-3	105.5	0.215	2.11	1658	0.8	0.5	0.018	1.0
KV-23	Phoscorite	107-72	36.6	0.781	10.0	848	1	1	0.016	
KV-24	Phoscorite	KI-17-V	74.2	0.360	4.40	1500				
KV-27	Carbonatite	154 -KS	179.9	0.291	15.9	3090	2	5	2.500	
KV-28	Carbonatite	158-KS	561.5	0.231	4.86	14625	2	6	3.200	
KV-29	*Clinopyroxene	158-KS	1054.3	0.181	2.33	7250				
KV-30	*Biotite	158-KS	7.04	1.56	3.14	50000				
KV-31	*Calcite	158-KS	1.3	1.3	17.3	7400				
KV-32	Carbonatite	159-KS	435.5	0.28	6.03	10950	3	19	2.300	
KV-37	Carbonatite	KI-15-V	9.40	0.79	5.96	1543			0.120	0.7
KV-41	Carbonatite	111-72	7.56	2.86	20.5	966	2	5	0.120	
KV-43	Carbonatite	117-72	49.3	1.43	9.04	1570	5	9	0.016	
KV-44	Carbonatite	KI-20-S	17.4	5.08	2.61	2107			0.140	0.2
KV-46	Carbonatite	NKV-30	29.3	1.98	3.20	3315				
SB-1	Olivinite	111-3/49,2	1716.0	0.064	10.8	808	1.4	3	0.450	4.6
SB-3	Olivinite	NSB138-160	1050.2	0.085	3.47	3344	1.1	4	0.520	2.0
SB-5	Olivinite	Sja -184/80	730.8	0.714	3.09	1684	18	16	0.298	2.2
SB-6	Clinopyroxenite	NSB-138-70	1983.8	0.078	5.22	1858	3	6	0.480	2.2
SB-7	Clinopyroxenite	Sja-114/55	1484.7	0.680	3.75	2294	4	51	0.149	1.2
SB-8	*Magn,fraction	Sja-114/55mf	4296.7	0.334	4.99	2185				
SB-9	*Clinopyroxene	Sja-114/55-pr	591.6	0.575	3.10	1644				
SB-10	*Perovskite	Sja-114/55-prs	129.1	76.9	5.68	687				
SB-13	Clinopyroxenite	SB-1	842.1	0.862	6.03	1691	10	47	0.744	2.2
SB-15	Phoscorite	SB-2	112.2	1.09	5.61	4934	8	24	2.133	2.2
SB-17	Phoscorite	SB-3	299.3	1.15	2.87	3549	6.1	27	1.975	5.8
SB-22	Carbonatite	BEG-10	18.4	3.39	11.4	1432	2.6	9.1	0.390	2.4
SB-23	Carbonatite	NSB-186-1	19.8	5.15	9.02	1408			0.191	4.5
SB-26	Carbonatite	BEG-13	8.99	2.66	19.5	584	5.1	20	0.406	2.1
SB-32	Carbonatite	16-333/249,8	214.1	0.126	8.99	801				
SB-33	*Pyrrhotite	16-333/249,8	19.3	0.233	2.35	383				
SB-34	*Dolomite	16-333/249,8	240.7	0.089	106.3	349				
SB-35	*Ankerite	16-333/249,8	53.5	0.505	9.98	952				
SB-36	Carbonatite	333/19	44.0	0.539	3.55	1220	1	16	0.008	
SB-37	Carbonatite	SB-4	77.3	0.150	3.31	936	0.5	9	0.057	3.4
SB-40	Carbonatite	NSB-351-6	74.3	0.157	5.83	721	0.5	2	0.062	3.2

Table 2. Continuation

Sample	Rock/ mineral	Number	^3He 10^{-12}cc/g	$^4\text{He}/^3\text{He}$ 10^6	(^{36}Ar) 10^{-9}cc/g	$(^{40}\text{Ar})/^{36}\text{Ar}$ g	U ppm	Th ppm	K %wt	Li ppm
OV-6	Clinopyroxenite	OV-2057/116	42.1	3.92	4.64	3901	1.9	12	0.530	3.1
OV-11	Ijolite	BEG-2	12.1	4.37	5.37	6921	0.7	7.1	2.000	1.9
OV-15	Carbonatite	348-D	59.7	1.96	7.71	1894	1	5	0.040	
OV-16	*Clinopyroxene	348-D	110.9	1.78						
OV-17	*Calcite	348-D	22.3	2.53	16.5	885				
OV-19	Carbonatite	OV-2044/282,5	7.28	2.67	5.54	4041	1	10	0.190	1.3
LV-1	Olivinite	GIM-3287	79.0	0.172	5.41	665	0.5	3	0.021	2.2
LV-5	*Ti-magnetite	LVM-2mgt	37.9	0.069	1.54	2931				
LV-2	Olivinite	LV-1	9.68	2.22	4.57	394	0.1	1.3	0.018	1.1
LV-4	*Olivine	LVM-2/ol	2.14	2.38	2.67	1438				
SG-20	Turjaite	S-19	139.0	0.97	3.61	5313			0.730	2.2
VR-1	Olivinite	25V-229/256,8	242.1	2.02	5.01	3371				
VR-17	Carbonatite	NVV-279/174	2.53	9.09	11.2	2144			0.680	4.3
VR-22	Carbonatite	NVV-295/127	8.19	47.62	6.39	3774			0.199	0.5
VR-26	Carbonatite	NVV-430/202	248.9	1.27	10.5	1261			0.083	8.8
TP-7	Turjaite	T-63	99.5	0.161	3.03	4451				
DC-1	Lamprophyre	37-46	11.7	2.94	18.7	2500	5	7	1.818	80.0
DC-2	*Amphibole	37-13	32.6	1.33	7.30	3395	0.2	6	1.326	9.0
DC-3	*Amphibole	37-1	33.2	1.23	8.93	2800	1	5	1.244	9.0
DC-4	Lamprophyre	E-1	15.3	2.94	8.14	9210			1.511	
DC-5	Lamprophyre	50-4	16.5	11.8	8.28	3792	5.1	24	1.370	37.0
DC-6	*Amphibole	50-1	34.3	1.05	3.22	4780	0.4	5	1.069	4.0
DC-7	*Amphibole	50-10	39.8	1.06	3.67	4900	0.3	5	0.978	40.0
DC-12	Carbonatite	73-3	10.9	12.5	17.76	2798	0.9	6	2.084	4.0
DC-13	*Amphibole	73-6	3.54	3.39	10.4	2232	0.4	6	1.111	12.0
DC-14	Kimberlite	25-1	33.9	3.12	13.5	1355.85	2.3	16	0.755	8.0
DC-18	Nephelinite	1-15	85.3	2.77	11.2	2670	6.1	5	1.345	12.0
DC-19	*Amphibole	1-1	43.2	1.39	3.35	9240	1	8	1.716	7.0
DC-20	Carbonatite	23-6	1.43	71.4	4.92	4270	10	23	1.303	30.0
DC-21	*Amphibole	23-5	5.58	3.11	5.33	3395	0.6	7	1.268	73.0
DC-22	Granulite	37-20	6.42	1.93	3.21	4366	0.2	3	0.696	15.0
DC-23	Granulite	E-3	4.62	3.03	11.5	1385			0.481	
DC-24	Granulite	37-2(2)	3.23	3.96	4.26	6542	0.2	3	1.699	5.0
DC-25	*Garnet	37-2(2)	1.05	3.04	1.06	1227				
DC-26	*Pyroxene	37-2(2)	17.6	2.49	5.90	2424	0.3	1	0.141	17.0
DC-28	Granulite	E/96-10(2)	14.7	5.08	8.12	3080				
DC-30	Granulite	E/96-2(1)	15.2	2.47	13.3	1379				
DC-33	Carbonatite	23-6	1.43	71.4	4.92	4270	10	23	1.303	30.0
DC-37	Carbonatite	73-12	4.84	0.455	4.94	2570	0.2	3	0.647	2.0
DC-40	Carbonatite	16-7	44.4	1.35	12.6	2260	2.2	4	1.810	47.0
DC-41	*Amphibole	16-1	30.7	0.595	8.89	2924	1	13	1.194	3.0
DC-42	**Amphibole	17-17	16.9	2.01	5.42	6990	1.5	13	2.479	78.0
DC-44	Amphibolite	17-20	162.6	1.02	3.67	6485			1.600	
DC-45	Amphibolite	17-1a	28.3	0.847	3.63	7710	0.4	25		26.0
DC-46	Amphibolite	E-4	23.2	1.64	12.9	2940			1.210	
DC-47	Amphibolite	40-1	3.08	4.81	7.90	9600	0.3	3	1.594	10.0
DC-48	Amphibolite	40-2	4.88	7.81	5.45	11962	0.3	3	0.780	10.0
DC-49	Amphibolite	40-3	3.63	7.52	5.82	18200	1.1	8	0.979	12.0
DC-50	Pyroxenite	41-5	38.1	1.23	8.38	2734	0.5	7	0.141	18.0
DC-51	Pyroxenite	1-18	65.5	1.695	3.84	5210	0.4	4		5.0
DC-52	Pyroxenite	19-13	17.1	2.04	3.32	6030	0.7	5	1.028	30.0
DC-54	Metasomatite	37-52	35.5	1.27	7.99	4486	0.7	12	0.638	20.0
DC-55	Metasomatite	37-50	5.61	3.03	13.8	1385	0.3	8	0.597	27.0

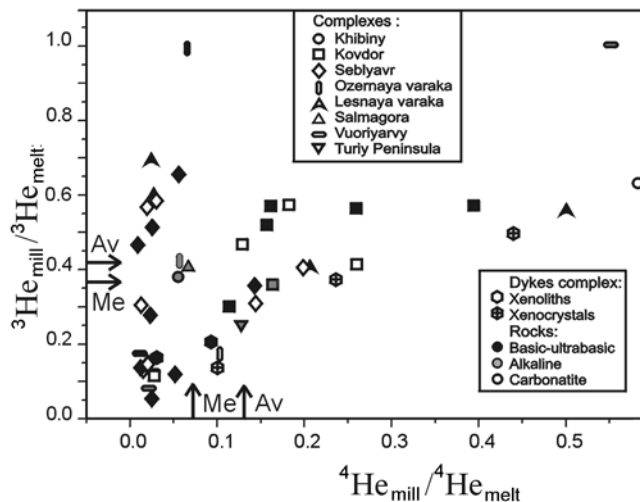


Figure 13. Comparison of ^3He and ^4He concentrations in whole-samples (melt) and in vehicles (mill). Milling (Section 3.1) generally liberates a considerable portion of ^3He (Average and Median ≈ 0.4) and a smaller portion of ^4He (Av and Me ≈ 0.1). This comparison shows that ^3He -bearing vesicles are larger and can be open (by milling) easier than radiation damage tracks containing radiogenic ^4He .

with as high ^3He as $\sim 10^{-9} \text{ cm}^3 \text{ STP g}^{-1}$ still show $^4\text{He}/^3\text{He}$ varying within a factor of ~ 20 . The parent-daughter relationships allows to understand whether initial $^4\text{He}/^3\text{He}$ ratios varied substantially in magmatic He trapped 370 Ma ago or a post-magmatic contribution of in-situ produced $^4\text{He}^*$ is a reason of this spread.

4.1.4. Relationships between helium isotopes, parent element concentrations and age. Enhanced concentrations of U, the major generator of radiogenic He, are typical of ultrabasic rocks from Kola UACC, $\text{U} \leq 20$ ppm, by a factor of 100 exceeding usual concentrations [Taylor and McLennan, 1985]. The Average U concentrations and Medians (both in ppm) are decreasing from ultrabasic rocks of UACC, 3.2 and 1.2 (13 samples) through carbonatites 2.40 and 1 (23 samples) to rocks of the dyke Complex 1.8 and 0.6 (29 samples). Th concentrations are quite high in some carbonatites and rocks from dykes, up to 70 ppm, which affect the average Th/U ratios observed in these rocks, 11 and 12, respectively. The average Th/U in ultrabasic rocks, 5.6, is also above the mean crustal value, 3.9 [Kramers and Tolstikhin, 1998].

A comparison of the combination $\text{U} + 0.24\text{Th}$ proportional to ^4He production [Zartman et al., 1961], and the whole-rock helium isotope abundances definitely shows an important role of the contribution of radiogenic $^4\text{He}^*$: the higher is the ratio of $(\text{U} + 0.24\text{Th})/^3\text{He}$ the higher is the $^4\text{He}/^3\text{He}$ ratio (Figure 15). Assuming the closed

system evolution for UACC, i.e., no gain/loss of species of interest since the formation age, 370 Ma ago, the data points would have been situated on the evolution line having slope of $^4\text{He}/(\text{U} + 0.24\text{Th}) = 45$ [cc/g] (solid line in Figure 15). Indeed the data-points are approaching the evolution line or lay below indicating an open system behaviour, i.e., helium loss. In regards to U-Th-He systematics, such a behaviour is quite typical for both igneous and sedimentary rocks [Mamyrin and Tolstikhin, 1984; Tolstikhin et al., 1996]. Importantly, several data-points having low whole-rock $^4\text{He}/^3\text{He}$ ratios almost approach the evolution line, implying a narrow interval for the initial $^4\text{He}/^3\text{He}$ ratio in helium trapped by these rocks.

To estimate the initial ratio several samples with low $^4\text{He}/^3\text{He}$ and $(\text{U} + 0.24\text{Th})/^3\text{He}$ ratios are presented in a linear co-ordinate plot (Figure 16). The regression line indicates the initial $^4\text{He}/^3\text{He} = 30,000$ which is exactly the same as the lowest measured ratio in helium released by milling (sample SB-1, Table 3). Slope of the regression is lower than that of the reference evolution line, indicating a moderate He loss.

Summarising, relationships between helium isotopes and parent radioactive elements (Figures 15 and 16) reveal the identical initial ratio of $^4\text{He}/^3\text{He} \approx 30,000$ in trapped helium and its highly variable concentrations. This initial ratio is intermediate between the mean MORB value, 89,000 [Tolstikhin and Marty, 1998] and the lowest value observed in Loihi basalt glasses 20,000 [Honda, 1993]. Subsequent variable contribution of radiogenic in-situ produced He^* ensure a wide spread of present-day He isotope abundances in UACC, depending on relative abundance of the parent elements, $(\text{U} + 0.24\text{Th})/^3\text{He}$, and portion of He^* retained in a sample (see also Section 5.2).

4.2. Neon and He-Ne Relationships

The conventional three-isotope plot (Figure 17) shows a good correlation between $^{21}\text{Ne}/^{22}\text{Ne}$ and $^{20}\text{Ne}/^{22}\text{Ne}$ ratios in Ne extracted by milling. $^{20}\text{Ne}/^{22}\text{Ne}$ ratios vary from 10.5 to 12.1 (Table 4) implying mixing between the atmospheric, 9.8, and the solar, 13.7, end-members [Honda, 1991, 1993]. The slope of regression line, $\text{SR}(\text{Kola}) = 190 \pm 40$, is slightly below that observed for Loihi samples, $\text{SR}(\text{Loihi}) = 250 \pm 25$ but well above the MORB regression, $\text{SR}(\text{MORB}) = 90 \pm 4$, corroborating a conclusion on a plume-related fluid component inferred from the study of He isotope abundances.

Tolstikhin et al. [1985] reported an extremely radiogenic Ne in 5 samples of Khibiny carbonatites having the average ratios $^{20}\text{Ne}/^{22}\text{Ne} = 5.3$ and $^{21}\text{Ne}/^{22}\text{Ne} = 0.1$; because of high fluorine concentrations in Kola UACC, contribution of radiogenic $^{22}\text{Ne}^*$ appears to be impor-

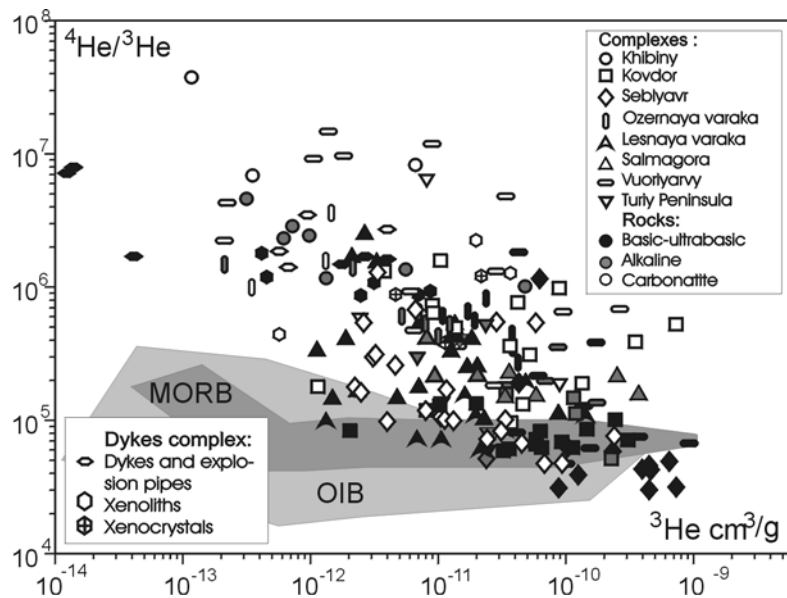


Figure 14. Helium isotope abundance in samples from Kola ultrabasic-alkaline-carbonatite Complexes: a fluid component (gas extraction by milling). Both $^4\text{He}/^3\text{He}$ ratios and ^3He concentrations in vesicles vary within ~ 4 orders of magnitude. The lowest ratios are well below MORB values indicating a contribution of high- ^3He plume component. The general tendency is the higher ^3He concentrations, the lower $^4\text{He}/^3\text{He}$ ratios. A moderate range of $^4\text{He}/^3\text{He}$ ratios in samples greatly enriched with ^3He could result from inhomogeneity of trapped fluid or mixing of trapped and in-situ produced He. This dilemma is discussed in Sections 4.1.4 and 5.2. See Figure 11 for sources of MORB and OIB data.

tant. Other UAC Complexes show less radiogenic signature with Ne compositions following approximately along the MORB trend (Figure 17).

Subtraction of the in-situ produced Ne isotopes using U-He-Ne systematics allow the plume-related compositions to be revealed in the less radiogenic samples from the Kovdor and other UACC. Measured isotope composition of neon (for example, point M in Figure 17, corresponding to sample KV-28, Table 4) reflects proportion of mixing of atmospheric, solar and radiogenic components. The first two end-members are well known and their adequate mixture is defined hereafter as the initial composition (SA in Figure 17). A plausible candidate for radiogenic “end-member” appears to be neon from Khibiny carbonatites; the corresponding data-point is situated to the right off Figure 17; direction to this point is shown by R. The end members, i.e., initial (SA) and radiogenic R compositions, as well as measured M, and plume-related P compositions resulting from end-member mixing must all lay on one and the same line in the co-ordinate used. Data-points R and M, which co-ordinates are known from measurements, determine this line SAPMR. Shift of a data-point from the initial composition (SA) to the right along SAPMR is proportional to the addition of radiogenic Ne^* , other things being equal. Proportion

$$\frac{[(^{21}\text{Ne}/^{22}\text{Ne})_{\text{plume}} - (^{21}\text{Ne}/^{22}\text{Ne})_{\text{SA}}] / [(^{21}\text{Ne}/^{22}\text{Ne})_{\text{meas}} - (^{21}\text{Ne}/^{22}\text{Ne})_{\text{SA}}]}{[(^4\text{He}/^3\text{He})_{\text{plume}} - (^4\text{He}/^3\text{He})_{\text{prim}}] / [(^4\text{He}/^3\text{He})_{\text{meas}} - (^4\text{He}/^3\text{He})_{\text{prim}}]} \approx 0.12$$

allow the shift from initial to plume related composition to be quantified. This proportion relies on the constant production ratio $^4\text{He}^*/^{21}\text{Ne}^* \approx (1.5 \pm 0.5) \times 10^7$ and known $(^4\text{He}/^3\text{He})_{\text{plume}} = 30,000$ (Sections 4.1.3 and 4.1.4), $(^4\text{He}/^3\text{He})_{\text{prim}} = 3,000$ [e.g., *Anders and Grevesse, 1989*], $(^4\text{He}/^3\text{He})_{\text{meas}} = 230,000$ (KV-28, Table 2) and gives the composition of plume-related Ne in this sample shown as P. While P deviates to the left from Kola UACC array, other 4 corrected compositions are well within this array corroborating occurrence of plume-related Loihi-like Ne even in samples containing a substantial radiogenic component.

4.3. Argon and Lighter Noble Gases

4.3.1. Parent-daughter and Ne-Ar relationships and $^{40}\text{Ar}/^{36}\text{Ar}$ ratio in trapped fluid $^{40}\text{Ar}/^{36}\text{Ar}$ ratio appears to be important characterisation of the

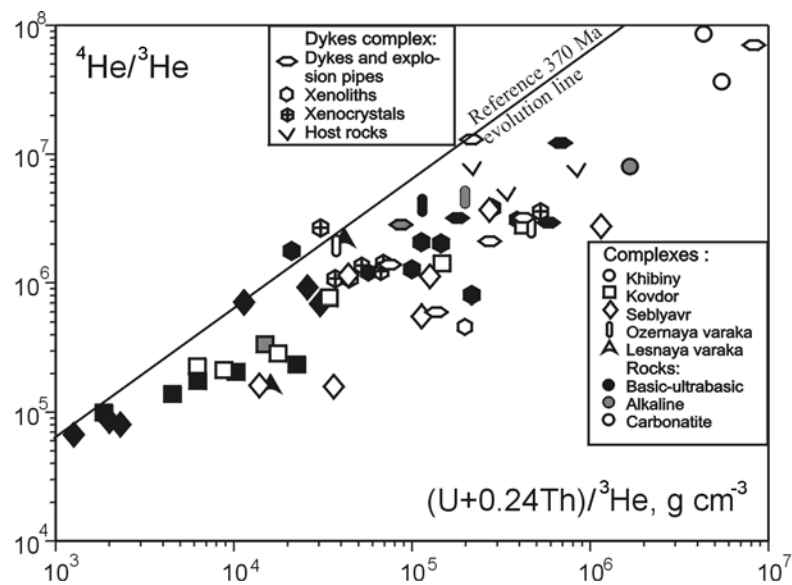


Figure 15. Relationships between whole-rock abundances of parent and daughter species indicates mixing between isotopically-homogeneous trapped He and radiogenic in-situ produced He*. Most samples are below the reference evolution line, therefore they have partially lost helium. Because of the bi-logarithmic scale of this plot, the initial $^4\text{He}/^3\text{He}$ ratio in trapped He can not be derived (see Figure 16).

trapped fluid particularly taking into account a poor knowledge of this ratio in a plume source [Allegre *et al.*, 1986, 1987; Ozima and Zahnle, 1993; O'Nions and Tolstikhin, 1994, 1996; Porcelli and Wasserburg, 1995; Tolstikhin and Marty, 1998]. In contrast to He, three sources of Ar are significant for samples from Kola UACC: atmospheric Ar, $^{40}\text{Ar}^*$ produced in-situ, and trap-

ped Ar. $^{40}\text{Ar}/^{36}\text{Ar}$ ratios in Ar extracted from the samples by milling vary within an order of magnitude, from air value 296 to $\sim 3,000$, implying a substantial contribution of atmospheric Ar in initially homogeneous (Section 4.1.4) trapped fluid.

Within the conventional $^{40}\text{Ar}/^{36}\text{Ar}$ versus $\text{K}/^{36}\text{Ar}$ plot the data points mainly cluster around the reference

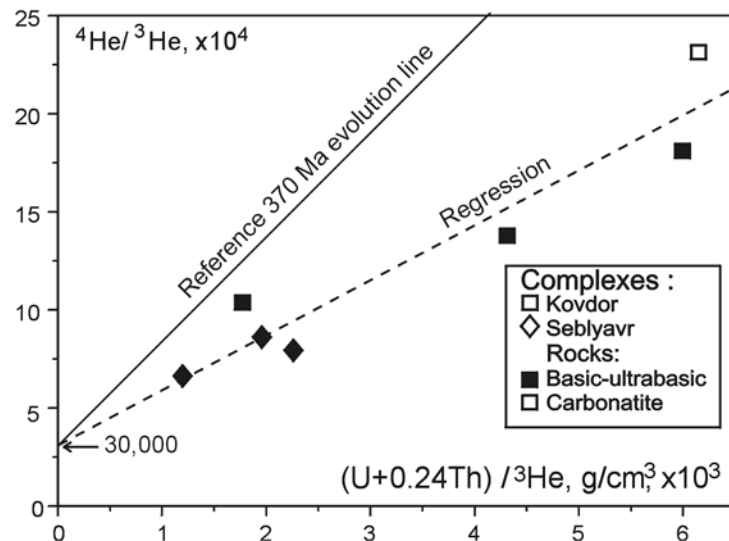


Figure 16. Samples with low $(\text{U}+0.24\text{Th})/^3\text{He}$ and $^4\text{He}/^3\text{He}$ ratios, even though lost some helium, show a good correlation, indicating initial $^4\text{He}/^3\text{He} = 30,000$, which is exactly the same as the lowest ratio in helium extracted by milling (samples SB-1, SB-2, and SB-6, Table 3).

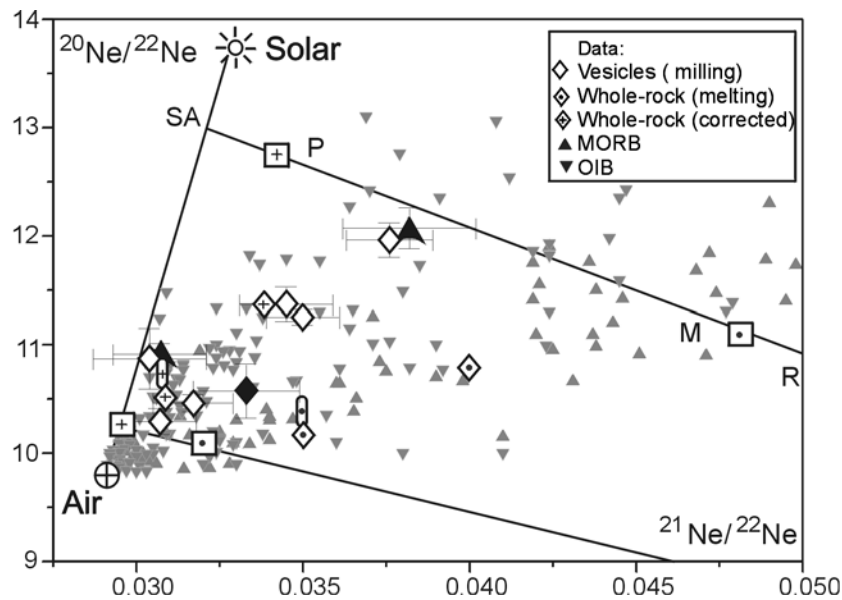


Figure 17. Conventional Ne three-isotope plot indicates mixing between atmospheric, primordial (solar-like) and radiogenic end-members.

The isotopic ratios in Ne extracted by crushing [Marty *et al.*, 1998] follow the plume-like trend traced previously by basalts from Loihi seamount, Hawaii; whereas the ratios in bulk samples [Tolstikhin *et al.*, 1985] approach the MORB array. When in-situ produced $^{21}\text{Ne}^*$ and $^{22}\text{Ne}^*$ were subtracted from the bulk abundances using He-Ne systematics [Honda, 1993], the corresponding data-points shift to the left-top and joint the plume trend. See definitions of symbols in Figure 15 and sources for MORB and OIB data in Figure 11.

370 Ma isochrone crossing atmospheric initial $^{40}\text{Ar}/^{36}\text{Ar}$ ratio (Figure 18). However several Kovdor samples deviate to the top off the isochrone, indicating an elevated initial $^{40}\text{Ar}/^{36}\text{Ar} \sim 4,000$ in the trapped fluid.

$^{20}\text{Ne}/^{22}\text{Ne}$ versus $^{40}\text{Ar}/^{36}\text{Ar}$ correlation (Figure 19) allows an independent estimate for the initial $^{40}\text{Ar}/^{36}\text{Ar}$ ratio [Marty *et al.*, 1998]. This correlation resulting from mixing of atmospheric and mantle species definitely shows that the mantle end-member must have $^{40}\text{Ar}/^{36}\text{Ar} > 3,000$. Generally mixing trajectory is a curve in these coordinates and extrapolation of this curve to solar $^{20}\text{Ne}/^{22}\text{Ne}$ requires special assumptions about the mantle end-member(s). If mixing of material from 3 reservoirs (Section 5.4) would have occurred, the extrapolation is not allowed. Assuming two end-member mixing, i.e., the atmosphere and the plume source, Marty *et al.* [1999] obtained the limiting $^{40}\text{Ar}/^{36}\text{Ar}_{\text{plume}} \sim 5,000 - 6,000$.

4.3.2. $^4\text{He}/^{40}\text{Ar}^*$ ratio in trapped fluid. Two post-magmatic processes appears to evolve $^4\text{He}/^{40}\text{Ar}^*$ ratios in a trapped fluid. The first is addition of in-situ produced nuclides, particularly tacking into account that the mean K/U ratio observed in UAC samples (with the exception of the Dyke Complex, see Table 3) is by a factor of ≈ 5 less than the canonical mantle K/U

$= 12700$ [Johum *et al.*, 1983]. The second is a preferential helium loss. Indeed, the whole-rock $^4\text{He}/^{40}\text{Ar}^*$ versus $(\text{U}+0.24\text{Th})/\text{K}$ plot demonstrates that the two processes account for the observed distribution of data-points (Figure 20).

To avoid a substantial contribution of in-situ-produced nuclides, 23 samples with $^4\text{He}/^3\text{He}_{\text{mill}} \leq ^4\text{He}/^3\text{He}_{\text{MORB}}$ were selected giving the average $^4\text{He}/^{40}\text{Ar}^* = 6.4 \pm 5.3$ and $\text{Me} = 5.0$. Among those several carbonatites show insignificant fractionation between ^4He and $^{21}\text{Ne}^*$ (See Figure 24) and $^4\text{He}/^{40}\text{Ar}^*$ ratios in this sub-set vary within a narrow range averaging at 3.1 ± 1.1 which is in a good agreement with the model estimations of mantle ratios, 2.5 ± 1.5 for the upper and ≈ 3 for the lower mantle reservoirs [Tolstikhin and Marty, 1998].

5. Discussion

5.1. Carriers of Mantle Fluids: Inclusions and Host Minerals

To understand relationships between the crystallisation consequence, the mineral structures, the morphology and density of defects in crystalline lattices, and the trapped component abundances, mineral separates

Table 3. He and Ar abundances in vesicles

Sample	Rock/ mineral	Number	^3He 10^{12} cc/g	$^4\text{He}/^3\text{He}$ 10^6	(^{36}Ar) 10^9 cc/g	$(^{40}\text{Ar})/(^{36}\text{Ar})$
KH-1	Foyaite	KH-2909	1.0	2.38	n.d.	n.d.
KH-2	Foyaite	KH-2914	5.5	1.34	n.d.	n.d.
KH-3	Foyaite	KH-2918	0.7	2.85	n.d.	n.d.
KH-4	Foyaite	KH-2921	46.8	1.02	n.d.	n.d.
KH-5	Foyaite	KH-2941	0.3	4.54	n.d.	n.d.
KH-6	Foyaite	KH-2944	0.6	2.32	n.d.	n.d.
KH-7	Foyaite	KH-2945	1.3	1.16	n.d.	n.d.
KH-8	Carbonatite	NKH-581-1	6.4	8.19	11.0 9	866
KH-10	Carbonatite	13-KHk	0.4	6.84	n.d.	n.d.
KH-11	Carbonatite	14-KHk	0.1	37.0	n.d.	n.d.
KV-1	Olivinite	D-52	32.1	0.06	0.30	1621
KV-2	Olivinite	KR-59-1/268.1	64.2	0.064	0.82	2193
KV-3	Olivinite	KR-62-1/276	91.6	0.068	n.d.	n.d.
KV-4	Olivinite	KR41-1/199	34.8	0.060	n.d.	n.d.
KV-5	Olivinite	KR80-1/357.8	109	0.063	n.d.	n.d.
KV-8	Olivinite	KR-133-1/997.3	10.1	0.129	n.d.	n.d.
KV-9	Olivinite	KR-18-1/126	2.0	0.084	n.d.	n.d.
KV-10	Olivinite	KR-55-1/257.8	62.0	0.084	1.44	2985
KV-11	Clinopyroxenite	KR-35-1/171.4	239	0.100	n.d.	n.d.
KV-12	Clinopyroxenite	KR-5s/152-1598	145	0.086	n.d.	n.d.
KV-13	**Diopside	KD-2	57.8	0.074	0.43	2818
KV-14	**Magnetite	KD-1	298	0.071	n.d.	n.d.
KV-15	Melilitolite	KI-22-A	55.7	0.068	n.d.	n.d.
KV-16	Melilitite	D-54	19.8	0.132	n.d.	n.d.
KV-17	Turjaite	GIM-4652	221	0.051	n.d.	n.d.
KV-18	Ijolite	19/83KS	114	0.148	n.d.	n.d.
KV-19	Ijolite	KR-193	33.7	0.152	n.d.	n.d.
KV-20	Ijolite	KI-16	116	0.111	n.d.	n.d.
KV-21	**Magnetite	KD-3	44.4	0.132	0.51	1509
KV-22	Phoscorite	KI-17-A	7.9	0.120	n.d.	n.d.
KV-24	Phoscorite	KI-17-B	35.2	0.097	n.d.	n.d.
KV-25	Phoscorite	KI-20-A	49.6	0.318	n.d.	n.d.
KV-26	Phoscorite	KI-20-B	86.0	1.00	n.d.	n.d.
KV-33	Carbonatite	KR-69-1/305.1	13.2	0.476	n.d.	n.d.
KV-34	Carbonatite	D-56	3.8	1.32	n.d.	n.d.
KV-35	Carbonatite	KI-15-A	9.2	0.633	n.d.	n.d.
KV-36	Carbonatite	KI-15-C	35.3	0.360	n.d.	n.d.
KV-37	Carbonatite	KI-15-B	1.1	0.179	n.d.	n.d.
KV-38	**Magnetite	4/83-KS/m	133	0.195	n.d.	n.d.
KV-39	**Calcite	4/83-KS/k	336	0.398	n.d.	n.d.
KV-40	Carbonatite	KI-18	9.0	0.714	n.d.	n.d.
KV-42	Carbonatite	KR-128-1/795.5	710	0.526	n.d.	n.d.
KV-44	Carbonatite	KI-20-C	10.0	1.61	n.d.	n.d.
KV-45	Carbonatite	KV-ZH-14	39.7	0.781	n.d.	n.d.
SB-1	Olivinite	111-3/49.2	85.9	0.030	4.13	435.4
SB-2	*Magn.fraction	111-3/49.2	405	0.030	3.25	593
SB-3	Olivinite	NSB138-160	120	0.036	n.d.	n.d.
SB-4	Olivinite	Sja-184/82.5	40.8	0.179	n.d.	n.d.
SB-5	Olivinite	Sja-184/80	98.1	0.060	n.d.	n.d.
SB-6	Clinopyroxenite	NSB-138-70	694	0.031	2.94	1200

Table 3. Continuation

Sample	Rock/ mineral	Number	^3He 10^{12} cc/g	$^4\text{He}/^3\text{He}$ 10^6	(^{36}Ar) 10^9 cc/g	$(^{40}\text{Ar})/(^{36}\text{Ar})$
SB-7	Clinopyroxenite	Sja-114/55	412	0.045	1.78	1685.5
SB-8	*Magn,fraction	Sja-114/55mf	601	0.046	2.64	1325
SB-9	*Clinopyroxene	Sja-114/55-pr	388	0.042	1.56	1603
SB-10	*Perovskite	Sja-114/55-prs	59.8	1.099	2.46	1016
SB-11	Clinopyroxenite	Sja-114/65	215	0.055	1.02	1564
SB-12	Clinopyroxenite	Sja-186/130	424	0.041	3.89	1130
SB-13	Clinopyroxenite	BEG-16	429	0.040	0.99	1359
SB-14	Ijolite	BEG-12	23.6	0.051	n.d.	n.d.
SB-15	Phoscorite	BEG-6	66.3	0.047	0.62	2185
SB-16	Phoscorite	BEG-11	4.4	0.248	n.d.	n.d.
SB-17	Phoscorite	BEG-8	89.4	0.045	0.87	1204
SB-18	Phoscorite	BEG-9	7.8	0.113	n.d.	n.d.
SB-19	Phoscorite	BEG-15	32.5	0.099	n.d.	n.d.
SB-20	Carbonatite	Sja-101/180,5	11.3	0.159	n.d.	n.d.
SB-21	Carbonatite	NSB-341-13	2.1	0.172	n.d.	n.d.
SB-22	Carbonatite	BEG-10	10.4	0.101	n.d.	n.d.
SB-23	Carbonatite	NSB-186-1	2.5	0.518	n.d.	n.d.
SB-24	Carbonatite	NSB-341-3	3.0	0.294	n.d.	n.d.
SB-25	Carbonatite	NSB-341-4	3.1	0.304	n.d.	n.d.
SB-26	Carbonatite	BEG-13	3.3	1.23	n.d.	n.d.
SB-27	Carbonatite	NSB-341-2	2.4	0.154	n.d.	n.d.
SB-28	Carbonatite	NSB-359-1	6.3	0.637	n.d.	n.d.
SB-29	Carbonatite	NSB-341-1	229	0.073	n.d.	n.d.
SB-30	Carbonatite	NSB-351-1	10.9	0.097	n.d.	n.d.
SB-31	Carbonatite	NSB-362-1	12.6	0.095	n.d.	n.d.
SB-37	Carbonatite	BEG-14	23.5	0.070	1.58	668
SB-38	*Pyrrhotite	BEG-14	3.9	0.096	0.80	465
SB-39	*Dolomite	BEG-14	43.4	0.064	2.59	735
SB-40	Carbonatite	NSB-351-6	29.7	0.077	n.d.	n.d.
OV-1	Clinopyroxenite	OV-2048/117,4	23.5	0.809	n.d.	n.d.
OV-2	Clinopyroxenite	OV-2048/118	38.2	0.345	n.d.	n.d.
OV-3	Clinopyroxenite	OV-2050/302,8	18.5	0.556	n.d.	n.d.
OV-4	*Clinopyroxene	OV-2050/302,8py	17.1	0.654	n.d.	n.d.
OV-5	*Ti-magnetite	OV-2050/302,8mg	37.0	0.441	n.d.	n.d.
OV-6	Clinopyroxenite	OV-2057/116	41.6	0.265	n.d.	n.d.
OV-7	Clinopyroxenite	OVS-33/95	10.5	0.564	n.d.	n.d.
OV-8	Ijolite	OV-2057/212	9.7	0.435	5.03	636
OV-9	Ijolite	NOV-2053/1	12.0	0.518	n.d.	n.d.
OV-10	Ijolite	OV-2044/230	7.0	0.633	n.d.	n.d.
OV-11	Ijolite	BEG-2	5.1	0.588	n.d.	n.d.
OV-12	Ijolite-urtite	OV-2057/12	7.3	0.549	n.d.	n.d.
OV-13	Syenite	OV-2048/87,6	2.1	1.38	n.d.	n.d.
OV-14	Syenite	OV-79/95	0.2	1.44	n.d.	n.d.
OV-18	Carbonatite	OV-2044/121	0.3	0.952	n.d.	n.d.
OV-19	Carbonatite	OV-2044/282,5	1.3	1.58	0.94	1021
OV-20	Carbonatite	OVS-2050/139,6	1.4	3.66	n.d.	n.d.
LV-1	Olivinite	GIM-3287	32.5	0.086	0.67	1061
LV-2	Olivinite	LV-1	6.7	0.074	0.11	2790.6
LV-3	Olivinite	LVM-2/nn	10.2	0.072	0.67	863
LV-4	*Olivine	LVM-2/ol	1.3	0.101	0.35	345

Table 3. Continuation

Sample	Rock/ mineral	Number	^3He 10^{12} cc/g	$^4\text{He}/^3\text{He}$ 10^6	(^{36}Ar) 10^9 cc/g	$(^{40}\text{Ar})/(^{36}\text{Ar})$
LV-5	*Ti-magnetite	LVM-2mgt	21.2	0.061	0.31	3000
LV-6	**Ti-magnetite	GIM-343	48.5	0.196	0.79	2463
LV-7	**Ti-magnetite	LV-8/117mgt	141.1	0.110	n.d.	n.d.
LV-8	**Clinopyroxene	LV-80/1pr	19.7	0.112	n.d.	n.d.
LV-9	**Ti-magnetite	LV-80/1mgt	16.0	0.156	n.d.	n.d.
SG-1	Olivinite	S-2011/118,5	1.5	0.144	0.34	767
SG-2	Olivinite	S-2011/13	2.3	0.167	n.d.	n.d.
SG-3	Olivinite	S-2011/183,3	18.0	0.427	0.57	1230
SG-4	Olivinite	S-2011/189,5	2.6	2.55	0.66	531
SG-5	*Olivine	S-2011/189,5ol	1.1	0.346	0.44	519
SG-6	*Ti-magnetite	S-2011/189,5mgt	2.1	1.71	0.62	438
SG-7	Olivinite	S-2011/191	6.9	0.552	0.51	1356
SG-8	Olivinite	S-2011/195	3.3	1.56	0.35	662
SG-9	Olivinite	S-2011/199	1.9	0.424	2.04	588
SG-10	Olivinite	S-2011/253,5	12.3	0.334	0.39	1673
SG-11	Olivinite	S-2011/304,5	7.0	0.186	n.d.	n.d.
SG-12	Olivinite	S-2032/268	21.5	0.107	n.d.	n.d.
SG-13	Olivinite	S-45	13.5	0.526	n.d.	n.d.
SG-14	Olivinite	S-50a	13.6	0.418	n.d.	n.d.
SG-15	Clinopyroxenite	S-2011/72	86.4	0.113	n.d.	n.d.
SG-16	Clinopyroxenite	S-2032/13	4.7	0.148	n.d.	n.d.
SG-17	Clinopyroxenite	S-2011/183,3a	19.6	0.260	1.25	1840
SG-18	Clinopyroxenite	S-62	12.4	0.444	n.d.	n.d.
SG-19	Clinopyroxenite	S-2011/199a	16.5	0.254	2.76	2683
SG-20	Turjaite	S-19	56.5	0.157	n.d.	n.d.
SG-21	Turjaite	S-2033/261	354.5	0.158	n.d.	n.d.
SG-22	Turjaite	S-2033/290	245.4	0.212	n.d.	n.d.
SG-23	Melteygite	S-11	9.3	0.218	n.d.	n.d.
SG-24	Ijolite-melteygite	NSG-2030/5	13.0	0.408	n.d.	n.d.
SG-25	Ijolite-melteygite	NSG-2031/2	19.8	0.222	n.d.	n.d.
SG-26	Ijolite-melteygite	S-48	7.9	0.417	n.d.	n.d.
SG-27	Ijolite	S-2015/349	34.1	0.148	n.d.	n.d.
SG-28	Ijolite	S-2011/184,5	34.6	0.231	2.38	2268
SG-29	Carbonatite	NSG-2026/2	55.4	0.527	n.d.	n.d.
SG-30	Carbonatite	S-5	26.5	0.521	n.d.	n.d.
VR-1	Olivinite	25V-229/256,8	42.0	0.145	n.d.	n.d.
VR-2	Olivinite	44-2/48,0	93.9	0.048	n.d.	n.d.
VR-3	Olivinite	NVV-288-202	40.9	0.083	n.d.	n.d.
VR-4	Olivinite	NVV-288-296	34.9	0.083	n.d.	n.d.
VR-5	Olivinite	NVV-288-152	56.8	0.063	n.d.	n.d.
VR-6	Clinopyroxenite	N-426/226	170.2	0.376	n.d.	n.d.
VR-7	**Ti-magnetite	N-384/288	42.0	1.79	n.d.	n.d.
VR-8	Clinopyroxenite	NVV-258-96	148.2	0.063	n.d.	n.d.
VR-9	Clinopyroxenite	NVV-307/126	360.3	0.074	1.94	1754
VR-10	*Clinopyroxene	NVV-307/126pr	60.0	0.213	1.74	1493
VR-11	*Ti-magnetite	NVV-307/126mgt	907.1	0.067	1.95	1586
VR-12	Clinopyroxenite	NVV-95/140	134.6	0.126	n.d.	n.d.
VR-13	Ijolite	N-417/158	186.9	0.152	n.d.	n.d.
VR-14	Ijolite-urtite	NVV-289/325	66.5	0.191	n.d.	n.d.
VR-15	Ijolite	NVV-289/325-1	78.1	0.352	n.d.	n.d.

Table 3. Continuation

Sample	Rock/ mineral	Number	^3He 10^{12} cc/g	$^4\text{He}/^3\text{He}$ 10^6	^{36}Ar 10^9 cc/g	$^{40}\text{Ar}/^{36}\text{Ar}$
VR-16	Ijolite-urtite	NVV-438/102	32.4	0.188	n.d.	n.d
VR-17	Carbonatite	NVV-279/174	0.2	2.21	n.d.	n.d
VR-18	Carbonatite	29V-128/161	14.1	0.355	n.d.	n.d
VR-19	Carbonatite	V-48-125/69	27.6	0.181	n.d.	n.d
VR-20	Carbonatite	NVV-200/680	8.9	11.8	n.d.	n.d
VR-21	Carbonatite	NVV-467/2	1.7	9.71	n.d.	n.d
VR-22	Carbonatite	NVV-295/127	1.0	9.09	n.d.	n.d
VR-23	Carbonatite	NVV-328/84	0.2	4.29	n.d.	n.d
VR-24	Carbonatite	13V-206/234,5	29.0	1.31	n.d.	n.d
VR-25	Carbonatite	NVV-288-248	95.1	0.662	n.d.	n.d
VR-26	Carbonatite	NVV-430/202	250.0	0.696	n.d.	n.d
VR-27	Carbonatite	NVV-440/158	5.9	0.917	n.d.	n.d
VR-28	Carbonatite	NVV-200/311	1.3	14.7	n.d.	n.d
TP-1	Clinopyroxenite	S-92/4,2	24.5	0.057	n.d.	n.d
TP-2	Clinopyroxenite	GIM-3010	10.3	0.136	n.d.	n.d
TP-3	Clinopyroxenite	GIM-3012	24.1	0.079	n.d.	n.d
TP-4	Turjaite	GIM-4680	14.6	0.389	n.d.	n.d
TP-5	Turjaite	GIM-4696	6.7	0.305	4.59	1286
TP-6	Turjaite	S-45N12	23.0	0.521	n.d.	n.d
TP-7	Turjaite	T-63	24.8	0.081	n.d.	n.d
TP-8	Carbonatite	TPN-26	2.4	0.551	n.d.	n.d
TP-11	Carbonatite	TPN-29	85.7	0.186	n.d.	n.d
TP-12	Carbonatite	TPN-57	7.7	6.49	n.d.	n.d
DC-3	* Amphibole	37-1	.6	0.87	1.97	760
DC-8	Lamprophyre	E/96-1(2)	4.0	1.58	3.87	2350
DC-9	Lamprophyre	E/96-20(2)	3.5	1.31	6.99	930
DC-10	Lamprophyre	E/96-1(1)	2.6	1.69	18.18	506
DC-11	Lamprophyre	E/96-20(1)	1.7	1.49	3.14	1177
DC-15	Kimberlite	K/97-6	0.0	7.69	n.d.	n.d
DC-16	Kimberlite	K/97-4	0.0	7.94	n.d.	n.d
DC-17	Kimberlite	K/97	0.0	1.82	n.d.	n.d
DC-19	* Amphibole	1-1	21.6	1.22	3.29	1548
DC-27	Granulite	E/96-10(1)	7.1	0.893	2.74	1132
DC-28	Granulite	E/96-10(2)	2.4	0.893	2.65	1282
DC-29	Granulite	E/96-10(3)	8.4	0.943	1.21	2032
DC-30	Granulite	E/96-2(1)	3.1	1.09	4.33	531
DC-31	Granulite	E/96-20(3)	0.4	1.8	5.39	649
DC-32	Carbonatite	N/96-1(74)	0.7	1.41	2.81	807
DC-34	Carbonatite	66	19.6	2.1	1.92	2417
DC-35	Carbonatite	67	0.6	0.431	1.97	1521
DC-36	Carbonatite	T/96-11(64)	36.6	1.26	4.75	1537
DC-38	Carbonatite	73-10	1.0	3.57	4.71	1359
DC-39	Carbonatite	68	0.6	1.85	3.20	1250
DC-41	* Amphibole	16-1	11.4	0.376	1.84	924
DC-43	Carbonatite	E/96-11(71)	4.1	2.75	3.31	2839
DC-53	Pyroxenite	E/96-1(3)	0.4	1.18	0.77	1092

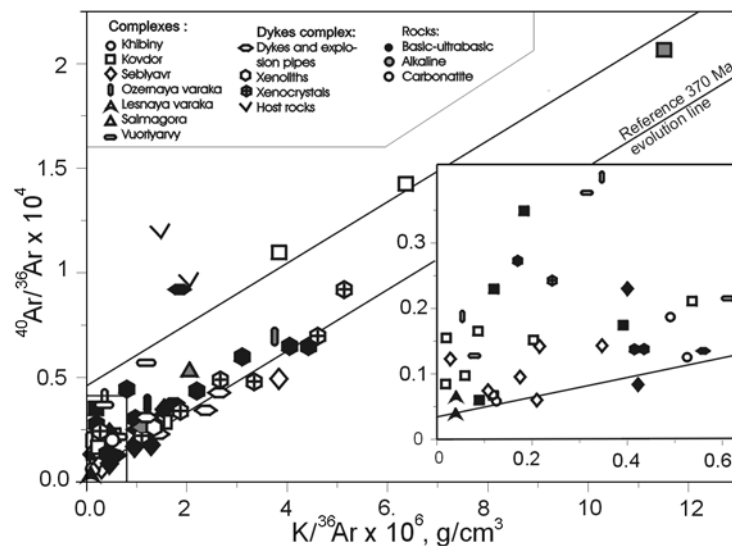


Figure 18. K-Ar evolution diagram.

Most samples approach the reference 370 Ma isochrone crossing atmospheric $^{40}\text{Ar}/^{36}\text{Ar}$ ratio. However several samples from the Kovdor and Vuoriyarvi Complexes are well above the isochrone implying trapped Ar with initial $^{40}\text{Ar}/^{36}\text{Ar} \sim 4,000$. Samples having low $\text{K}/^{36}\text{Ar}$ ratios (inset) also show occurrence of excess trapped Ar with $^{40}\text{Ar}/^{36}\text{Ar} \geq 3,000$. Host rocks of the dyke Complex are not considered because of their older age.

were investigated. Ultrabasic rocks showing the highest abundances of trapped He appears to be the most interesting for this study. Table 5 comprises He isotope abundances in olivine, pyroxene and magnetite concentrates from olivinite SB-3 (Tables 1, 2). It should be noted that the whole-rock U, Th, and He data indi-

cate a good retention, $\geq 50\%$, of radiogenic $^4\text{He}^*$ by this sample. As it is shown below in this Section, even better ^3He retention is expected. Therefore the present-day measured ^3He concentrations should approach those trapped initially. ^3He concentrations are almost constant in the clinopyroxene and Ti-magnetite separates

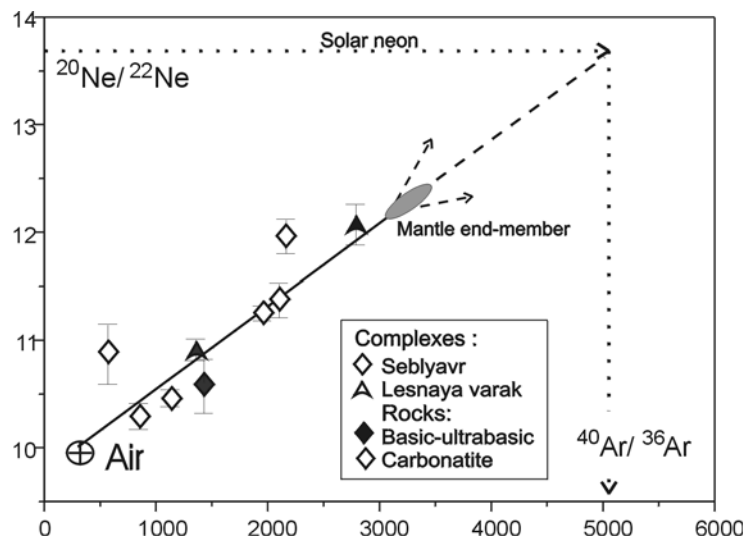


Figure 19. Ar-Ne isotope plot (after Marty et al., 1999). Notice relatively low $^{40}\text{Ar}/^{36}\text{Ar} \sim 3,000$ ratio measured in a mantle “end-member” together with the least contaminated Ne. This ratio is somewhat lower than the model-derived lower mantle values and much lower than values inferred from observation for the upper mantle, $\approx 40,000$ (see Tolstikhin and Marty, 1998, and references therein). Extrapolation could lead to a somewhat higher value for the mantle source. However the extrapolation trends and even possibility of the extrapolation are not clear.

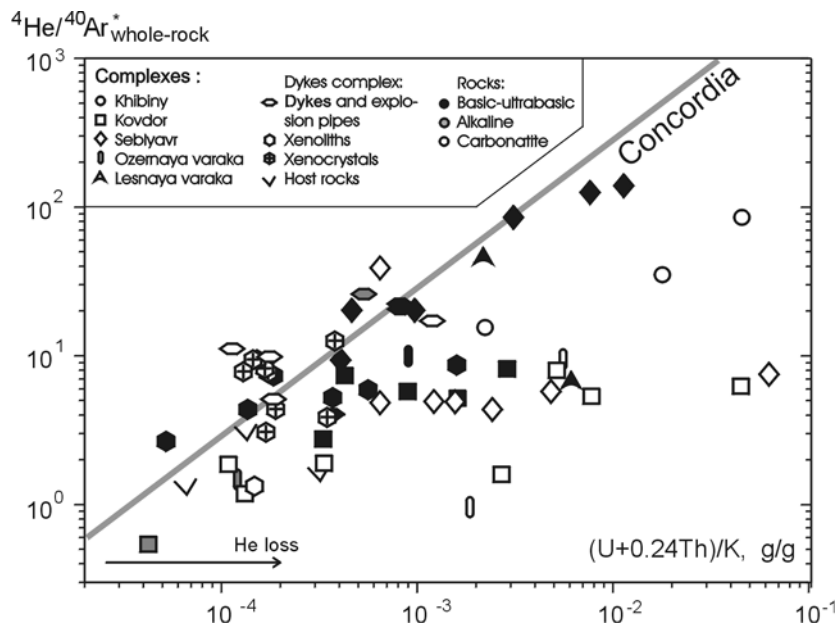


Figure 20. Generally samples from Kola UACC (excepting those from the Dyke Complex) show whole-rock ${}^4\text{He}/{}^{40}\text{Ar}^*$ ratios lower than those predicted by parent elements.

These relationships imply a preferential loss of radiogenic ${}^4\text{He}$. Some carbonatites show especially low ${}^4\text{He}/{}^{40}\text{Ar}^*$ resulted from insufficient ability to preserve helium (see Figure 15). A correlation between ${}^4\text{He}/{}^{40}\text{Ar}^*$ melt and ${}^4\text{He}/{}^{40}\text{Ar}^*$ mill (not presented in this paper) indicates a contribution of the in-situ produced species into the trapped fluid (see Figure 23).

In contrast, the ratios in host rocks of the Dyke Complex are below the concordia, whereas these in several samples from dykes themselves are above this line indicating that the dykes could be considered as a complementary reservoir to the host rocks (Mamyryn and Tolstikhin, 1984; Tolstikhin et al., 1996).

but vary mildly in the olivine slightly increasing with its size. ${}^3\text{He}$ concentrations in the pyroxene and in bigger fractions of the olivine are similar, $\approx 18 \times 10^{-9}$ cc/g. The Ti-magnetite shows much higher abundance of trapped mantle He. This enrichment could originate from the consequence of mineral crystallisation governing magnetite segregation after olivine and clinopyroxene. Rare gases are incompatible elements and a rare gas enrichment (~ 10 times) adequate to the mass balance ($\sim 10\%$ of magnetite in the rocks) is expected in the last portion of basic melt producing magnetite. Also the crystalline lattice of magnetite shows channel-like interstitials between elementary crystal domains with cross size ≈ 2 Å which is similar to diameter of He atom. In contrast to that, crystalline lattice of olivine is rather dense and defects/inclusions are needed to accommodate trapped species.

Generally olivine is used as a proper carrier of trapped He [e.g., Marty and Tolstikhin, 1998, and references therein]. Taking into account high concentrations of trapped He and its rather good retention in magnetite (see Figure 22), this mineral can be recommended as a promising natural sampler of trapped rare gases. High ${}^3\text{He}$ concentrations and low ${}^4\text{He}/{}^3\text{He}$ ratios in several

other magnetite separates (e.g., samples KV-13, 14, 21; SB-7-9, LV-4, 5, Table 2) support this suggestion.

${}^4\text{He}$ concentrations in the mineral separates varies more widely than ${}^3\text{He}$ implying inhomogeneity of U (Th) concentrates, or different retention of radiogenic ${}^4\text{He}^*$, or a contribution of U-bearing mineral, like perovskite (SB-10, Table 2) having the highest concentration of ${}^4\text{He}$ among UAC samples. The last column in Table 5 shows hypothetical contributions of perovskite which are able to reconcile ${}^3\text{He}$ and ${}^4\text{He}$ inventories in all separates.

Step-wise heating experiments with Ti-magnetites and olivine (Figure 21) clearly indicate different settings for ${}^4\text{He}^*$, always related to radiation damage tracks, and ${}^3\text{He}$. At low temperatures $\leq 800^\circ\text{C}$ fluid inclusions are decipitated liberating a dominant portion of major fluid components, CO_2 and H_2O , and variable portions of ${}^4\text{He}^*$ and ${}^3\text{He}$. In Ti-magnetite BEG-1 (Figure 21b) portion of ${}^3\text{He}$ released within these low-temperature steps coincides with that liberated by crushing, $\sim 10\%$. Because of the mean size of the post-crushing powder is about 0.001-0.01 cm, the inclusions in this mineral should be of a similar size or somewhat less.

${}^4\text{He}^*$ is mainly released under moderate tempera-

Table 4. Neon isotopes in vesicles and bulk samples

Sample	Rock/mineral	Extraction	^{22}Ne 10^{12} cc/g	$^{20}\text{Ne}/^{22}\text{Ne}$	$^{21}\text{Ne}/^{22}\text{Ne}$
SB-13	Clinopyroxenite	Milling	46.7	10.57	0.0333
SB-15	Phoscorite	Milling	31.2	11.96	0.0376
SB-15	Phoscorite	Milling	36.6	11.25	0.035
SB-17	Phoscorite	Milling	8.8	11.37	0.0345
SB-17	Phoscorite	Milling	12.0	10.46	0.0317
SB-37	Carbonatite	Milling	35.1	10.29	0.0307
SB-37	Carbonatite	Milling	62.9	10.87	0.0304
LV-2	Olivinite	Milling	7.6	12.07	0.0382
LV-2	Olivinite	Milling	4.5	10.91	0.0307
KV-23	Phoscorite	Melting	435.6	10.1	0.032
KV-28	Carbonatite	Melting	245.5	11	0.048
SB-32	Carbonatite	Melting	236.5	10.15	0.035
SB-34	*Dolomite	Melting	370.4	10.8	0.04
OV-15	Carbonatite	Melting	288.5	10.4	0.035
KV-23	Carbonatite	Melting (corr)	-	10.25	0.0296
KV-28	Carbonatite	Melting (corr)	-	12.56	0.0337
SB-32	Carbonatite	Melting (corr)	-	10.52	0.0309
SB-34	*Dolomite	Melting (corr)	-	11.37	0.0338
OV-15	Carbonatite	Melting (corr)	-	10.77	0.0310

tures, from 600 to 1100°C. Radiation tracks especially those crossing grain boundaries and/or fluid-bearing vesicles clearly play an important role stimulating $^4\text{He}^*$ loss under low and moderate temperatures.

In contrast to $^4\text{He}^*$, trapped ^3He is dominantly released under rather high temperatures, >1100°C, almost together with destruction of the crystalline lat-

tices. An adequate amount of ^{40}Ar is also released under the same high temperature so that measured $^4\text{He}/^{40}\text{Ar}^*$ ratios are close to this ratio in the magmatic fluid ≈ 3 (Section 4.3.2). Vacuum conditions during step-wise heating experiments shows that large high-temperature portions of ^3He (and relevant portion of $^{40}\text{Ar}^*$) are not accompanied by adequate amounts of the major volatile

Table 5. Helium and argon isotopes in mineral separates from sample SB-3 (gases extracted by melting under 1600°C)

Mineral	Size mm	^4He 10^{-6} cc/g	^3He 10^{-9} cc/g	$^4\text{He}/^3\text{He}$ 10^{-6}	SB-10 mass-fr.
Clinopyroxene	>0.315	186.5	0.207	0.901	0.018
Clinopyroxene	>0.16	375	0.167	2.24	0.037
Olivine I	>0.2	12.6	0.087	0.144	0.001
Olivine I	>0.315	8.9	0.141	0.0628	0.0005
Olivine II	>0.16	50	0.135	0.369	0.0047
Olivine II	>0.2	7.8	0.088	0.0885	0.0005
Olivine II	>0.315	38.4	0.246	0.155	0.0031
Olivine II	>0.4	54.2	0.165	0.327	0.005
Ti-magnetite	>0.16 (3 A)	338	2.74	0.123	0.025
	>0.20 (3 A)	340	2.48	0.136	0.027
	>0.315 (3 A)	250	2.38	0.104	0.017
	>0.315 (6 A)	426	2.41	0.176	0.036

The whole-rock sample has lost less than 0.5 of the radiogenic in-situ produced He, therefore the present-day concentrations of less movable ^3He at least in Ol and Ti-Mgt should be similar to the initial values. In the last column mass-fraction of Perovskite SB-10 is shown; addition of this fraction to the host mineral (col. 1) would explain observed range of ^4He concentrations. A means Ampers: current under which the separation has been performed.

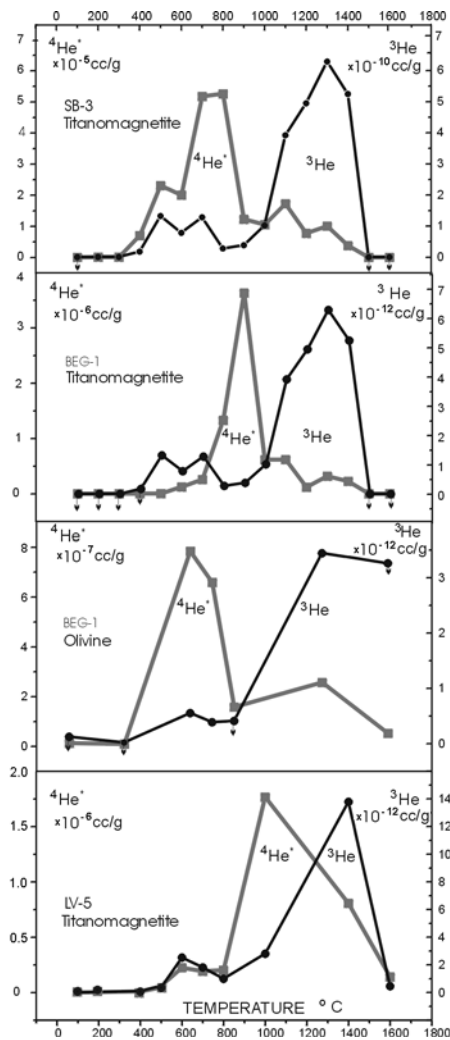


Figure 21. Step-wise heating experiments for magnetites and olivine separated from ultrabasic rocks (see Tables 1-3 for SB-3 and KV-5, and Table 5 for BEG-1). Notice three separated loss events: (1) Low temperature loss which is most probably related to decipitation of large vesicles; both trapped ^3He (see Figures 12, 14) and radiogenic $^4\text{He}^* = ^3\text{He}$ ($^4\text{He}/^3\text{He}_{\text{meas}} - ^4\text{He}/^3\text{He}_{\text{initial}}$) are releasing at this low temperature, $<800^\circ\text{C}$. (2) Preferential loss of $^4\text{He}^*$ from related radiation α -tracks under moderate temperature from 600°C to 1100°C . (3) Preferential loss of ^3He under high temperature, 1400°C . Arrows indicate that the upper limits of ^3He concentrations are shown.

components. The separation calls for extremely small volumes of trapped-He-bearing sites, somewhat between size of He atom and CO_2 molecule.

More work is needed to understand and quantify observations discussed above. However the conclusion on a good trapping capacity and rare gas rateability of magnetites is fortified by the step-wise-heating data.

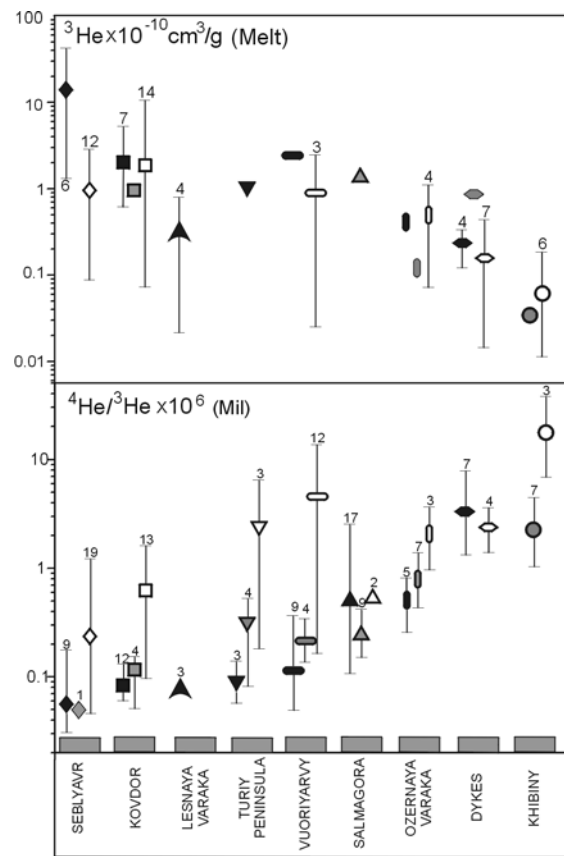


Figure 22. $^4\text{He}/^3\text{He}$ ratios and ^3He concentrations in different rocks and Complexes. Notice variations of both parameters within a factor of 1,000 implying that the rate of melt degassing and subsequent retention of trapped He are the principal factors controlling observed $^4\text{He}/^3\text{He}$ ratios. The parent elements, U and Th, vary on a much narrower scale (Table 3) and cause limited variations of $^4\text{He}/^3\text{He}$ (Figure 23). Solid - ultrabasic, shadowed - alkaline, open - carbonatitic rocks, numbers are numbers of samples.

5.2. Carriers of Mantle Fluids: Rocks and Complexes

Figure 22 reveals the two general tendencies: increasing of $^4\text{He}/^3\text{He}$ ratios in trapped helium (liberated by milling) from basic through alkaline to carbonatitic rocks and elevated ratios in samples from the Ozer-naya Varaka, Khibiny, and Dike Complexes. These tendencies could result from varying post-crystallisation abundances of trapped helium governed by different degassing rates or trapping capacities of host minerals together with subsequent variable contributions of in-situ produced helium. $^4\text{He}/^3\text{He}_{\text{mill}}$ versus $(\text{U}+0.24\text{Th})/^3\text{He}_{\text{mill}}$ plot allows to check this explanation (Figure 23). At first glance low and similar parent/daughter ratios for Kovdor and Seblyavr ultrabasic rocks, and slightly enhanced $^4\text{He}/^3\text{He}_{\text{mill}}$ in

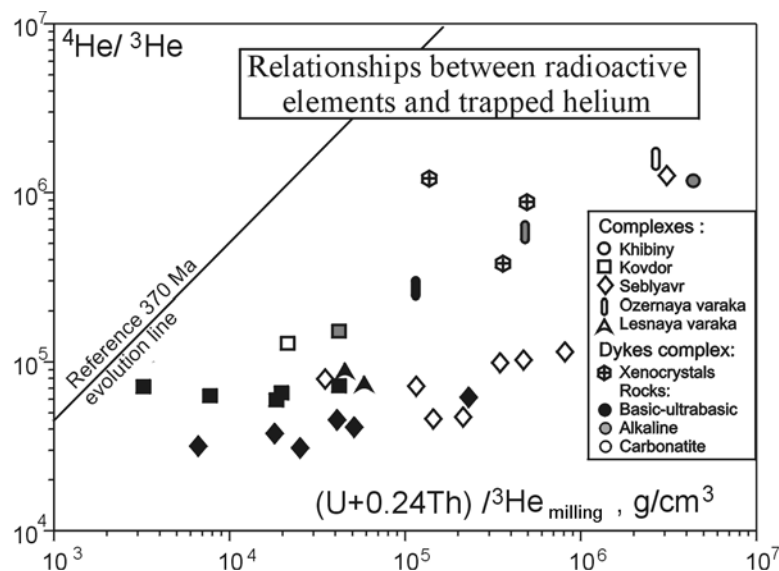


Figure 23. Contribution of radiogenic in-situ produced He in helium extracted from vesicles by milling.

samples from the Kovdor (Figure 23) would have implied an isotopic heterogeneity of trapped helium, in contrast to previous conclusions (Section 4.1.4). However, a more detail look at the data shows, that Kovdor ultrabasic rocks (minerals) had lost a larger portion of radiogenic $^4\text{He}^*$ ($\approx 35\%$) than relevant samples from Sebyavr ($\approx 10\%$). Some portion of $^4\text{He}^*$ releasing from related α -tracks penetrates into vesicles already containing trapped He. A small contribution of this $^4\text{He}^* \sim 0.1$ ($^4\text{He}_{\text{cal}}^* - ^4\text{He}_{\text{meas}}^*$), could ensure the observed enhanced $^4\text{He}/^3\text{He}_{\text{milling}}$ in all but one Kovdor samples. Moreover, this contribution is also recorded by $^4\text{He}_{\text{milling}}/^4\text{He}_{\text{melt}}$ ratios which are higher in the Kovdor samples (the Average $^4\text{He}_{\text{milling}}/^4\text{He}_{\text{melt}} = 0.22$) relative to the Sebyavr (0.037). Enhanced $^4\text{He}/^3\text{He}_{\text{milling}}$ ratios in carbonatites could also result from the particularly low retention of radiogenic $^4\text{He}^*$ in these rocks (see Figure 15) and its partial migration into vesicles.

The data presented in Figure 23 indicate that migration of in-situ produced He and its admixture to trapped He retained in vesicles do increase $^4\text{He}/^3\text{He}_{\text{milling}}$ ratios. While Figure 23 comprises a limited data-set, this mechanism could be responsible for $^4\text{He}/^3\text{He}_{\text{milling}}$ variations within a factor of 1000 seen in Figure 14 and 22 which include all available data. It should be emphasised that a great range of $(\text{U}+\text{Th})/^3\text{He}_{\text{milling}}$ ratios is dominantly due to $^3\text{He}_{\text{milling}}$ variations: U and Th concentrations cluster within a relatively narrow diapason (Section 4.1.4). For example, the average values for ultrabasic rocks from the Sebyavr, $\text{U} = 6.2$ ppm, $\text{Th}/\text{U} = 3.4$, are quite similar to those for the relevant samples from Dykes Complex, $\text{U} = 4.1$ ppm and $\text{Th}/\text{U} = 3.8$

(Table 2), whereas ^3He concentrations in these Complexes differ by ~ 2 orders of magnitude.

Therefore melt degassing and trapping capacities of host minerals appear to be the principal parameters controlling present-day helium isotope composition both in mineral lattices and in vesicles. The compositional array basic \rightarrow alkaline \rightarrow carbonatitic rocks corresponds to the intrusion - crystallisation stages, and also to decreasing densities and viscosities of parent melts. These patterns predict a better degassing of the later intrusive stages, and the increasing $^4\text{He}/^3\text{He}_{\text{milling}}$ ratios along the array, e.g., the Kovdor, Turiy, Vuoriyarvy and Ozeraya Varaka Complexes in Figure 22, are in full accord with this prediction. The degassing conditions during the last carbonatitic intrusion stage appear to be especially variable causing adequate variations of $^4\text{He}/^3\text{He}_{\text{milling}}$ and ^3He (Figure 22). For example, ^3He concentration in Kovdor Vuoriyarvy carbonatites varies within 2 orders of magnitude. A highly variable trapped He concentrations in carbonatites reflect multi-pulse intrusions of these rocks together with different degassing conditions at each pulse.

As it is seen in Figures 11, 14 and 16, the ultrabasic rocks preserve initial $^4\text{He}/^3\text{He}$ ratios better than the others. Figure 22 presents the Complexes in order of increasing average $^4\text{He}/^3\text{He}_{\text{milling}}$ in these rocks. Again the different degassing rate appears to be responsible for increasing of $^4\text{He}/^3\text{He}_{\text{milling}}$ from one Complex to another.

Degassing history is controlled, among other factors, by conditions of crystallisation differentiation in magma chambers, including depths of the chambers. These conditions could be partially restored using geological and

petrographical data: position of intrusions within the cross section of supracrustal rocks, quenching phases near contacts and eruptive breccias in internal parts, fingerprints of explosive processes, structural and textural peculiarities of rocks especially in contact zones.

The above features imply that the Khininy alkaline massif and the Dykes Complex belong to the uppermost subsurface formations [Polkanov and U-Li-Zhen', 1961; Galakhov, 1975]; the dykes are considered as eruptive channels to volcanic explosion fields removed by erosion [Bulakh and Ivannikov, 1984]. This is in full agreement with the low ^3He abundances and the high $^4\text{He}/^3\text{He}$ ratios indicating a substantial pre-crystallisation degassing [Figure 22, see also Figure 14].

In contrast, the Kovdor, Seblyavr, Vuoriyarvy, and Lesnaya Varaka Complexes composed by ultrabasic, alkaline and carbonatitic rocks and showing signatures of hypabyssal intrusions were formed at greater depths [Kukhareenko et al., 1965], in agreement with He isotope data (Figures 23, 14). Mineral - fluid inclusions in early apatites (the Kovdor) recorded the minimal fluid pressure ~ 1500 atm corresponding to ≥ 5 km depth [Sokolov, 1981].

Intermediate depths suggested to other Complexes are considered to be formed at [Kukhareenko et al., 1965]. This agrees with He isotope data for all but one Complex: according to Figure 23, the Tury Peninsula belongs to the least degassed group.

The degassing rate of a Complex could be recorded by the related development of host rocks, i.e., fenitization [Le Bas, 1989]. For example, the Lesnaya Varaka mainly composed by basic rocks with low $^4\text{He}/^3\text{He}$ ratios is surrounded by a thin rim of fenitised rocks which is in contrast to the mainly alkaline Ozernaya Varaka Complex having higher $^4\text{He}/^3\text{He}$ ratio and a thicker rim [Ikorsky et al., 1998].

Resuming, the simplest explanation of the available data envisages two processes: (i) trapping of initially isotopically homogeneous helium ($^4\text{He}/^3\text{He}$ initial $\sim 30,000$) by growing crystals; concentrations of trapped He were controlled by progressive crystallisation, variable degassing and trapping capacities and (ii) subsequent migration of trapped and in-situ produced radiogenic He. Conclusion on a homogeneous pre-crystallisation fluid also followed from study of primary inclusions in silicate rock of the Kovdor Complex [Sokolov, 1981]. Several deep sources of helium having different isotopic compositions are not required to satisfy the data contrary to the inferences from Rb-Sr and Sm-Nd systematics [e.g., Kramm, 1993; Zaitsev and Bell., 1995].

Variable mixing of mantle and crustal materials during the magmatic and early post-magmatic stages followed by trapping of He with variable $^4\text{He}/^3\text{He}$ ratios have not been clearly recorded by the UAC rocks in

contrast to the Monche layered intrusion [Tolstikhin et al., 1991]. However these processes can not be completely ruled out either. Ne isotope mixing array [see Figure 17] and low $^{40}\text{Ar}/^{36}\text{Ar}$ ratios in the mantle end-member (Figure 19 and 20) imply a contribution of air-related component.

5.3. Primordial and Radiogenic He and Ne in Kola UACC, MORB and OIB

The production $^4\text{He}^*/^{21}\text{Ne}^*$ ratio is almost constant independently on natural environments, e.g., U-bearing minerals or ordinary rocks of various composition [Kyser and Reason, 1982; Verkhovsky and Shukolyukov, 1991; Yatsevich and Honda, 1997]. A production ratio is known reasonably well, He-Ne isotope relationships are able to quantify the rate of noble gas elemental fractionation and shed light on related processes [Verkhovsky et al., 1983]. $^3\text{He}/^{22}\text{Ne}_{\text{prim}}$ versus $^4\text{He}^*/^{21}\text{Ne}^*$ plot presents He-Ne relationships for Kola UACC samples along with MORB and OIB data. All ^3He measured in the samples is considered as the primordial component (subscript prim), and $^{22}\text{Ne}_{\text{prim}}$, $^4\text{He}^*$ and $^{21}\text{Ne}^*$ are calculated from equations:

$$^{22}\text{Ne}_{\text{prim}} = \frac{^{22}\text{Ne}_m ({}^{20}\text{Ne}/^{22}\text{Ne}_m - {}^{20}\text{Ne}/^{22}\text{Ne}_{\text{atm}})}{({}^{20}\text{Ne}/^{22}\text{Ne}_{\text{prim}} - {}^{20}\text{Ne}/^{22}\text{Ne}_{\text{atm}})}$$

$$^4\text{He}^* = {}^3\text{He}_m ({}^4\text{He}/^3\text{He}_m - {}^4\text{He}/^3\text{He}_{\text{prim}})$$

$$\begin{aligned} {}^{21}\text{Ne}/^{22}\text{Ne}_{\text{ini}} = & {}^{21}\text{Ne}/^{22}\text{Ne}_{\text{atm}} + \\ & + ({}^{21}\text{Ne}/^{22}\text{Ne}_{\text{prim}} - {}^{21}\text{Ne}/^{22}\text{Ne}_{\text{atm}}) \times \\ & \times [({}^{20}\text{Ne}/^{22}\text{Ne}_m - {}^{20}\text{Ne}/^{22}\text{Ne}_{\text{atm}}) / \\ & / ({}^{20}\text{Ne}/^{22}\text{Ne}_{\text{prim}} - {}^{20}\text{Ne}/^{22}\text{Ne}_{\text{atm}})] \end{aligned}$$

$$^{21}\text{Ne}^* = {}^{22}\text{Ne}_m ({}^{21}\text{Ne}/^{22}\text{Ne}_m - {}^{21}\text{Ne}/^{22}\text{Ne}_{\text{ini}})$$

where subscripts m, atm and ini define measured, atmospheric and initial values, respectively. The relevant primordial isotope compositions are considered to be solar [Anders and Grevesse, 1989] and the calculated initial values depend on proportion of mixing of solar and atmospheric species in each individual sample. In contrast to almost constant production $^4\text{He}^*/^{21}\text{Ne}^*$ ratio, the measured ratios of both radiogenic and primordial species vary within 4 orders of magnitude and correlate. The primordial nuclides, ^3He and $^{22}\text{Ne}_{\text{prim}}$, were stored in a less degassed mantle reservoir since the earth accretion, 4.5 Ga [O'Nions and Oxburgh, 1983; Kellogg and Wasserburg, 1990; O'Nions and Tolstikhin, 1994, 1996]. The radiogenic nuclides, $^4\text{He}^*$ and $^{21}\text{Ne}^*$, were mainly produced within the upper mantle reservoir having much higher $(\text{U}+0.24\text{Th})/{}^3\text{He}$ ratio than the less degassed mantle [O'Nions and Tolstikhin, 1994]. Estimates of the mean residence time of a highly incompatible elements in the upper mantle results in ≈ 1

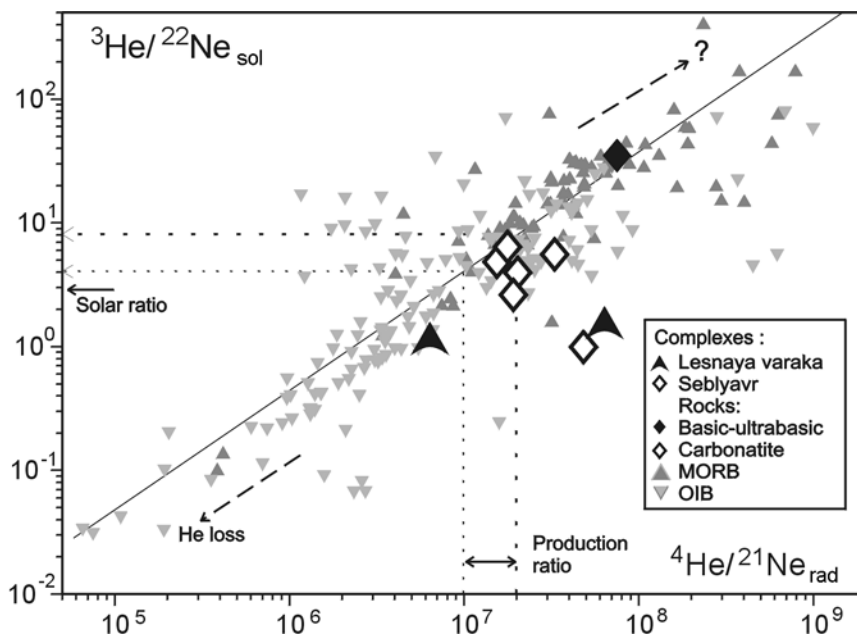


Figure 24. A comparison of primordial and radiogenic He and Ne isotope abundances in samples from Kola UACC, MORB and OIB.

While the ${}^4\text{He}^*/{}^{21}\text{Ne}^*$ production ratio is almost constant, this ratio and the ratio between primordial species vary within a great range which can be approximated by a straight line. Projection of the production ratio via the approximation line to the primordial ratio indicates ${}^3\text{He}/{}^{22}\text{Ne}$ similar to the actual solar value implying solar-like ${}^3\text{He}/{}^{22}\text{Ne}$ in the mantle before the fractionation. Possible mechanisms responsible for the fractionation are discussed in the text.

Ga [Galer and O'Nions, 1985; Kellogg and Wasserburg, 1990; O'Nions and Tolstikhin, 1994, 1996]. These time constraints imply that the direct correlation in Figure 24 should result from fractionation process(es) occurred only slightly before, during or even after the gases were trapped by solids: otherwise the ratios between ancient (${}^3\text{He}$, ${}^{22}\text{Ne}_{\text{prim}}$) and young (${}^4\text{He}^*$ and ${}^{21}\text{Ne}^*$) species would not have correlated.

The straight line shown in Figure 24 reasonably well fit the correlation; the product of the slope of this line, 3.5×10^{-7} , and the mean ${}^4\text{He}^*/{}^{21}\text{Ne}^*$ production ratio, 1.5×10^{-7} , allows the initial ${}^3\text{He}/{}^{22}\text{Ne}_{\text{prim}}$ ratio (preceded the fractionation) to be recovered, ${}^3\text{He}/{}^{22}\text{Ne}_{\text{prim}} \approx 5$, which is similar to the solar system primordial ratio ≈ 3 [Anders and Grevesse, 1989]. The similarity envisages the unfractionated solar-like primordial gases in the less degassed reservoir, in accord with inferences from steady-state models of layered mantle [e.g., O'Nions and Tolstikhin, 1994]. The samples from Kola UACC do not deviate far from the production/primordial ratio (Figure 24) in contrast to those from MORB and OIB. A substantial decrease of He/Ne ratios (relative to the primordial/production values) could result out of preferential migration of He isotopes from fluid inclusions in OIB and MORB samples. He shows much higher penetrability through silicates than Ne and Ar [Morozova

and Ashkinadze, 1971; Ashkinadze, 1980] and specifically through silicate glasses, major noble gas hosts in ocean ridge and seamount environments. While He is migrating from the inclusions through basalt glass into free fluids, the residual He/Ne ratios are decreasing.

A 50 fold increase of He/Ne ratios requires a special explanation. Such a trend could originate from partial melts degassing owing to the better solubility of He in silicate melts than the solubilities of heavier gases [Jambon et al., 1986; Lux, 1987]. Noble gas partitioning among solid, gas and silicate melt in a magma chamber is described as [Spasennykh and Tolstikhin, 1993]:

$$L_m = (L_n)^{\frac{(S_m + b/RT + S_m f K_m)}{(S_n + b/RT + S_n F K_n)}}$$

where L_n and L_m are final over initial concentration ratios for species m and n , and S , b , R , T , F and K in the power are the solubility, the volume gas/melt ratio, the Boltzman gas constant, the temperature, the volume solid/melt ratio, and the solid/melt partition coefficient, respectively. The maximal fractionation would be expected if $b \rightarrow 0$, $K \rightarrow 0$, and for the conventional solubility [cc/(g atm)] $S(\text{He}) = 0.0006$ and $S(\text{Ne}) = 0.00025$ [Jambon et al., 1986, Lux, 1987] the required 50-fold increase of He/Ne ratio could originate if $\geq 95\%$ of He had been lost from degassing melts and only $\leq 5\%$

retained. At first glance such rate of degassing seems reasonable. However analysis of the data presented in Figure 24 shows that among 250 data-points, 50 samples having highest ^3He concentrations, $> 1 \times 10^{-10}$ cc STP g^{-1} , all deviate to the right-top off the production/primordial ratios. The ratio of this concentration and the helium retention coefficient predicted by fractional degassing (≤ 0.05) gives the expected ^3He concentration in undegassed melts, $\geq 2 \times 10^{-9}$ cc STP g^{-1} or even $\geq 2 \times 10^{-8}$ cc STP g^{-1} for the most ^3He -rich MORB glasses. These values are by 10 to 100 times exceed the initial ^3He abundance in basaltic melts estimating from steady-state and evolutionary degassing models $(5.6 \pm 3) \times 10^{-10}$ cc STP g^{-1} [Tolstikhin and Marty, 1998]. Also the present day production of the oceanic crust, 6×10^{16} g a^{-1} [Crisp, 1984; Reimer and Schubert, 1984], and ^3He flux into the oceans, 2.24×10^7 cc STP a^{-1} [Craig et al., 1975; Farley et al., 1995], give ^3He concentration in MORB melts at 3.56×10^{-10} cc STP g^{-1} , similar to the above estimation but at least an order of magnitude less than that required to satisfy the fractional degassing hypothesis. The preferential helium diffusion from vesicles through silicate glasses proposed above produces high $^4\text{He}/^{21}\text{Ne}^*$ ratios in a complementary pore fluid phase. Helium concentrations in pore fluids could be by an orders of magnitude higher than those in the fluid-bearing rocks [e.g., Tolstikhin et al., 1996]. If the fluid would have been trapped into “secondary” inclusions of host rocks/minerals, ^4He concentrations and $^4\text{He}/^{21}\text{Ne}^*$ ratios could both be high in a qualitative accord with the data. Also a non-equilibrium degassing process, when He migrates into ascending bubbles faster than Ne, could be responsible for the enhanced He/Ne ratios. More work is needed to understand and quantify this alternative mechanism.

5.4. Mantle Sources of Plume-related Component

Similar isotopic and chemical characteristics of small-volume continental magmas, including alkaline melts, and alkali basalts from small oceanic islands or seamounts calls for related source(s) and processes involved. While both asthenospheric [Nelson et al., 1988; Kwon et al., 1989] and lithospheric [McKenzie and O’Nions, 1995] source regions were suggested using isotopic arguments, models of carbon- and alkali-rich melt generation and development generally envisaged a metasomatically enriched lithospheric source [Wyllie et al., 1990]. The following discussion agrees with the model [McKenzie and O’Nions, 1995] which reconciled isotopic, geochemical, geochronological and geophysical data. The model envisages: (i) the subcontinental lithosphere including a MORB-source-like bottom layer and a depleted (relative to the MORB source) layer above as the most plausible environments, and (ii) processing of these lay-

ers by addition of 10 to 30 % of a metasomatic melt originated by extraction of $\sim 0.3\text{--}0.5$ % melt from the MORB-source asthenospheric mantle. Because the subcontinental lithosphere is a long-life conservative reservoir [e.g., Kramers, 1979, 1991; Richardson, 1984], time interval between the metasomatic processing and the mobilisation of parent alkaline magmas (intruded into the continental crust) or detachment of the processed domains (entrained into the thermal convection within the asthenospheric mantle) could be long and variable which allows enriched (relative to the MORB) isotopic signatures to be generated.

This time interval is crucial to constraint the ^3He -bearing source for parent melts of the Kola UAC Complexes. It should be emphasised that both trace-element- [McKenzie and O’Nions, 1995] and major-element-related [Wyllie et al., 1990] models do not envisage a deep-mantle plume-like source for the metasomatic low-partial-melting melts. In the past the upper mantle could also show lower $^4\text{He}/^3\text{He}$ ratios due to e.g. a higher flux of ^3He rich material from the lower mantle. To understand whether the ancient upper mantle could be a source of the metasomatic low $^4\text{He}/^3\text{He}$ -melts, the age when this reservoir has had $^4\text{He}/^3\text{He}$ ratio similar to that in parent melts of Kola Devonian UACC should be compared with the age of metasomatism inferring from other isotopic systematics, e.g., Rb-Sr or Sm-Nd.

Figure 25 comprises $^4\text{He}/^3\text{He}$ upper mantle evolutionary trends compiled from several recent degassing models. While segments of the trends related to the early earth are different depending on assumptions involved, all post-3-Ga segments show higher $^4\text{He}/^3\text{He}$ ratios than that obtained above for UACC (Section 4.1.1, see Figure 16). The model-derived upper mantle $^4\text{He}/^3\text{He}$ ratios were similar to those initial for Kola UAC rocks approximately 3 Ga ago.

In contrast to the above quite ancient age, a shorter metasomatism-extraction interval is inferred from Rb-Sr systematics. Sr isotope composition of UAC Complexes is well constraint by Rb-Sr isochrone dating and low Rb/Sr rocks/minerals, such as apatites or carbonatites: initial $^{87}\text{Sr}/^{86}\text{Sr}$ varies from within 0.7030 – 0.7040 exceeding the present day average normal MORB ratio 0.7024 [Ito et al., 1987]. The average Rb/Sr of highly differentiated UAC Complexes appears to be less reliable. Two values suggested by Gerasimovsky [1966] for the Lovozero massif, Rb/Sr ≈ 0.377 [see also Kramm et al., 1993], and by Kukharensko et al. [1984] for the Khibiny ≈ 0.15 are available. These estimates together with the model Sr isotope evolution trend for the upper mantle [Azbel and Tolstikhin, 1988] give the model age of the upper mantle metasomatism within 420 - 700 Ma, substantially less than that predicted by U-He systematics. This difference rules out the upper mantle as a source of He-bearing $\leq 700\text{-Ma}$ -old material and

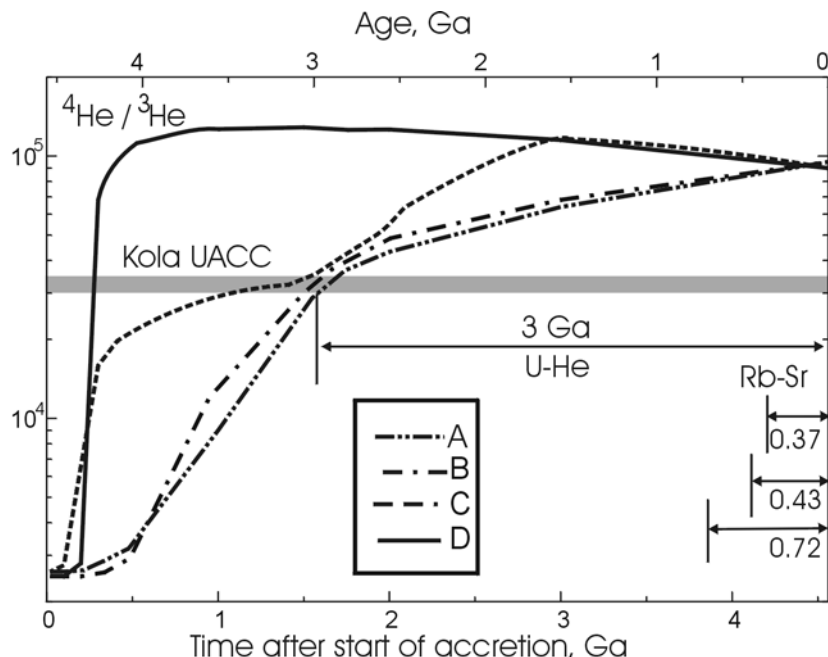


Figure 25. Model evolutionary trends for $^4\text{He}/^3\text{He}$ ratio in the upper mantle. All models outlined below envisage: the upper mantle as severely degassing reservoir; the parent elements are accumulating into the continental crust growing through time as in [Kramers and Tolstikhin, 1998]. $^4\text{He}/^3\text{He}$ ratios in the upper mantle were similar to those trapped by the UACC ~ 3 Ga ago or earlier, in contrast to the age of mantle metasomatism derived from Rb-Sr systematics, 0.43 - 0.72 Ga, depending on accepted Rb/Sr, $^{87}\text{Sr}/^{86}\text{Sr}_{\text{initial}}$ and models of Sr isotope compositions in the upper mantle, i.e., at most 350 Ma before the formation age of the Complexes, 370 Ma (Section 2). Models: A - a completely isolated (during whole history of the earth) lower mantle having the bulk silicate earth concentrations of U and Th [Azbel and Tolstikhin, 1992]; B - a moderately degassed lower mantle having ignorantly low abundances of the parent elements [O'Nions and Tolstikhin, in preparation]; the model is similar to that suggested by Albarede (1998); C - a moderately degassed substantially isolated lower mantle having the bulk earth abundances of the parent elements; this model satisfies the Pu-U-I-Xe systematics [O'Nions and Tolstikhin, in preparation]; D - same as C but satisfies to U-Th-K-He-Ne-Ar systematics [Tolstikhin and Marty, 1998].

suggests the lower mantle (or its stagnant less-degassed domain) as a host reservoir for primordial rare gases in UACC.

Available model estimates of noble gas abundances in the principal terrestrial reservoirs [Tolstikhin and Marty, 1998] allow contribution of the three reservoirs,

the lower mantle, the upper mantle, and the crust (represented by groundwater containing presumably atmospheric gases) to be quantified (Table 6). A minor contribution from the less degassed reservoir imply that the plume itself only stimulated metasomatism of the subcontinental lithosphere and the major role in this

Table 6. Contribution of principal terrestrial reservoirs to plume source

Reservoir	Contribution (by weight %)	^{22}Ne 10^{-14} mole/g	$^{20}\text{Ne}/^{22}\text{Ne}$	$^{21}\text{Ne}/^{22}\text{Ne}$ lm	$^4\text{He}/^3\text{He}$ 10^6	$^{40}\text{Ar}/^{36}\text{Ar}$ lm	$^3\text{He}/^{22}\text{Ne}$	$^{36}\text{Ar}/^{22}\text{Ne}$
Lower mantle (lm)	1.8	6.05	13.7	0.0336	0.0055	5300	5.6	1.82
Upper mantle	98.2	0.07	13.7	0.0596	0.09	40000	5.56	5.34
Fresh water	0.06	95	9.8	0.0289	100	296	0	80
Plume calculated	100	-	12.7	0.04	0.036	3200	4.23	21.1
Plume observed	-	-	12.6	0.04	0.03	3400	6.8	<38

processes belongs to melts from the upper mantle, in accordance with recent geochemical and petrological models [Wyllie *et al.*, 1990; McKenzie and O'Nions, 1995].

Acknowledgements. Partially supported by INTAS Grant 94-2621 and by Project 3461 from Russian Academy of Sciences. All authors greatly appreciate the contribution by Rita Vetrina in preparing of the manuscript.

References

- Albarede F., Time-dependent models of U-Th-He and K-Ar evolution and the layering of mantle convection. *Chemical Geol.* 145, 413–429, 1998.
- Allegre C. J., T. Staudacher, and P. Sarda, Rare gas systematics: formation of the atmosphere, evolution and structure of the Earth's mantle. *Earth Planet. Sci. Lett.* 81, 127–150, 1986.
- Amelin YU. V., and Semenov V. S., Nd and Sr isotopic geochemistry of mafic layered intrusions in the eastern Baltic Shield: implications for the evolution of Paleoproterozoic continental mafic magmas. *Contrib. Mineral. Petrol.* 124, 255–272, 1996.
- Amelin YU. V., Heaman L. M., and Semenov V. S., U-Pb geochronology of layered mafic intrusions in the eastern Baltic Shield: implications for the timing and duration of Paleoproterozoic continental rifting. *Precamb. Res.* 75, 31–46, 1995.
- Andersen T., Mantle and crustal components in a carbonatite Complex, and the evolution of carbonatite magma: REE and isotopic evidence from the Fen Complex, Southeast Norway. *Chem. Geol. (Isot. Geosci. Sect.)* 65, 147–166, 1987.
- Anders E. and Grevesse N., Abundances of the elements: Meteoritic and solar. *Geochim. Cosmochim. Acta* 53, 197–214, 1989.
- Arzamastseva L. V., Arzamastsev A. A., Ultrabasic fooidolites in alkaline massifs of the Kola region: estimate of phosphate capacity. In: *Alkaline magmatism of NE part of the Baltic shield* (ed. T. N. Ivanova), Kola Sci Centre of USSR Acad. Sci. 26–37, 1990, (in Russian).
- Arzamastseva L.V., Balaganskaya E.G., Pavlov V.P., Prichapkin V.A. and Shpachenko A.K., *New data on apatite deposits of Khibina. In Apatite capacity of alkaline massifs of the Kola region* (ed. O. B. Dudkin). Kola Sci Centre of USSR Acad. Sci., 47–67, 1991, (in Russian).
- Azbel I.Ya. and Tolstikhin I.N., *Radiogenic isotopes and the evolution of the earth's mantle, crust and atmosphere.* Kola Sci. Centre Pub. 140 p., 1988, (in Russian).
- Azbel I.Ya. and Tolstikhin I.N., Geodynamism, magmatism and degassing of the earth. *Geochim. Cosmochim. Acta* 54, 139–154, 1992.
- Balaganskaya E. G., Breccias of Kovdor phosphorite-carbonatite deposit of Fe - ore and their geological significance. *Zapiski VMO*, 2, 21–36, 1994, (in Russian).
- Balaganskaya E. G. and Savchenko E. E., Perovskite in rocks of ijolite - urtite arc of Khibina massif. *Zapiski. VMO*, 1, 85–96, 1998, (in Russian).
- Balashov Yu. A., Mitrofanov F. P. and Balagansky V. V., *New geochronological data on Archaean rocks of the Kola Peninsula. Correlation of Precambrian formations of the Kola-Karelian region and Finland* (Eds. V. V. Balagansky, F. P. Mitrofanov), Kola Sci Centre of USSR Acad. Sci. 13–34, 1992.
- Balashov Yu. A., Bayanova T. B., and Mitrofanov F. P., Isotope data on the age and genesis of layered basic-ultrabasic intrusions in the Kola Peninsula and northern Karelia, north-eastern Baltic Shield. *Precamb. Res.* 64, 197–205, 1993.
- Bayanova T. B., Kirnarsky Y. M., and Levkovich N. V., U-Pb study of baddeleyite from the Kovdor massif. *Doklady RAS* 356, 509–511, 1997.
- Beard A. D., Downes H., Vetrin V., Kempton P. D., Maluski H., Petrogenesis of Devonian lamprophyre and carbonatite minor intrusions, Kandalaksha Gulf (Kola Peninsula, Russia), *Lithos* 39, 93–119, 1996.
- Beard A. D., Downes H., Hegner E., Sablukov S. M., Vetrin V. R., and Balogh K., Mineralogy and geochemistry of Devonian ultramafic minor intrusions of the southern Kola Peninsula, Russia: implications for the petrogenesis of kimberlites and melilitites. *Contrib. Mineral. Petrol.* 130, p. 288–303, 1998.
- Belkov I.V. (Editor), *Evolution of Earth's crust and endogenous metallogenic zonation in NE part of Baltic Shield.* Nauka, 109, 1987. (in Russian).
- Bell K. and Blenkinsop J., Neodymium and strontium isotope geochemistry of carbonatites. In: *Carbonatites: Genesis and Evolution* (editor K. Bell). Unwin Hyman 278–299, 1989.
- Berthelsen A., and Marker M., Tectonics of the Kola collision suture and adjacent Archaean and Early Proterozoic terrains, the north-eastern region of the Baltic Shield. *Tectonophysics* 126, 31–55, 1986.
- Borodin L.S., Nephelinization of pyroxenites and paragenesis of rock-forming minerals of ijolite from massifs of ultrabasic-alkaline rocks. In: *Physical-chemical problems of formation of rocks and minerals* (Ed. G. A. Sokolov), USSR Acad. Sci., 1, 187–199, 1961, (in Russian).
- Bulakh A. T., and Ivannikov V. V., *Problems of mineralogy and petrology of carbonatites.* Leningr. St. Univ., 244 p., 1984. (in Russian).
- Craig H., Clarke W. B., and Beg M. A., Excess ^3He in deep water on the east Pacific rise. *Earth Planet. Sci. Lett.* 26, 125–132, 1975.
- Crisp J. A., Rates of magma emplacement and volcanic output. *J. Volcanol. Geotherm. Res.* 20, 177–211, 1984.
- Dudkin O. B., and Kirnarsky Yu. M., Complex of deposits of Kovdor massif. *Geologiya Rudnich Mestorozdeniy*, 36, 31–41, 1994. (in Russian).
- Dudkin O. B., Savitsky A. V., and Kuleshov G. V., Mineral associations of alkaline rock Complex of Ozernaya Varaka massif. In: *Mineral Complexes and minerals of the Kola Peninsula* (Ed. I. V. Belkov). Kola Branch of USSR Acad. Sci. 126–140, 1980. (in Russian).
- Dudkin O. B., Minakov F. V., Kravchenko M. P., Kravchenko

- E. V., Kulakov A. N., Polezhaeva L. I., Pripachkin V. A., Pushkarev Yu. D., and Rjungenen G. I., *Carbonatites of Khibina*. Kola Branch of USSR Acad. Sci., 98 p., 1984. (in Russian).
- Evdokimov M. D., *Fenites of Turiy alkaline Complex of the Kola Peninsula (mineral associations and geochemical features)*. Nauka, 248 p., 1982. (in Russian).
- Farley K. A., Maier-Reimer E., Schlosser P., and Broecker W. S., Constraints on mantle ^3He fluxes and deep-sea circulation from an oceanic general circulation model. *J. Geophys. Res.* 100 (B3), 3829–3839, 1995.
- Galakhov A. V., *Petrology of Khibina alkaline massif*. Nauka, 256 p., 1975. (in Russian).
- Galakhov A. V., Khibina massif - a complicate multichambers intrusive of central type. *Dokl. USSR Acad. Sci.* 302, 673–675, 1988. (in Russian).
- Galer S. J. G. and O'Nions R. K., Residence time of thorium, uranium and lead in the mantle and implications for mantle convection. *Nature* 316, 778–782, 1985.
- Gerling E. K., Tolstikhin I. N., Drubetskoy E. R., Levkovsky R. Z., Sharkov E. V. and Kozakov I. K., Helium and argon isotopes in rock-forming minerals. *Geokhimiya*, 11, 1603–1611, 1976. (in Russian).
- Gogol O. V. and Delenitsin A. A., Rb-Sr data for diamond-bearing kimberlites and alkaline massifs in NE Fennoscandia. Submitted, 1999.
- Gogol O. V., Bayanova T. B., Balaganskaya E. G., and Delenitsin A. A., Duration of the Paleozoic plume in the Northeastern Baltic Shield (from Rb-Sr and U-Pb isotope data). ICOG-9, Beijing, China, *Chinese Science Bulletin*, 43, 45, 1998.
- Gorschkov G. V., Zjabkin V. A., Ljatkovskaya N. M., and Tsvetkov O. S., *Natural neutron background of atmosphere and Earth's crust*. Atomizdat, 410 p., 1966. (in Russian).
- Grunenfelder M. H., Tilton G. R., Keith B., and Blenkinsop J., Lead and strontium isotope relationships in the Oka carbonatite Complex, Quebec. *Geochim. et Cosmochim. Acta* 50, 461–468, 1986.
- Hawkesworth C. J., Kempton P. D., Rogers N. W., Elam R. M. and van Alsteren P. W., Continental mantle lithosphere, and shallow level enrichment processes in the Earth's mantle. *Earth Planet. Sci. Lett.*, 96, 256–258, 1990.
- Hiyagon H., Ozima M., Marty B., Zashu Z. and Sakai H., Noble gases in submarine glasses from mid-oceanic ridges and Loihi seamount: Constraints on the early history of the earth. *Geochim. Cosmochim. Acta* 56, 1301–1316, 1992.
- Honda M., McDougall I., Patterson D. B., Doulgeris A. and Clahue D., Possible solar noble gas component in Hawaiian basalts. *Nature*, 349, 149–151, 1991.
- Honda M., McDougall I., Patterson D. B., Doulgeris A., and Lague D. A., Noble gases in submarine pillow basalt glasses from Loihi and Kilauea, Hawaii: A solar component in the earth. *Geochim. Cosmochim. Acta* 57, 859–874, 1993.
- Ikorsky S. V., and Kusth V. D., Nitrogen in fluid inclusions of alkaline rocks of Khibina massif and method of its chromatographic determination. *Geochimija*, 7, 962–970, 1992. (in Russian).
- Ikorsky S. V., Kamensky I. L., and Nivin V. A., Helium isotopic variations in the Paleozoic (380–360 Ma) Complexes of the Kola Alkaline Province: High $^3\text{He}/^4\text{He}$ ratios age sings of Devonian mantle plume?. *EUG-9*, Strasbourg, 56 p., 1997.
- Ikorsky S. V., Kamensky I. L., and Nivin V. A., Mamanov V. P., Juvenile helium migration into host rocks during formation of alkaline-ultramafic central type intrusions (on an example of Ozeraya Varaka massif, Kola Peninsula) *Dokl. Akad. Nauk RAS* 362, 242–244, 1998. (in Russian).
- Ito E., White W. M. and Gopel C., The O, Sr, and Pb isotope geochemistry of MORB. *Chem. Geol.* 62, 157–176, 1987.
- Ivanova T. N., Dudkin O. B., Kozireva L. V., and Poljakov K. I., *Ijolite-urtites of Khibina Tundra*. Nauka 179 p., 1970. (in Russian).
- Jambon A., Weber H. and Braun O., Solubility of He, Ne, Ar, Kr and Xe in basalt melt in the range 1250 - 1600°C. Geochemical implications. *Geochim. Cosmochim. Acta* 50, 401–408, 1986.
- Jochum K. P., Hofmann A. W., Ito E., Seufert H. M. and White W. M., K, U and Th in mid-ocean ridge basalt glasses and heat production, K/U and K/Rb in the mantle. *Nature* 306, 431–436, 1983.
- Kalinkin M. I., Arzamastsev A. A., and Poljakov I. V., Kimberlites and related rocks of the Kola Region. *Petrologija*, 1, 205–214, 1993. (in Russian).
- Kamensky I. L., Tolstikhin I. N., Sharkov I. V., and Pushkarev Yu. D., The first results of measuring helium isotopic composition on single-cascade mass-spectrometer MI-1201. *Geokhimiya*, 3, 439–443, 1984. (in Russian).
- Kaneoka I., Takaoka N., and Upton B. G. J., Noble gas systematics in basalts and a dunite nodule from Reunion and Grand Comore Islands, *Indian Ocean*. *Chem. Geol.*, 59, 35–42, 1986.
- Kellogg L. H. and Wasserburg G. H., The role of plumes in mantle helium fluxes. *Earth Planet. Sci. Lett.* 99, 276–289, 1990.
- Kogarko L. N., Kononova V. A., Orlova M. P., and Woolley A. R., *Alkaline Rocks and Carbonatites of the World*. Chapman and Hall, 230 p., 1995.
- Kramers J. D., Lead, uranium, strontium, potassium and rubidium in inclusion-bearing diamonds and mantle derived xenoliths from Southern Africa. *Earth Planet. Sci. Lett.* 42, 58–70, 1979.
- Kramers J. D., Paradoxes of the mantle lithosphere underneath Archaean continents and models for its origin. *Schweiz. Mineral. Petrogr. Mitt.* 71, 175–186, 1991.
- Kramers J. D. and Tolstikhin I. N., Two major terrestrial Pb isotope paradoxes, forward transport modelling, core formation and the history of the continental crust. *Chem. Geol.* 139, 75 – 110, 1998.
- Kramm U., Mantle components of carbonatites from the Kola alkaline province, Russia and Finland: a Nd-Sr study. *Europe J. Miner.* 5, 985–989, 1993.
- Kramm U., and Kogarko L. N., Nd and Sr isotope signatures of the Khibina and Lovozero apaitic centres, Kola Alkaline Province. Russia. *Lithos* 32, 225–242, 1994.
- Kramm U., Kogarko L. N., Kononova V. A. and Vartiainen H., The Kola Alkaline Province of the CIS and Finland:

- Precise Rb-Sr ages define 380–360 Ma age range for all magmatism. *Lithos* 30, 33–44, 1993.
- Kratz K. O. (Editor), *Earth's crust of Eastern part of the Baltic Shield*. Nauka, 232., 1978. (in Russian).
- Kukharenko A. A., Alkaline magmatism in Eastern part of the Baltic Shield. *Zapiski VMO* 5, 547–566, 1967. (in Russian).
- Kukharenko A. A., Orlova M. P., Bulakh A. G., Bagdasarov E. A., Rimskaya-Korsakova O. M., Nefedov E. I., Il'insky G. A., Sergeev A. S., and Abakumova N. B., *Kaledonian Complex of ultrabasic, alkaline rocks and carbonatites of Kola Peninsula*. Nedra, 772 p., 1965. (in Russian).
- Kukharenko A. A. and Il'insky G. A., Corrected data on average concentrations of elements in rocks of the Khibiny massif. *Zap. Vses. Miner. Ob. CXIII* 4, 393–397, 1984.
- Kwon S.-T., Tilton G. R., and Grunefelder M. H., Lead isotope relationships in carbonatites and alkalic complexes: An overview. In: *Carbonatites: Genesis and Evolution* (editor K. Bell). Unwin Hyman 360–387, 1989.
- Kyser T. K. and Rison W., Systematics of rare gas isotopes in basic lavas and ultramafic xenoliths, *J. Geophys. Res.* 87, 5611–5630, 1982.
- Le Bas M. J., Nephelinites and carbonatites In: Fitton J. G. and Upton B. G. (eds) *Alkaline Igneous Rocks Geol. Soc. Special Publications* 30, 53–83, 1987.
- Le Bas M. J., Diversification of carbonatite In: K. Bell (ed) *Carbonatites: Genesis and Evolution*. Unwin Hyman 428–446, 1989.
- Levchenkov O. A., Levsky L. K., Nordgulen O., Dobizhinetskaya L. F., Vetrin V. R., Cobbing J., Nilsson L. P., and Sturt B., U-Pb zircon ages from Sorvaranger, Norway, and the western part of the Kola Peninsula, *Russia. Nor. Geol. Unders. Special Publ.* 7, 29–47, 1995.
- Lux G., The behaviour of noble gases in silicate liquids: solution, diffusion, bubbles and surface effects, with implications to natural samples. *Geochim. Cosmochim. Acta* 51, 1549–1560, 1987.
- Mamyrin B. A. and Tolstikhin I. N., *Helium isotopes in nature*. Elsev. Sci. Publish. B.V. 273 p., 1984.
- Marty B., Neon and xenon isotopes in MORB: implications for the Earth-atmosphere evolution. *Earth Planet. Sci. Lett.*, 94, 45–56, 1989.
- Marty B. and Humbert F., Nitrogen and argon isotopes in oceanic basalts, *Earth Planet. Sci. Lett.* (In press), 1997.
- Marty B. and Tolstikhin I. N., CO₂ fluxes from mid-ocean ridges, arcs and plumes. *Chemic. Geol.* 145, 233–248, 1998.
- Marty B., Tolstikhin I., Kamensky I. L., Nivin V., Balagan-skaya E., and Zimmermann J.-L., Rare gas systematics of 380 Ma carbonatites from the Kola region, Russia: Evidence for a deep plume origin and constraints on the rare gas state of the mantle. *Earth Planet. Sci. Lett.*, accepted, 1999.
- McKenzie D. and O'Nions R. K., *The source regions of ocean Island basalts*. Oxford Univ. Press. 133–159, 1995.
- Mitrofanov F.P., (ed.). *Geology of the Kola Peninsula*. Ap- atity, 145 p., 1995.
- Mitrofanov F. P., Ikorsky S. V., and Kamensky I. L., He isotopes in Paleozoic alkaline intrusives of Kola Peninsula and Northern Karelija. *Dokl. Russian Acad. Sci.* 345, 243–246, 1995. (in Russian).
- Moreira M., Staudacher Th., Sarda Ph., Schilling J.-G. and Allegre C. J., A primitive plume neon component in MORB: the Samoa ridge-anomaly, South Atlantic, 51–52°S). *Earth Planet. Sci. Lett.* 133, 367–377, 1995.
- Morozova I. M., and Aschkinadze G. Sch., *Migration of rare gas atoms in minerals*. Nauka, 120 p., 1971. (in Russian).
- Morrison P. and Pine J., Radiogenic origin of the helium isotopes in rocks. *Ann. N.Y. Acad. Sci.* 62, 69–92, 1955.
- Nelson D. R., Chivas A. R., Chappell B. W. and McCulloch M. T., Geochemical and isotopic systematics in carbonatites and implications for the evolution of ocean-island sources. *Geochim. et Cosmochim. Acta* 52, 1–17, 1988.
- O'Nions R. K. and Oxburgh E. R., Heat and helium in the Earth. *Nature* 306, 29–432, 1983.
- O'Nions R. K. and Tolstikhin I. N., Behaviour and residence times of lithophile and rare gas tracers in the upper mantle. *Earth and planetary science letters* 124, 131–138, 1994.
- O'Nions R. K. and Tolstikhin I. N., Limits on the mass flux between lower and upper mantle and stability of layering. *Earth Planet. Sci. Lett.* 139, 213–222, 1996.
- Orlova M. P., Melilite rocks of Salmagora massif (Kola Peninsula). Information issue of Vses. Geol. Inst., N7, *Petrographija*, 67–79, 1959. (in Russian).
- Ozima M. and Zashu S., Noble gases in submarine pillow volcanic glasses. *Earth Planet. Sci. Lett.* 62, 24–40, 1983.
- Ozima M. and Zahnle K., Mantle degassing and atmospheric evolution: Noble gas view. *Geochem. J.* 27, 185–200, 1993.
- Panina L. I., Temperature conditions on crystallization of Salmagora ijolite massif (Kola Peninsula). In: *Termobarochimistry and genetic mineralogy* (Ed. Yu. A. Dolgov), Siberian Depart. of USSR Acad. Sci. 55–58, 1975. (in Russian).
- Polkanov A. A., and U Li Jen, On genesis and evolution of alkaline magma of Khibina subvulkano. Questions of geochronology and geology. *USSR Acad. Sci.*, 12, 176–186, 1961. (in Russian).
- Porcelli D. and Wasserburg G. J., Mass transfer of helium, neon, argon and xenon through a steady-state upper mantle. *Geochim. Cosmochim. Acta* 59, 4921–4937, 1995.
- Poreda R. J. and Farley K. A., Rare gases in Samoan xenoliths. *Earth Planet. Sci. Lett.* 113, 129–144, 1992.
- Poreda R. J. and Radicati Di Brozzolo F., Neon isotopic variation in Mid-Atlantic Ridge basalts. *Earth Planet. Sci. Lett.* 69, 277–289, 1984.
- Pushkarev Yu. D., *Megacycles of crust - mantle evolution*. Nauka, 216 p., 1990. (in Russian).
- Richard D., Marty B., and Chaussidon M., Helium isotopic evidence or a lower mantle component in depleted Archean komatiite. *Nature* (submitted), 1996.
- Richardson S. H., Gurney J. J., Erlank A. J., and Harris J. W., Origin of diamonds in old enriched mantle *Nature* 310, 198–202, 1984.
- Samoilov V. S. and Afanas'ev B. V., New data about carbonatites from alkaline-ultrabasic complex Turiy Mys. *Zap. VMO* 107, 291–304, 1978. (in Russian).
- Sarda P., Staudacher T. and Allegre C. J., ⁴⁰Ar/³⁶Ar in MORB lasses: constraints on atmosphere and mantle evo-

- lution. *Earth Planet. Sci. Lett.* 72, 357–375, 1985.
- Sarda P., Staudacher T. and Allegre C. J., Neon isotopes in submarine basalts. *Earth Planet. Sci. Lett.* 91, 73–88, 1988.
- Sasada T., Hiyagon H., Bell K. and Ebihara M., Excess ^{129}Xe and relatively low $^{40}\text{Ar}/^{36}\text{Ar}$ ratios in carbonatites from Canada and Brazil. *Geochim. Cosmochim. Acta* (accepted), 1997.
- Shpachenko A. K., Stepanov V. A., New data on morphology of ore-containing structures in northern segment of ijolite - urtite arc of Khibina. *Dokl. USSR Acad. Sci.* 319, 1413–1417, 1991. (in Russian).
- Solopov Yu. A., Using of olivinites of Lesnaja Varaka. Location and structure of ore deposits. *Zapiski. Leningr. Gogn. Inst.* 72, 77–83, 1977. (in Russian).
- Solopov Yu. A., Structure of apatite - magnetite deposit of Vuorijarvi massif. Geology and prospecting of deposits. *Zap. Leningr. Gorn. Inst.* 75, 34–36, 1978. (in Russian).
- Spasennykh M. Yu. and Tolstikhin I. N., Noble gas fractionation during degassing of melts. *Geochim. J.* 27, 213–217, 1993.
- Staudacher T. and Allegre C. J., Terrestrial xenology, *Earth Planet. Sci. Lett.* 60, 389–406, 1982.
- Staudacher T., Kurz M. D. and Allegre C. J., New noble-gas data on glass samples from Loihi seamount and Hualalai and on dunites samples from Loihi and Reunion Island. *Chem. Geol.* 56, 193–205, 1986.
- Staudacher Th., Sarda Ph., Richardson S. H., Allegre C. J., Sanga I., and Dmitriev L. V., Noble gases in basalt glasses from a Mid-Atlantic ridge topographic high at 14°N : Geodynamic consequences, *Earth Planet. Sci. Lett.* 96, 119–133, 1989.
- Subbotin V. V., Structure control and zonation of rare metal ores in Vuorijarvi massif. In: *Alkaline magmatism of NE part of the Baltic Shield* (Ed. T. N. Ivanova). Kola Sci. Center Russian Acad. Sci. 76–79, 1990. (in Russian).
- Subbotin V. V., Mihaelis S. A., Genetic types of apatite ores from Sebljavr complex deposit. In: *Deposits of un-ore raws from Kola Peninsula* (Ed. O. B. Dudkin). Kola Sci. Center Russian Acad. Sci., 27–35, 1986. (in Russian).
- Taylor S. R. and McLennan S. M., *The continental crust: its composition and evolution*. Blackwell Sci. Public. 312 p., 1985.
- Ternovoy V. I., *Carbonatite massifs and their deposits*. Leningr. Univ. 168 p., 1977. (in Russian).
- Ternovoy V. I., Afanas'yev B. V., and Sulimov B. I., *Geology and prospecting of Kovdor vermiculite - phlogopite deposit*. Leningrad, Nedra, 287 p., 1969. (in Russian).
- Timmerman M. J., and Daly J. S., Sm-Nd evidence for late Archaean crust formation in the Lapland-Kola Mobile belt, Kola Peninsula, Russia and Norway. *Precamb. Res.* 72, 97–107, 1995.
- Tolstikhin I. N., and Marty B., The evolution of terrestrial volatiles: A view from helium, neon, argon and nitrogen isotope modelling. *Chemical Geol.* 147, 27–52, 1998.
- Tolstikhin I. N., Kamensky I. L., Sharkov I. V., Dudkin O. B., and Pripachkin V. A., Isotopes of light noble gases in carbonatites of the Kola Peninsula. *Kola Sci. Center, Russian Acad. Sci.* 42 p., 1985. (in Russian).
- Tolstikhin I. N., Dokuchaeva V. S., Kamensky I. L., and Amelin Yu. V., Juvenile helium in ancient rocks: II. U-He, K-Ar, Sm-Nd and Rb-Sr systematics in the Monche Pluton. $^3\text{He}/^4\text{He}$ ratios frozen in uranium-free ultramafic rocks. *Geochim. Cosmochim. Acta* 56, 987–999, 1992.
- Tolstikhin I. N., Lehmann B. E., Loosli H. H., and Gautschi A., Helium and argon isotopes in rocks, minerals and related groundwaters: A case study in Northern Switzerland. *Geochim. Cosmochim. Acta* 60, 1497–1514, 1996.
- Valbracht P. J., Honda M., Matsumoto T., Mattielli N., McDougall I., Agettli R., and Weis D., Helium, neon and argon isotope systematics in Kerguelen ultramafic xenoliths: implication for mantle source signatures. *Earth Planet. Sci. Lett.* 138, 29–38, 1996.
- Verkhovskiy A. B. and Shukolukov Yu. A., *Element and Isotope Fractionation of Noble Gases in Nature*. Moscow, Nauka, 294 p., 1991. (in Russian).
- Verkhovskiy A. B., Yurgina E. K. and Shukolukov Yu. A., Element and isotope ratios of juvenile noble gases. *Geokhimiya* 11, 1559–1576, 1983. (in Russian).
- Vetrin V. R., and Kalinkin M. M., Reconstruction of the processes of intracrustal and crustal-mantle magmatism and metasomatism *Kola Sci. Centre Publ.* 106 p., 1992.
- Vrevskiy A. B., and Krymsky R. Sh., Sm-Nd systematics and geochemistry of Archean peridotite komatiite of the Baltic Shield. *Dokl. Russian Acad. Sci.* 352, 80–82, 1997. (in Russian).
- Woolley A. R., and Kempe D. R. C., Carbonatites: nomenclature, average chemical compositions, and element distribution In: K. Bell (editor), *Carbonatites: Genesis and Evolution*. Unwin Hyman 1–13, 1989.
- Wyllie P. J., Baker M. B., and White B., Experimental boundaries for the origin and evolution of carbonatites. *Lithos* 26, 3–19, 1990.
- Yatsevich I. and Honda M., Production of nucleogenic neon in the Earth from natural radioactive decay. *J. Geophys. Res.* 102, B5, 10, 291–10, 298, 1997.
- Zaitsev A. N., Rhombohedral carbonates from carbonatites of the Khibina massif, Kola Peninsula, Russia. *Can. Miner.* 34, 453–468, 1996.
- Zaitsev A. N. and Bell K., Sr and Nd isotope data of apatite, calcite and dolomite as indicators of source and the relationships of phoscorites and carbonatites from the Kovdor massif, Kola Peninsular, Russia. *Contrib. Miner. Petrol.* 121, 324–335, 1995.
- Zaitsev A. N., Bell K., Wall F., and Le Bas M. J., Alkaline-REE carbonates from carbonatites of Khibina massif: mineralogy and genesis. *Dokl. Akadem. Nauk* 355, 241–245, 1997. (in Russian)
- Zartman R. E., Wasserburg G. J. and Reynolds J. H., Helium, argon and carbon in some natural gases. *J. Geophys. Res.* 66, 1, 277–306, 1961.

(Received December 5, 1998.)